



Synthesis and Performance Evaluation of Co/H-ZSM-5 Bi-functional Catalyst for Fischer-Tropsch Synthesis

MSc Dissertation

Prepared by

Khuthadzo Matamela (351237)

Submitted to

School of Chemical and Metallurgical Engineering, Faculty of Engineering and the Built Environment, University of the Witwatersrand, Johannesburg, South Africa in Fulfillment of the Award of the Degree of MSc (ENG) in Chemical Engineering

Supervisor: Prof. M.O. Daramola

25 October 2016

DECLARATION

1. I know that plagiarism is wrong. Plagiarism is using another's work and to pretend that it is one's own.
2. I have used the Harvard Referencing method for citation and referencing. Each significant contribution to, and quotation in, this proposal from the work, or works of other people has been attributed and have been cited and referenced.
3. This MSc dissertation is my own work.
4. I have not allowed, and will not allow, anyone to copy my work with the intention of passing it off as his or her own work.
5. I acknowledge that copying someone else's assignment or essay, or part of it, is wrong, and declare that this is my own work

SIGNATURE: _____

DATE: _____

ACKNOWLEDGEMENTS

I would like acknowledge the following individuals for their inputs:

- My Supervisor Dr. Michael Olawale Daramola for his guidance, supervision, ideas, patience, and support throughout this work and related projects.
- Mr. Basil Ecurie Chaussoulus for all his technical advice and setting up of the FTS rig.
- Pathutshedzo Sikhwari and Hopwell Gumede, Thank you for your enormous strength.
- Ms. Sibongile Maswaganyi for administration.
- A great thank you! To Mr. Bruce Mothibedi and his team with all the lab equipment provided and assistance.
- School of Chemical and Metallurgical engineering, Wits University
- National Research Foundation (NRF) for financial assistance
- North-West University – Wits project for financial assistance
- To my Family, Thank You! For supporting me all the way.

And finally, a Glorious Thanks, to the Almighty God for seeing me through it all.

Presentations and Publications

Conference proceedings and publications that have originated from this research project are listed below.

Publications:

1. Khuthadzo Matamela, M.O. Daramola, Conversion Of Syngas Derived From Waste Tyres To Liquid Fuel Over A Bi-Functional Co/H-ZSM-5 Catalysts: Effect Of Operating Conditions, *Manuscript submitted and accepted for publication and Oral presentation at: VENICE, ITALY, 2016 - 6th International Symposium on Energy from Biomass and Waste conference*
2. Khuthadzo Matamela, M.O. Daramola, Conversion Of Syngas Derived From Waste To Liquid Fuel Over Bi-Functional Co/H-ZSM-5 Catalyst In The Presence Of CO₂ Co-Feeding, *under review by the Journal of Environmental Chemical Engineering, 2016*

Conference Proceedings:

1. **Khuthadzo Matamela**, M.O. Daramola, Conversion Of Syngas Derived From Waste Tyres To Liquid Fuel Over A Bi-Functional Co/H-ZSM-5 Catalysts: Effect Of Operating Conditions, **Oral Presentation**, 14 – 17 November, VENICE, ITALY, 2016 - 6th International Symposium on Energy from Biomass and Waste - Abstract Accepted
2. **Khuthadzo Matamela**, M.O. Daramola, Conversion Of Syngas Derived From Waste To Liquid Fuel Over Bi-Functional Co/H-ZSM-5 Catalyst In The Presence Of CO₂ Co-Feeding, **Oral Presentation** , 8 -12 August , CAPE TOWN, SOUTH AFRICA , The 2016 Pittsburgh Coal Conference, University of Pittsburgh, Swanson School of Engineering, Cape Town International Convention Centre - Abstract Accepted

Contents

DECLARATION	i
ACKNOWLEDGEMENTS	ii
Presentations and Publications.....	iii
Publications:.....	iii
Conference Proceedings:	iii
ABSTRACT.....	vii
LISTS OF FIGURES	x
LISTS OF TABLES	xi
Nomenclature	xiii
CHAPTER 1: INTRODUCTION	1
1.1. Motivation and background.....	1
1.2. Research Questions	4
1.3. Research Objectives.....	4
1.4. Outline of Dissertation.....	4
1.5. References	5
CHAPTER 2: LITERATURE REVIEW	7
2.1. Introduction	7
2.1.1. Feedstock for FT Synthesis.....	8
2.1.2. FTS Catalyst Type	9
2.1.3. FTS Product Distribution	10
2.1.4. FTS Process Conditions (LTFT & HTFT)	15
2.1.5. FTS Reactors.....	16
2.1.6. Industrial Commercialization of FTS	18
2.2. Research development	19
2.3. Synthetic Gas and Catalyst for Fischer-Tropsch Synthesis.....	20
2.3.1. Gasification and Pyrolysis	20
2.3.2. FTS Catalyst	21
2.3.3. Synthesis of Fischer-Tropsch Catalyst.....	23
2.4. Effect of Operating Conditions on Catalyst Performance.....	24
2.5. Characterization of FTS Catalysts.....	24

2.6.	Conventional and Synthetic Diesel Fuel.....	25
2.7.	Summary and Future Outlook.....	27
2.8.	References	28
CHAPTER 3: EXPERIMENTAL PROCEDURE.....		33
3.1.	Introduction	33
3.2.	Materials	33
3.3.	Physicochemical Characterization of the Catalyst	34
3.3.1.	N ₂ Physisorption.....	34
3.3.2.	X-Ray Diffraction (XRD) Analysis	34
3.3.3.	Scanning Electron Microscopy (SEM) & Energy Dispersion Spectroscopy (EDS) Analysis ..	34
3.3.4.	Thermal Gravimetric Analysis (TGA)	35
3.3.5.	Temperature-Programmed Reduction (TPR).....	35
3.3.6.	Transmission-Electron-Microscopy (TEM)	35
3.4.	Reactor Design & Catalyst Loading	36
3.4.1.	Reactor specification.....	36
3.5.	Gas Chromatography	37
3.6.	Catalyst Activation\Reduction	38
3.7.	Summary	38
3.8.	References	39
CHAPTER 4: SYNTHESIS AND CHARACTERIZATION OF CATALYST.....		40
4.1.	Introduction	40
4.2.	Synthesis of the Bi-functional Co/H-ZSM-5 and the traditional Co/SiO ₂ Catalyst	40
4.3.	Results and Discussion	41
4.3.1.	N ₂ Physisorption.....	41
4.3.2.	XRD Analysis.....	45
4.3.3.	SEM Analysis	49
4.3.4.	EDS Analysis	51
4.3.5.	TGA Analysis.....	54
4.3.6.	TPR Analysis	56
4.3.7.	TEM Analysis	59
4.4.	Summary	61
4.5.	References	61

CHAPTER 5: PERFORMANCE EVALUATION OF THE BI-FUNCTIONAL Co/H-ZSM-5 CATALYST DURING FISCHER-TROPSCH SYNTHESIS.	64
5.1. Introduction	64
5.2. Experimental Procedure for the Evaluation of the Performance of the Catalyst.....	65
5.3. Results and Discussion	67
5.4. Comparison of the Bi-functional Catalyst with a Commercial Catalyst: Effect of operating conditions.....	78
5.5. Summary	82
5.6. References	83
CHAPTER 6: EFFECT OF CO ₂ CO-FEEDING ON THE PERFORMANCE OF THE BI-FUNCTIONAL Co/H-ZSM-5 CATALYST DURING FTS.....	85
6.1. Introduction	85
6.2. Results and Discussion	86
6.3. Comparison of the bi-functional catalyst and commercial catalyst in the presence of CO ₂	88
6.4. Summary	90
6.5. References	91
CHAPTER 7: CONCLUSION & RECOMMENDATIONS	92
7.1. Conclusion.....	92
7.2. Recommendations	98
7.3. Process Optimization	99
7.4. References	100
APPENDICES	102
Appendix A: CATALYST SYNTHESIS IMAGES.....	102
Appendix B: N ₂ PHYSISORPTION AND BET DATA	103
Appendix C: PERFORMANCE EAVALUATION AND GC PICS.....	109
Appendix D: CONVERSION AND SELECTIVITY CALCULATIONS.....	112
D1. Conversion Calculations	112
D2. Selectivity Calculations	115

ABSTRACT

The motivation behind this study is the need to manage and reduce wastes, in particular waste tyre and biomass, while in turn recovering energy from these carbonaceous materials. These wastes were gasified to produce synthetic gas which served as a feed to the Fischer-Tropsch Synthesis process to produce hydrocarbons. The formed hydrocarbons can be used as fuels for different purpose like transportation, domestic and industrial heating systems. Cobalt supported on zeolite catalysts are used because of their high acidic sites present in the zeolite that can break the Anderson-Schultz-Flory polymerization kinetics and also because cobalt-based catalysts are preferred for low temperature Fischer-Tropsch (LTFT) synthesis process due to their negligible water and carbon dioxide formation as well as stability and life span.

In this research, a bi-functional Co/H-ZSM-5 catalyst was synthesized, characterized and evaluated for direct production of hydrocarbons at different process conditions. The bi-functional catalyst was prepared by incipient wetness impregnation method of an aqueous cobalt solution as the source of cobalt metal onto an H-ZSM-5 zeolite support, thereafter dried at 120 °C and calcined at 400 °C to obtain the finished Co/H-ZSM-5 catalyst. Physicochemical analyses performed included, Nitrogen Physisorption at 77 K to determine the surface area, pore volume and size of the synthesized catalyst. Also the N₂ adsorption was used to determine the adsorptive properties of the catalyst. X-ray diffraction at 2θ region between 10 to 90 ° by using Co-Kα radiation ($\lambda=1.79026 \text{ \AA}$) was used to determine the material crystallinity, structure and composition. For the morphology and elemental composition of the catalyst, a Scanning Electron Microscopy coupled with an Energy Dispersive X-ray Spectroscopy was used. Thermal stability of the catalyst was checked using a Thermal Gravimetric Analyzer to determine how the catalyst degraded with time when temperature was increased uniformly. Reducibility of the catalyst was determined by using Temperature Programmed Reduction equipment in a hydrogen environment from room temperature to 900 °C. Transmission Electron Microscopy was used to check the catalyst morphology, and the dispersion of the metal-oxide particles within the catalyst support.

The bi-functional zeolite supported catalyst was found to possess a surface area of 292 m²/g, pore volume of 0.18 cm³/g and pore size of 2.83 nm. The catalyst morphology was found to be irregular and aggregated-circular shape with a particle size of about $2.5 \pm 0.5 \text{ }\mu\text{m}$. The embedded cobalt-oxide particles were obtained to be about $8 \pm 3 \text{ nm}$ located closer to the surface of the

support and were reduced to metallic cobalt of 25% composition, at 330 °C in a hydrogen rich environment with an expected hydrogen consumption of 133 %.

The process conditions under study involved flow rate, pressure and temperature and synthetic gas of different H₂/CO ratio. The Synthetic gas mixture was purchased from Afrox and prepared in a way to mimic or simulate the syngas mixture expected from gasification of the waste tyre and biomass. However the study mainly focused on Hydrogen, Carbon Monoxide and Carbon dioxide as the dominant constituents of a waste tyre produced syngas. The bi-functional, Co/H-ZSM-5 performance evaluation was compared to commercial Co/SiO₂ catalyst under similar conditions. The performance evaluation and comparison was made based on conversion and selectivity at different conditions. The process conditions considered were a flow rate of 1200, 2400 and 3600 GHSV (ml/gcat.hr), a pressure of 2, 8 and 15 bar, Low Temperature Fischer-Tropsch (LTFT) process at 220 and 250 °C was used, with a syngas composition that included H₂/CO ratio of 1.5, 2.5 and 2.5 with 5 % of CO₂ present in the reactant feed.

The combination of 2 bar, 1200 GHSV and temperature of 220 °C and 1.5 of ratio was considered as low process conditions. While the combination of 15 bar, 1200 GHSV, 250 °C and ratio of 2.5 was considered as high process condition. Three pre-calibrated GCs (two online and one offline) were used to analyze the reaction products and the feed and the integrated peak-data analyses was captured by the use of a Data Apex Chromatograph software package known as Clarity ® (v. 2.5). The captured and analyzed data was used to calculate conversion and selectivity according to the methods reported in literature.

With regard to the effect of process conditions, at low process conditions, the bi-functional catalyst, Co/H-ZSM-5, resulted in a 3 % CO conversion, while the commercial Co/SiO₂ catalyst, resulted in 15 % of CO conversion. However the bi-functional catalyst was more selective to gasoline range products and 16 % selectivity to C₅ hydrocarbons was obtained and 79 % to C₆₊, as compared to selectivities of 4 and 75 % for C₅ and C₆₊ respectively, for Co/SiO₂ catalyst. Also Co/SiO₂ was found to be more selective to Olefins, the undesired products, with a selectivity of about 91 % to C₆₊ hydrocarbons as compared to a selectivity of 87 % for C₆₊ hydrocarbon obtained by using the bi-functional Co/H-ZSM-5 catalyst. Methane production was high for the Co/SiO₂ catalyzed reaction, (about 13 % selectivity) with some quantity of water produced, as compared to 3 % methane selectivity for Co/H-ZSM-5 catalyst with no water produced during

the reaction. At low process condition, both catalysts were less prone to middle distillates hydrocarbon production.

At high process conditions, a CO conversion of about 54 and 68 % was obtained by Co/H-ZSM-5 and Co/SiO₂ catalyst respectively. At these conditions the H-ZSM-5 supported catalyst was observed to produce more methane, about 53 % selectivity while for Co/SiO₂ catalyst it was obtained to be 35 % selective to methane, with 66 and 7 % of C₆₊ olefin and paraffin selectivity respectively. Co/H-ZSM-5 offered 9 % selectivity to C₆₊ per olefin and paraffin hydrocarbons. The commercial catalyst showed an orderly manner of distributing products at these conditions while the bi-functional catalyst randomly distributed the formed products with a high selectivity to middle olefin distillates.

In terms of CO₂ co-feeding in the reactant feed, both CO and CO₂ were hydrogenated to hydrocarbons. A CO conversion of about 73 % was obtained by Co/H-ZSM-5 catalyzed reaction while for Co/SiO₂ catalyzed reaction a conversion of 70 % was obtained. About 63 and 75 % of CO₂ conversion was obtained by H-ZSM-5 and SiO₂ supported catalyst. These results were obtained at high process conditions. No change in paraffin selectivity was observed when comparing a state in which CO₂ was present and absent, however olefin selectivity is significantly affected by the presence of CO₂. Thus, an increase in olefin selectivity is observed with Co/SiO₂, achieving 76 % of C₆₊ Olefin from 66 % and Co/H-ZSM-5 increasing middle olefin distilled from 25 to about 30 % of selectivity.

Based on the performance evaluation the bi-functional catalyst was proven to yield higher hydrocarbons from a simulated waste-tyre synthetic gas with no requirement of downstream hydrocracking, since the bi-functional catalyst cut-off higher hydrocarbons due to its acidic sites. While the metallic sites of the catalyst, catalyzes the reaction of synthetic gas to hydrocarbons. This type of catalyst with both metallic sites and acidic sites is a hybrid-catalyst commonly known as bi-functional catalyst (Kang *et al.*, 2014).

At low process conditions the bi-functional Co/H-ZSM-5 catalyst is found to be more preferred while at higher process conditions the commercial catalyst was found to be more preferred, however in the presence of CO₂ co-feeding, either catalyst can be used, but if water elimination is required the bi-functional catalyst is more suitable for the process.

LISTS OF FIGURES

Figure 2.1: Production of liquid fuel (e.g. diesel) via the Fischer-Tropsch Synthesis Process	7
Figure 2. 2: Product Distribution for FT Synthesis over Cobalt Catalyst (adapted from Rao & Gormley, 1990)	13
Figure 2.3: Comparison of the hydrocarbon Product distribution (ASF Plot) and Selectivity Model Predictions (taken from, Todic <i>et al.</i> , 2013)	14
Figure 2.4 Variation of Yield with Chain Growth Parameter for specific products (taken from, Rao & Gormley, 1990)	15
Figure 2.5: Types of Fischer-Tropsch Reactors in commercial use at present, adapted from Subiranas (2009)	16
Figure 3.1: Schematic Diagram of Reactor Specifications	36
Figure 4.1: Bifunctional catalyst Synthesis procedure	41
Figure 4.2: Surface Areas of the Support and the catalyst	42
Figure 4.3: Pore size of the support and the catalyst	43
Figure 4.4: Pore Volume of the support and the catalyst.....	44
Figure 4.5: XRD Patterns of the Support and Synthesized Catalyst.....	46
Figure 4.6: XRD Patterns of Co/H-ZSM-5 final catalyst.....	48
Figure 4.7: SEM image for (a) ZSM-5 and (b) H-ZSM-5	50
Figure 4.8: SEM Image for Co/H-ZSM-5	51
Figure 4.9: Elemental Composition of ZSM-5	52
Figure 4. 10: Elemental Composition of Co/H-ZSM-5.....	53
Figure 4.11: Change in Sample mass with Temperature	54
Figure 4.12: Optimum Sample Decomposition Conditions	55
Figure 4.13: Co/H-ZSM-5 catalyst TPR profile.....	57
Figure 4.14: TEM images of (a) H-ZSM-5 support and (b) Co/H-ZSM-5 bi-functional catalyst.....	60
Figure 4.15: TEM images of (a) SiO ₂ support and (b) Co/SiO ₂ commercial catalyst	60
Figure 5.1: Olefin: (a) Ethylene, Paraffin: (b) Butane (c) isobutane which is a Butane isomer	65
Figure 5.2: Fischer-Tropsch Experimental Setup	66
Figure 5.3: Olefin & Paraffin Selectivity at flow rate of (a) 1200 (b) 2400 and (c) 3600 GHSV (ml/gcat.hr)	68
Figure 5.4: Olefin & paraffin Selectivity at low pressure and (a) 220 and (b) 250 degrees.....	70
Figure 5.5: Olefin & paraffin Selectivity at High Pressure and (a) 220 and (b) 250 degrees	72
Figure 5.6: Olefin & Paraffin Selectivity at Pressure of (a) 2 bar (b) 8 bar and (c) 15 bar	74
Figure 5.7: Olefin & Paraffin Selectivity at different syngas composition	76
Figure 5.8: Hydrocarbon selectivity for (a) Co/H-ZSM-5 and (b) Co/SiO ₂	79
Figure 5. 9: olefin & Paraffin Selectivity based on (a) Co/H-ZSM-5 and (b) Co/SiO ₂ catalyst.....	81

Figure 6.1: Change in Olefin & Paraffin Selectivity in the absence of CO₂ (a) and in presence of CO₂ (b) . 88
 Figure 6.2: Olefin and Selectivity in the presence of CO₂ for (a) Co/H-ZSM-5 and (b) Co/SiO₂ catalyst.... 89

Figure A. 1: Bifunctional catalyst Synthesis images 102

Figure B. 1: Sample Surface area, pore Volume and Size 103

Figure B. 2: Catalyst and Support Adsorption Isotherm Data..... 103

Figure B. 3: Sample Surface Area based on BET model 104

Figure B. 4: Sample Surface Area based on Langmuir model 104

Figure B.5: Catalyst and Supports Adsorption Isotherms 105

Figure B. 6: Point A and B of the Adsorption Isotherms 106

Figure B.7: BET Model Surface Area Plot 107

Figure B.8: Langmuir Model Surface Area 108

Figure C. 1: The Experimental Setup Components used for Catalyst Performance Evaluation 109

Figure C. 2: Thermal Conductivity Detector Gas Chromatograph peak image during reaction 110

Figure C. 3: Flame Ionized Detector Gas Chromatograph peak image during reaction 111

Figure D1. 1: Change of Conversion with Time at 250 °C, 15 bars and 1200 GHSV and various H₂/CO ratios 114

Figure D2. 1: Hydrocarbon Selectivity at 250 °C, 15 bars and H₂/CO ratio of 1.5..... 119

LISTS OF TABLES

Table 2.1: Comparison between coal-derived syngas and bio-syngas composition 9

Table 2.2: Comparison of Low Temperature Fischer-Tropsch Synthesis over Iron-based and Cobalt-based Catalyst..... 10

Table 2.3: Effect of Fischer-Tropsch active metals and operating range on the product distribution (adapted from De Klerk & Furimsky, 2011) 10

Table 2.4: Commercial FTS Process Conditions Based on the Catalyst Type..... 16

Table 2.5: Specification of FT-Diesel in comparison to conventional diesel, adapted from Laohalidanond *et al.*, 2006) 26

Table 3.1: N₂ Physisorption Analysis Conditions and Adsorptive Properties..... 34

Table 3.2: GC Properties & Specification 38

Table 4.1: Textural Properties of zeolite Samples	42
Table 4.2: Miller Indices and spacing of adjacent planes of cobalt metal	48
Table 4.3: Sample Optimum Decomposition Point.....	56
Table 4.4: Element Peak Reduction Temperature	58
Table 5.1: Effect of flow rate on conversion	67
Table 5. 2: Effect of Temperature on conversion at low pressure	70
Table 5.3: Effect of Temperature on conversion at High pressure	71
Table 5.4: Effect of Pressure on Conversion	73
Table 5.5: Effect of Syngas Composition on Conversion.....	75
Table 5.6: Comparison between Bi-functional and Commercial catalyst.....	78
Table 5.7: Comparison between Bi-functional and Commercial catalyst on Conversion.....	80
Table 6.1: Effect of CO ₂ co-feeding on the rate of conversion Co/H-ZSM-5 catalyzed reaction	86
Table 6.2: Comparison between Bi-functional and Commercial catalyst on Conversion in the presence of CO ₂	88
Table D1. 1: Syngas Calibration peaks before reaction	112
Table D1. 2: Peak Composition Area.....	112
Table D1. 3: Thermal Conductivity Detector Syngas mixture Peak Areas after reaction	113
Table D1. 4: Product Moles and Conversion.....	113
Table D2. 1: Calibration Gas Composition	115
Table D2. 2: Hydrocarbon Products Peak Areas	115
Table D2. 3: Hydrocarbon Molar Response Factor adopted from Motchelaho (2011) and Moyo (2012).....	116
Table D2. 4: Product moles and Selwectivity.....	116
Table D2. 5: Olefin and Selectivity Data in Fractions	118

Nomenclature

AMCSD	The American Mineralogists Crystal Structure Database
Ar	Argon gas
ASF	Anderson-Schultz-Flory
BC	Body-Centred
BET	Brunauer-Emmett-Teller
CO	Carbon Monoxide
Co	Cobalt-metal
$\text{Co}(\text{NO}_3)_2 \cdot 6\text{H}_2\text{O}$	Cobalt (II) Nitrate Hexa-hydrate as purchased from Sigma-Aldrich
Co/H-ZSM-5	Final cobalt-zeolite bi-functional catalyst, to be used in FTS
Co/H-ZSM-5_1	Zeolite support impregnated with $\text{Co}(\text{NO}_3)_2 \cdot 6\text{H}_2\text{O}$ solution
Co/SiO ₂	Cobalt-supported on silicon dioxide (commercial catalyst)
CO ₂	Carbon Dioxide
E.U	European Union
EDS	Energy Dispersion Spectroscopy
EDX	Energy Dispersion X-Ray
FC	Face-Centred
FCC	Face-Centred-cubic
Fe	Iron-metal
FID	Flame Ionization Detector

FT	Fischer-Tropsch
FTS	Fischer-Tropsch Synthesis
GC	Gas Chromatography
gcat	weight of catalyst in grams
H ₂	Hydrogen Gas
hcp	Hexagonal Closed Pack
He	Helium gas
HTFT	High Temperature Fischer-Tropsch System
H-ZSM-5	H-form of ZSM-5 / Hydron-Zeolite Socony Mobil-5
IZA	International Zeolite Association Database
LTFT	Low Temperature Fischer-Tropsch System
MTG	Methanol-to-Gasoline
MTO	Methanol-to-Olefins
Ni	Nickel-metal
PDF	Powder Diffraction File
FIXBR	Fixed-Bed Reactor
SC	Simple-Cubic
SEM	Scanning Electron Microscopy
TCD	Thermal Conductivity Detector
TEM	Transmission Electron Microscopy
TGA	Thermal Gravimetric Analysis

TPR Temperature Programmed Reduction

XRD X-Ray Diffraction

ZSM-5 Ammonium (NH_4^+) form Zeolite Socony Mobil-5



CHAPTER 1: INTRODUCTION

1.1. Motivation and background

Management of waste has always been a crucial and delegated responsibility, undertaken on behalf of the industry, public authorities and waste management specialists. Rapid population growth along with increasing productivity and resource consumption has intensified waste production and accumulation (Phale, 2005; Suhanya *et al.*, 2013). Waste accumulation has been known to create various problems to the environment and to the human health. These problems are worsened when accumulation of wastes occurs at incorrect landsite (Phale, 2005). However to solve environmental problems and ensure a sustainable living, we must rethink and restructure basic human systems, which includes waste management. Garbage control is also of greater concern to those interested in structuring a sustainable future. For this reason, the need for environmentally acceptable waste disposal has also become a priority in South Africa.

Tons of discarded tyres constitute an environmental problem in South Africa as they pollute the environment due to improper disposal methods (Phale, 2005). These problems caused by waste tyres are mainly because they are not biodegradable and can last for several decades (Suhanya *et al.*, 2013). The same properties that make tyres desirable, such as durability, in turn make their disposal and reprocessing a challenge (Nkosi *et al.*, 2013). There are neither regulations nor measurements in place, intended to reduce accumulation of used tyres or to control their disposal in South Africa (Phale, 2005). As a consequence, used tyres have been disposed haphazardly, mostly stockpiled and burnt, thus present an environmental problem (Phale, 2005). Apart from improper disposal methods of tyres, large quantities of faulty tyre casings end up as second-hand tyres on vehicles and this contribute to road accidents caused by tyre failure. The number of discarded tyre piles continues to grow and therefore imposes even greater environmental, safety and aesthetic problems due to the lack of suitable methods to discard them (Phale 2005).

According to Mahlangu (2009) about 160 000 tons of scrap used tyres are produced in South Africa every year and about 20 - 28 million used tyres are dumped illegally in land sites. In 2005 this amount was predicted to increase by 9.3 million in a year (Mahlangu, 2009). Other nations like the United States (U.S) produce around 290 million of waste tyres (in number) whereas the European Union (E.U) produced about 260 million based on the 2003 statistics stated by

(Donatelli *et al.*, 2010). About 40 % of waste tyres in Europe was landfilled, but after the implementation of E.U directive on waste landfill in 2006, this practice could no longer be practiced in the European countries (Donatelli *et al.*, 2010).

With the aim of recovering energy from waste tyres and biomass, many research studies such as Hu *et al.*, (2012), Rada *et al.*, (2012) and Peres *et al.*, (2013) have been focused on different utilization techniques, for instance gasification, pyrolysis and more recently, tyre refreshment and rubber regeneration. Waste tyres can be processed by gasification to capture hydrogen and carbon monoxide gas. Gasification in particular, is a thermal process that converts carbonaceous materials, such as coal, organic waste or biomass into carbon monoxide and hydrogen with a controlled amount of oxygen or steam (Donatelli *et al.*, 2010). This resulting gas mixture is called synthesis gas or simply syngas.

Syngas gas can be used to produce a variety of chemicals and liquid fuels. Domestic transportation and military operational interest have motivated continued focus on syngas-based fuel production. Liquid transportation fuels like gasoline and diesel may be made from syngas via four basic processes: (1) higher alcohols, (2) Fischer-Tropsch (FT), (3) Methanol-to-Gasoline (MTG), and (4) Methanol-to-Olefins (MTO) (Dagle *et al.*, 2014). Higher alcohol synthesis, is mainly focused on ethanol, and has enjoyed renewed attention, but still offers a low productivity and poor selectivity. Fischer-Tropsch (FT) produces a wide range of mainly linear paraffinic hydrocarbons, with the product distribution depending on the catalyst and the specific process configuration (Dagle *et al.*, 2014). Thereafter hydrocracking is required to maximize the desired product fraction. For example Sasol commercial plants in South Africa uses coal derived synthesis gas to produce liquid fuel (Dancuart & Steynberg 2007). Due to many circumstances including geo-political and economic factors, Sasol developed four Fischer-Tropsch processes, of which two are low temperature systems (LTFT) that uses either Fe- or Co-based catalyst and the other two are high temperature systems (HTFT) which uses Fe-based catalyst (Dancuart & Steynberg 2007). All these plants have been demonstrated commercially and are currently in operation in South Africa (Dancuart & Steynberg 2007).

Despite several advantages of FT, numerous studies such as Pour *et al.*, (2009), Mohanty *et al.*, (2011) and Sartipi *et al.*, (2013a) have evaluated the combination of Fischer-Tropsch Catalyst (e.g. Fe-, and Co-based) and zeolites (e.g. ZSM-5) for the conversion of syngas to hydrocarbons.

Hydrocracking and hydro-isomerization of the primary Fischer-Tropsch olefins are considered to occur on the acidic sites and in the pore channels of the zeolite, which breaks the limit of the Anderson-Schultz-Flory (ASF) hydrocarbon product distribution thus facilitating direct conversion of liquid fuel without the need for further hydro-treatment (Dagle *et al.*, 2014) and (Mohanty *et al.*, 2011). According to Sartipi *et al.*, (2013a) the ASF hydrocarbon distribution model implies that the number of carbon in the products is a function of the chain growth probability at the catalyst surface.

Cobalt (Co) and Iron (Fe) are the two most industrial employed metals in commercial FTS catalyst (Sartipi *et al.*, 2013a). Both these metals can catalyze FTS at temperatures below 523 K, also known as the Low-Temperature Fischer-Tropsch (LTFT) (Sartipi *et al.*, 2013a). Co-based catalyst is preferred at LTFT to Fe-based while Fe-based catalyst is preferred at HTFT systems when compared to Co-based catalyst (Dancuart & Steynberg 2007). Many efforts have been devoted in developing a catalyst able to couple FTS with hydrocracking or isomerization to break the ASF hydrocarbon product distribution and directly produce liquid fuel thereby eliminating downstream hydro-treatment processes in FTS. To achieve this, Sartipi *et al.*, (2013a) stated that a second functionality to the FTS should be added to the catalyst formulation in order to break the ASF selectivity. Since hydrocracking and isomerization is mostly based on acid catalyzed reactions, zeolites are considered a potential solution to this approach.

In this research, Co/H-ZSM-5 was synthesized and evaluated for the direct production of liquid fuel during FTS using a syngas mixture purchased from Afrox and prepared in a way to simulate the syngas mixture expected from gasification of the waste tyre and biomass. Fixed bed reactor (FIXBR) was used as reaction chamber at predetermined pressure, temperature, and reaction time, amount of catalyst and H₂/CO ratio. The overall conversion, selectivity, and hydrocarbon distribution was evaluated by using the reaction data that was captured by the pre-calibrated GCs. The Co/H-ZSM-5 catalyst acted as a bi-functional catalyst and Co/SiO₂ was the commercial catalyst. The catalytic performance of Co/H-ZSM-5 will be benchmarked with the catalyst performance of a commercial Co-based FTS catalyst that was evaluated at similar conditions as the bi-functional catalyst.

1.2. Research Questions

The following research questions were attended to, in this project:

- Can the use of bi-functional Co-based catalyst supported on H-ZSM-5 yield liquid fuel from waste-based syngas via FTS?
- How does the performance of this synthesized catalyst during FTS compare with the performance of the commercial Co-based FTS Catalyst?
- What will be the effect of CO₂ co-feeding with H₂/CO on the performance of the catalyst during FTS?
- What will be the effect of operating variables such as reaction temperature, pressure, reaction time and H₂/CO ratio on the performance of the catalyst?

1.3. Research Objectives

To answer the aforementioned research questions, the objectives of this research were as follows:

- Synthesis and characterization of a bi-functional Co-based catalyst supported on H-ZSM-5 zeolite.
- Evaluation of the performance of the synthesized catalyst in terms of reactivity (activity and selectivity) and hydrocarbon distribution during the conversion of syngas to liquid fuels via FTS and comparison between this performance and that of a commercial Co-based FTS catalyst (Co/SiO₂).
- Studying the effect of CO₂ co-feeding on the performance of the catalyst during FTS reaction
- Investigation of the effect of operating variables such as temperature, pressure, reaction time, H₂/CO ratio on the performance of the catalyst.

1.4. Outline of Dissertation

In Chapter 1 of this document, motivation of the research, research questions, aims and objectives were stated as well as the problem statement and an approach to answer and satisfy the research questions. Chapter 1 was preceded by Chapter 2 which gave a detailed review on Fischer-Tropsch processes history, its traditional catalysts, the use of zeolite as a catalyst and the process feedstock. Chapter 3 outlined the materials used, catalyst characterization methods and experimental procedure as adopted from different literature, catalyst activation and reactor

design while Chapter 4, reported on the procedure in which the bi-functional catalyst was synthesized, including discussion of physicochemical characterization results and findings. In Chapter 5, the performance evaluation obtained results are discussed in terms of conversion and selectivity based on the effect of the operating conditions while Chapter 6, reports on the obtained results and discussion on the effect of CO₂ co-feeding on the FTS product distribution. Lastly Chapter 7 draws conclusion on the findings and gives recommendation for future work as well as any useful information.

1.5. References

- Dagle R.A, Lizarazo-Adarme J.A, Dagle V.L, Gray M.J, White J.F, King D.L, Palo D.R, 2014, Syngas conversion to gasoline-range hydrocarbons over Pd/ZnO/Al₂O₃ and ZSM-5 composite catalyst system. *Fuel Processing Technology*, 123, pp.65–74. Available at: <http://dx.doi.org/10.1016/j.fuproc.2014.01.041>.
- Dancuart L.P, Steynberg A.P., 2007, Fischer-Tropsch based GTL technology: a new process? *Studies in Surface Science and Catalysis*, 163, pp.379–399.
- Donatelli A, Iovane P, Molino A, 2010. High energy syngas production by waste tyres steam gasification in a rotary kiln pilot plant . Experimental and numerical investigations. *Fuel*, 89(10), pp.2721–2728. Available at: <http://dx.doi.org/10.1016/j.fuel.2010.03.040>.
- Hu J, Yu F, Lu Y, 2012, Application of Fischer–Tropsch Synthesis in Biomass to Liquid Conversion. *Catalysts*, 2(2), pp.303–326.
- Mahlangu M.L, 2009. Waste Tyre Management Problems in South Africa and the Possible Opportunities that can be created through Recycling Thereof. ,Msc dissertation, University of South Africa
- Mohanty P, Pant K.K, Parikh J, Sharma D.K, 2011. Liquid fuel production from syngas using bifunctional CuO-CoO-Cr₂O₃ catalyst mixed with MFI zeolite. *Fuel Processing Technology*, 92(3), pp.600–608. Available at: <http://dx.doi.org/10.1016/j.fuproc.2010.11.017>.
- Nkosi N, Muzenda E, Zvimba J, Pilusa J., 2013. The Waste Tyre Problem in South Africa: An Analysis of the REDISA Plan. *International Conference on Chemical and Environmental*

- Engineering (ICCEE'2013)*. Available at:
[https://ujdigispace.uj.ac.za/bitstream/handle/10210/12485/Nhlanhla Nkosi, Edison Muzenda, John Zvimba and Jefrey Pilusa, 2013.pdf?sequence=1](https://ujdigispace.uj.ac.za/bitstream/handle/10210/12485/Nhlanhla%20Nkosi,%20Edison%20Muzenda,%20John%20Zvimba%20and%20Jefrey%20Pilusa,%202013.pdf?sequence=1) [Accessed June 13, 2015].
- Peres A.P. G, Lunelli B.H, Filho R.M, 2013. Application of Biomass to Hydrogen and Syngas Production, *Chemical Engineering Transactions*, Vol. 32, pp.589–594.
- Phale A.R., 2005. Environmental impact and waste management of used tyres in the RSA. Msc Dissertation, University of Johannesburg, South Africa.
- Pour A.L, Zare M, Shahri Kamali S.M, Zamani Y, Alaei M.R, 2009, Catalytic behaviors of bifunctional Fe-HZSM-5 catalyst in Fischer-Tropsch synthesis, *Journal of Natural Gas Science and Engineering*, 1(6), pp.183–189. Available at:
<http://dx.doi.org/10.1016/j.jngse.2009.11.003>.
- Rada, E.C, Ragazzi M, dal Maschio R, Ischia M, Panaitescu V.N, 2012. Energy recovery from tyres waste through thermal option. *UPB Scientific Bulletin, Series D: Mechanical Engineering*, 74(4), pp.201–210.
- Sartipi S, van Dijk J.E., Kapteijn F, 2013a, Applied Catalysis A : General Toward bifunctional catalysts for the direct conversion of syngas to gasoline range hydrocarbons : H-ZSM-5 coated Co versus H-ZSM-5 supported Co. “*Applied Catalysis A, General*”, 456, pp.11–22. Available at: <http://dx.doi.org/10.1016/j.apcata.2013.02.012>.
- Suhanya M, Kannadasan T, Thirumarimurugan M, 2013, Recovery of Oil From Waste Tyres Using Pyrolysis Method: a Review. *International Journal of Research in Engineering & Technology (IJRET)*, 1(2), pp.81–90. Available at:
<http://www.impactjournals.us/journals.php?id=77&jtype=2&page=2>.

CHAPTER 2: LITERATURE REVIEW

2.1. Introduction

Literature review serves to outline the most significant work done on the field or topic under study. In this case the bi-functional and commercial catalyst and the Fischer-Tropsch synthesis are discussed in detail. In this chapter, different types of feedstock, types of catalyst, and different process conditions involved in FTS are discussed. Reactors that are used in commercial FT are discussed as well. Current trend in research and innovation in FTS process also discussed. Furthermore, the chapter will dwell a bit on the production of synthetic gas using different methods, various synthesis techniques for the production of FT catalyst, characterization techniques for these catalyst and effect of operating conditions on the performance of these catalyst (obtained from previous studies) conversion and selectivity during FTS.

Producing liquid fuels via Fischer-Tropsch process involves several steps: conversion of carbon containing materials to synthetic gas, the Fischer-Tropsch process and finally product purification. Figure 2.1 illustrates the steps involved in the production of liquid fuels (e.g diesel) via FTS process from different carbon rich materials.

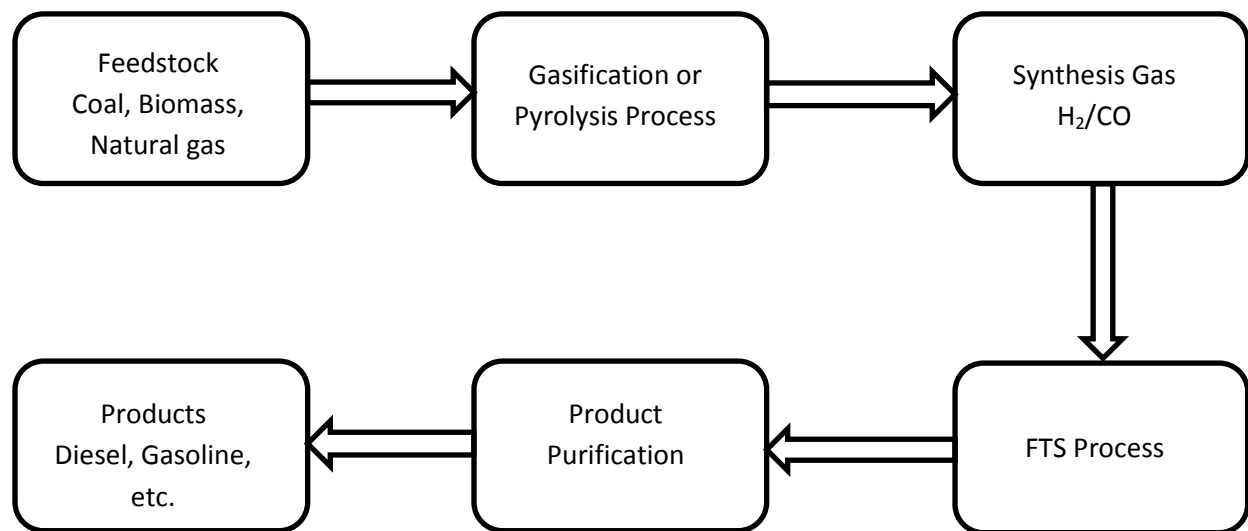


Figure 2.1: Production of liquid fuel (e.g. diesel) via the Fischer-Tropsch Synthesis Process

2.1.1. Feedstock for FT Synthesis

Fischer-Tropsch Synthesis is a set of catalytic processes that can be used to produce fuels and chemicals from synthesis gas that consist of a mixture of mainly CO and H₂. This gas mixture can be derived from the reforming of natural gas or gasification of used tyres, coal, or biomass (Hu *et al.* 2012a; Peres *et al.* 2013). Waste tyres, coal or biomass can be gasified to obtain the synthesis gas, and then a cleaning process can be applied to remove impurities in order to produce a clean syngas which meets the desired Fischer-Tropsch synthesis requirements (Peres *et al.*, 2013; De Klerk, 2011). The synthetic gas is the feed into the Fischer-Tropsch catalytic reactor to produce gasoline, diesel and other clean liquid fuels (Hu *et al.*, 2012; De Klerk, 2011).

The two main types of gas reforming are steam reforming and adiabatic oxidative reforming. The difference in these two types of reforming is the way in which energy is supplied to each of these processes. In steam reforming, heat is supplied by an external source to convert the natural gas and steam with or without CO₂, by an endothermic reaction in the presence of a catalyst (De Klerk, 2011). In adiabatic oxidative reforming process, irrespective of whether it employs a catalyst or not, the reaction takes place by exothermic partial combustion of the natural gas into syngas, with no external source of heat needed (De Klerk, 2011). Both processes have a coking side reaction which is due to the imbalance of CO or by catalyzed dehydration reaction of the natural gas feed. Some of the disadvantages associated with producing syngas from natural gas, is the need for gas cleaning and pre-reforming as pretreatment steps before gas reforming. The pretreatment steps are employed to prevent poisoning (Oar-arteta *et al.*, 2014) of the reformer catalyst and to ensure that the syngas produced by the FTS does not require further cleaning (De Klerk, 2011).

Production of synthetic gas from coal and natural gas has been a challenge in industries due to the limitation of these resources and environmental concern that they pose (Hu *et al.*, 2012). This has encouraged production of liquid fuels, by using syngas from biomass (bio-syngas). This process has been gaining increasing attention in recent years (see Peres *et al.*, 2013; Laohalidanond *et al.* 2006; Kreutz *et al.* 2008). For reason that, fuels from syngas obtained from biomass are usually much cleaner and environmental friendly and they contain little or no Sulphur and other contaminants (Hu *et al.*, 2012; Larsson, 2007; States & Agency, 1998).

Similar to syngas derived from coal, bio-syngas from biomass gasification contains CO, H₂, CO₂, CH₄ and N₂ in different proportions (Hu *et al.*, 2012). The average syngas from coal and bio-syngas from a downdraft gasifier that uses air as an oxidant contains the following composition shown in Table 2.1.

Table 2.1: Comparison between coal-derived syngas and bio-syngas composition

	Syngas	Bio-syngas
CO (%)	37.14	22.16
H ₂ (%)	36.67	17.55
CO ₂ (%)	20.58	11.89
CH ₄ (%)	1.71	3.07
N ₂ & other elements (%)	3.9	45.33

The composition of coal derived syngas in Table 2.1 is based on Wu *et al.*, (2005) and the bio-syngas composition is based on Hu *et al.*, (2012). In addition, according to Mitchell *et al.*, (2013) synthetic gas has a chemical composition of H₂ (20-40 %), CO (35-40 %), CO₂ (25-35 %), CH₄ (0-15%) and N₂ (0-5 %). If the FTS feedstock is synthesis gas from coal, natural gas, biomass or other solid carbon sources, traditional catalyst such as Fe-, Co-, and Ni-based can be used and they have been extensively studied in literature (Huang *et al.*, 2011; Pour *et al.*, 2009; Golodets, 1989).

2.1.2. FTS Catalyst Type

The distribution of the main products obtained from Fischer-Tropsch-active metal catalyst shows the effect of the catalyst type on the product composition (see Table 2.3.). In addition, the types of the promoters and the supports used for these catalysts do influence the performance of the catalyst during FT synthesis. Many studies and research have been focused, on two main types of FT catalyst namely, Iron (Fe) (see Pour *et al.* 2009) and cobalt (Co) (see Sartipi *et al.* 2013a and Sartipi *et al.* 2013b). The comparison between these two catalyst as reported by De Klerk & Furimsky, (2011) and is presented in Table 2.2.

Table 2.2: Comparison of Low Temperature Fischer-Tropsch Synthesis over Iron-based and Cobalt-based Catalyst

Catalyst Property	Fe-LTFTS	Co-LTFTS
Extensive Methanation	No	At increasing temperature & decreasing CO partial Pressure
Alkali promoters	Essential	No
Monomers	CH ₂	CH ₂ (CO, C ₂ H ₄)
Water Gas Shift (WGS) activity	Yes	Negligible
Branching Reaction	Static, Increases with time	Dynamic, decreases with time
Alkene hydrogenation	No / little	Extensive
Alkene isomerisation	No / little	Extensive

In addition to the catalyst properties listed in Table 2.2, different product distribution based on Fe- and Co-based catalysts is also shown in Table 2.3 below. This includes a Ni-based LTFT catalyst, which is advisable for use if longer carbon chains are desired as the product at low temperature ranges. However Ni-based catalyst is known to lose its activity at higher pressure due to side reaction that forms Nickel Tetra-carbonyl compound (De Klerk & Furimsky 2011).

Table 2.3: Effect of Fischer-Tropsch active metals and operating range on the product distribution (adapted from De Klerk & Furimsky, 2011)

Metal	Temperature (°C)	Pressure (MPa)	Nature of Products
Fe	200-250	1.0-3.0	Alkanes, Alkenes, Oxygenates
	320-340	1.0-3.0	Alkanes, Alkenes, Aromatics, Oxygenates
Co	170-220	0.5-3.0	Alkanes, some Alkenes and Oxygenates
Ni	170-205	0.1 *	Alkanes, some Alkenes

* At higher pressure, loss of Ni through Ni(CO)₄ formation becomes too high

According to De Klerk & Furimsky (2011), it has been noted that the Co-based LTFT catalysts gives a higher conversion rate (depending on the syngas conditions) and reportedly have a longer catalyst life. Co-based catalysts for LTFT are more easily prepared, cheaper, more robust and more resistant to Sulphur poisoning (De Klerk & Furimsky, 2011).

2.1.3. FTS Product Distribution

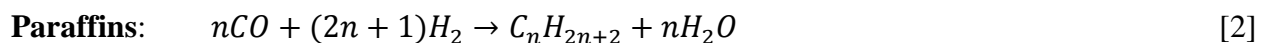
Several supports such as silica, aluminum and titanium (Dagle *et al.*, 2014; Silva *et al.*, 2013; Golodets, 1989) have been used for cobalt-based catalyst and their specific activity and selectivity properties studied, as well as their effect on liquid production from syngas have been reported. Bessell (1993), reported that the support material is a significant factor in influencing

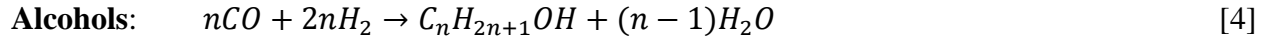
the specific activity of the catalyst, with the product selectivity being highly correlated with the extent of reduction of cobalt and its dispersion in the support.

Zeolites have also been investigated as a support for FT active metals (Bessell, 1993; Hassanpour *et al.* 2010; Mohanty *et al.* 2011), especially when liquid fuel production such as gasoline and diesel is being targeted. This is mostly done to impart a bi-functionality to the catalyst system, by using the zeolites to overcome the Anderson-Schultz-Flory (ASF) polymerization kinetics and maximize the selectivity of liquid fuels (Bessell, 1993). The product distribution from FTS is governed by ASF polymerization technique. According to Sartipi *et al.* (2013a) the ASF hydrocarbon distribution model implies that the number of carbon in the products is a function of the chain growth probability at the catalyst surface. In addition, the use of zeolites as support enhances isomerization and aromatization to yield a higher octane rating product (Bessell, 1993). Fornasari *et al.*, (1991) conducted a study to compare the performance of cobalt/Zeolite-Y and Co/ZSM-5 catalyst and reported that the Co/ZSM-5 displayed a higher activity than Co/Zeolite-Y. The decrease in the activity of the Co/Zeolite-Y was attributed to the formation of irreducible Co^{2+} ions on the Zeolite-Y supported catalyst.

The maximum selectivity of gasoline range products that could be obtained by catalytic conversion of synthetic gas over FT catalyst such as Co and Fe is about 48 % by weight of the total hydrocarbons produced (Bessell, 1993). However the use of H-ZSM-5 zeolite can convert olefins and oxygenated products to gasoline-range products containing aromatics (Dagle *et al.*, 2014; Bessell, 1993). In this manner, the FT products can be converted to a desired hydrocarbon cut. This method offers a possibility to overcome ASF polymerization kinetics and can increase the product selectivity of diesel and gasoline-range products above 30 and 48 % respectively (Rao & Gormley 1990; Bessell, 1993).

The conversion of synthetic gas to hydrocarbon, result in a number of synthesis reactions depicted by Eq. (1) to Eq. (4), these reaction are known to be exothermic with $\Delta H \approx -170$ kJ/ C-atom as reported by Bessell (1993).





Dancuart & Steynberg (2007) summarized the primary FT synthesis reaction as follows:



For other forms of the dominant Fischer-Tropsch Synthesis reactions, see Todic *et al.* 2013; Marvast *et al.* 2005; and Hu *et al.*, 2012 for more information. Two other important reactions that occur in different degrees of completion are syngas to alcohols (see Eq. (4)), and Water Gas Shift reaction (WGS) (Eq. (6)) (Dancuart & Steynberg, 2007) as follows:



Rao & Gormley (1990) also mentioned an occurrence of another reaction (also see, Hu *et al.* 2012) called Boudourd reaction (Eq. (7)) as follows:



The deactivation of the catalyst is due to the formation of coke by reaction in Eq. (7) that precipitates on the catalyst surface and decreases its activity (see Oar-arteta *et al.* (2014), for detailed study on causes of bifunctional catalyst deactivation). The relative importance of these reactions to each other depends on many factors including the FT catalyst type, the type of reactor and the composition of synthetic gas, in particular its H₂/CO ratio (Dancuart & Steynberg, 2007).

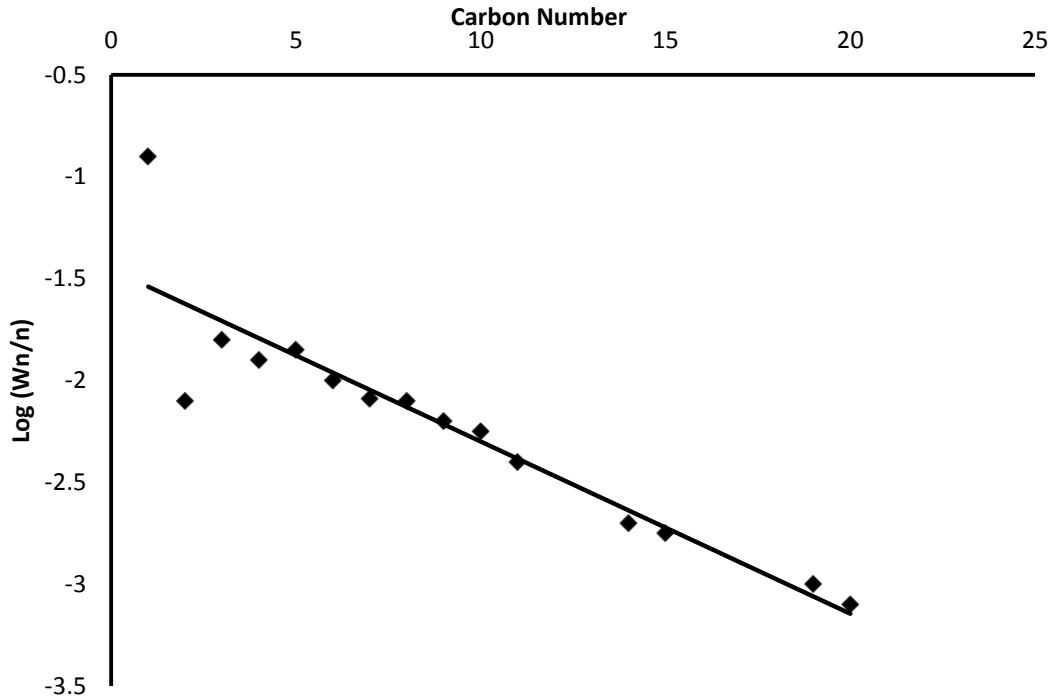


Figure 2. 2: Product Distribution for FT Synthesis over Cobalt Catalyst (adapted from Rao & Gormley, 1990)

Figure 2.2 illustrates the FTS product distribution over a cobalt based catalyst. It can be seen that the weight fraction (W_n) of carbon atoms increases as the number of carbon atoms (n) increases. This product distribution follows the Anderson-Schultz-Flory (ASF) polymerization technique. The chain growth probability is depicted with the quantity α and it represents the probability that a molecule with C_{n-1} carbon atoms will grow to a molecule with c_n carbon atoms (Rao & Gormley, 1990). Equation (8) is known as the ASF polymerization equation, where W_n is the weight fraction of C_n carbon atoms:

$$\log(W_n/n) = n \log \alpha + \log[(1 - \alpha)^2 / \alpha] \quad [8]$$

Rao & Gormley (1990) reported that if the FTS products follow the ASF product distribution polymerization technique, then one should expect a linear relation between $\log(W_n/n)$ and n , with the slope being $\log \alpha$ as depicted in Figure 2.3.

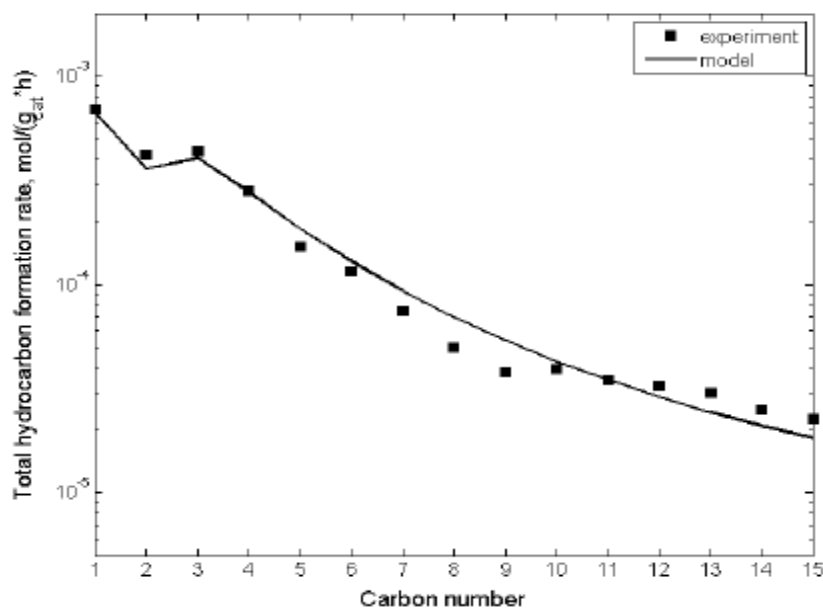


Figure 2.3: Comparison of the hydrocarbon Product distribution (ASF Plot) and Selectivity Model Predictions (taken from, Todic *et al.*, 2013)

Figure 2.3 illustrates a model of the hydrocarbon distribution and experimental data obtained by Todic *et al.*, (2013) at 533 K, 1.5 MPa, and H₂/CO ratio of 0.67 over Fe-based catalyst. Products in the C₂-C₁₀ range, alkenes in particular, were dominant but their formation decreases with increasing carbon number, at the range above C₁₀ paraffin production increased and alkenes decreased. This model is a good prediction of C₅₊ liquid hydrocarbon and performs better in lower hydrocarbon range products, and the increasing growth probability with the number of carbons. The apparent change of slope is due to the exponential decrease of C₂ to C₁₀ formation rate with carbon number, this behavior is also known as the non-ASF production which is also a possibility in FTS process.

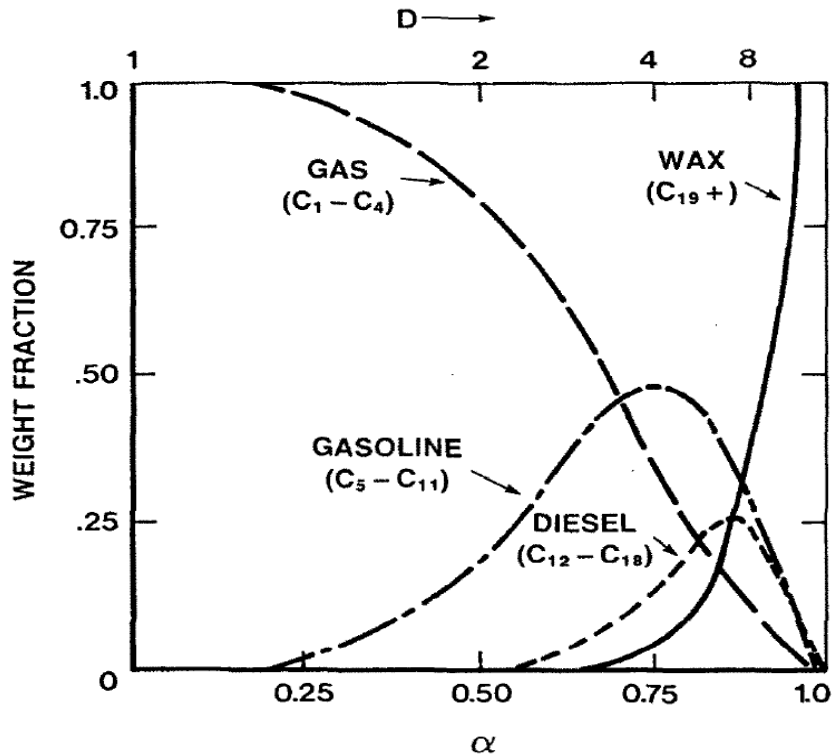


Figure 2.4 Variation of Yield with Chain Growth Parameter for specific products (taken from, Rao & Gormley, 1990)

The theoretical fraction for various hydrocarbon products such as gas (C_2-C_4), gasoline (C_5-C_{11}) and diesel ($C_{12}-C_{18}$) produced over FT Co-based catalyst is depicted in Figure 2.4, where $D = 1/(1 - \alpha)$ is the average degree of polymerization. From Figure 2.4, it can be seen that only gas (specifically methane) can be produced with 100 % selectivity. The maximum diesel yield is 30 % and for gasoline 48 % (Rao & Gormley, 1990; Bessell, 1993). These limitations arise from the ASF polymerization technique governing the chain growth. However, the use of zeolite supported catalysts is intended to circumvent these limitations and is expected to result in diesel and gasoline yields above 30 and 48 %, respectively (Rao & Gormley, 1990; Bessell, 1993).

2.1.4. FTS Process Conditions (LTFT & HTFT)

The operating conditions for the Low-Temperature Fischer-Tropsch (LTFT) and the High-Temperature Fischer-Tropsch (HTFT) with either Fe- or Co-based catalyst (Dancuart & Steynberg 2007; Subiranas 2009; Sartipi *et al.*, 2013a; Shah, 2011) are presented in Table 2.4.

Table 2.4: Commercial FTS Process Conditions Based on the Catalyst Type

FT Process	Low-Temperature (LTFT)	High-Temperature (HTFT)	References
Temperature	220-260 °C	320-350 °C	Dancuart, 2007
Catalyst	Co/Fe	Fe	
Pressure	Co: 0.5 - 3.0 MPa	1.0 - 3.0 MPa	De Klerk & Furimsky, 2010
	Fe: 1.0 - 3.0 MPa		

According to Subiranas (2009) the product range obtained from LTFT is wider than from HTFT. The LTFT mainly contains linear alkanes and lower contents of alkenes, oxygenates and iso-alkanes. The LTFT primary products require upgrading to middle distillates with naphtha as the main co-product. Another option is to process the produced wax for the production of lubricant base oils. The main HTFT products are low-boiling point hydrocarbons such as alkenes (propene, ethylene and butene) (Subiranas, 2009).

2.1.5. FTS Reactors

At present, there are three types of Fischer-Tropsch reactors in commercial use (Subiranas, 2009) (see Figure 2.5 for the schematic):

- (i) Tubular Fixed Bed Reactor
- (ii) Slurry Phase Reactor
- (iii) Fluidised-Bed Reactor (bubbling or circulating fluidised bed)

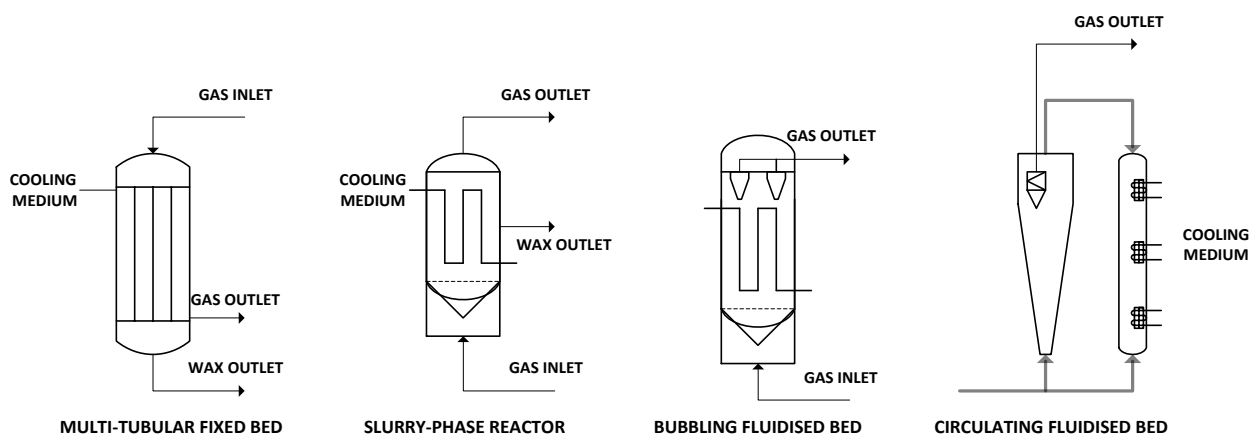


Figure 2.5: Types of Fischer-Tropsch Reactors in commercial use at present, adapted from Subiranas (2009)

Tubular fixed bed and slurry phase reactors are used preferably for the Low-Temperature FT system at about 220 -250 °C (Subiranas, 2009), to obtain long-chain hydrocarbons with either

Fe- or Co-based catalyst. When alkenes and/or alkanes are the desired products, then the use of high-Temperature FT system is recommended using a two-phase fluidized (FFB or CFB) with Fe-based catalyst (Subiranas, 2009).

In the tubular reactor the catalyst is packed into narrow tubes which are surrounded on the outside by water. Synthetic gas at a high flow rate is passed through the tubes resulting in a turbulent flow. These factors enable rapid heat exchange and minimize temperature rising in the axial and radial direction (Subiranas, 2009). Multi-tubular fixed-bed reactors are simple to operate and can be used over a wide range of temperature. The fixed bed reactor is known to have low cost, and easy to operate and maintain. In addition conventional fixed-bed reactors have been used by Sasol (the ARGE reactors) and Shell Company in their FT system (Subiranas, 2009; Narataruksa *et al.*, 2012; Davis, 2003; Dancuart & Steynberg, 2007). The five Sasol Arbeitsgemeinschaft (often abbreviated as ARGE) reactors in the Sasolburg plant are multi-tubular reactors with 3 m diameter, each containing 2050 tubes of 5 cm ID and 12 m long (Subiranas, 2009). These reactors use, Co-based or Fe-based catalyst (Steynberg *et al.*, 2004) at about 2.7 MPa and 230 °C with a production capacity of about 500 bpd/reactor (Subiranas, 2009). Shell also uses a multi-tubular reactor (~7 m diameter, < 5 cm ID) in Malaysia (Bintulu plant), operating with Co-based catalyst with a production capacity of 8000 bpd/reactor (Subiranas 2009). According to (Narataruksa *et al.*, 2012), fixed-bed reactors remain an attractive approach in economical aspect, because they offer a higher catalyst loading volume which enhances the hydrocarbon production.

The slurry phase reactor was developed during the World-War II by Kölbel and co-workers (Davis, 2003; Subiranas, 2009). In this type of reactor, the liquid wax product is the medium in which the catalyst is suspended resulting in a difficulty in its commercial application due to the need of separation of the wax product from the catalyst (Subiranas 2009). However in the 1990s, Sasol developed a reactor system to overcome this problem (Davis 2003; Subiranas 2009; Espinoza *et al.*, 1999) and the reactor was operated without problems for 10 years (Davis, 2003). The FT reaction rate is often pore diffusion-limited, even at low temperatures, and hence the smaller the catalyst particles the higher the obtained activity (Subiranas, 2009). For this reason, Subiranas (2009) stated that the slurry phase reactor offers a higher activity per mass of catalyst when compared to the fixed-bed reactor. The pressure drop in the slurry phase reactor is about

four times lower than of a multi-tubular reactor and results in a lower gas compression costs. In addition, the slurry phase offers better control of the product selectivity at high conversion, and is well mixed and deviates towards isothermal operation (Subiranas 2009). On-line catalyst removal can be performed with ease in slurry phase reactor. Presently, a slurry phase reactor with a capacity of 17000 bpd utilizing a Fe-based catalyst is being operated by Sasol in Qatar (Davis, 2003; Dancuart & Steynberg, 2007; Subiranas, 2009).

Fluidized bed reactors have inherent advantage with higher heat transfer coefficients which is important due to the large amount of heat needed to be removed from the FT reactors, in order to control their temperature (Dancuart & Steynberg, 2007). Two-phase fluidized bed reactors are preferred for high-temperature FTS (Subiranas 2009). The Kellogg company was a leader in developing fluidized bed reactors, which were applied by Sasol in Sasolburg, Secunda and Mossel Bay (Synthol reactors) (Dancuart & Steynberg, 2007; Subiranas, 2009; Davis, 2003). According to Steynberg *et al.*, (2004), the only circulating fluidized bed reactors operating are those at Mossel Bay. The other Sasol reactors have been replaced by bubbling fluidized bed reactor with capacities between 11000 and 20000 bpd (Davis, 2003; Subiranas, 2009). In the circulating fluidized bed reactor the catalyst is swept up the reaction chamber by the preheated feed gas, while the inside-reactor fitted cyclones returns the bulk of any catalyst entrained in the gas to the standpipe. To achieve a high conversion rate it is necessary to have a high catalyst loading in the reaction chamber. However, the pressure drop over the reaction chamber must not exceed the pressure drop over the standpipe and online catalysts removal and addition of fresh catalyst is required (Subiranas, 2009).

2.1.6. Industrial Commercialization of FTS

Ruhrchemie AG was one of the companies that used a FT system in their production plant in Oberhausen, Germany in the 1930s (Leckel, 2010). In the 1950s Sasol integrated its HTFT and LTFT plant in Sasolburg, South Africa (Leckel, 2010) and have been modified and improved for current use (Subiranas, 2009; Narataruksa *et al.*, 2012; Davis, 2003; Dancuart & Steynberg, 2007). British Petroleum (BP) has a demonstration Nikiski plant (Alaska) in operation that utilizes FT technology at a scale up to 300 bpd (BP, 2013). In 2005, PetroSA began to produce about 35000 tons of FT fuels per year in a pilot plant located in Mossel Bay (Larsson, 2007).

2.2. Research development

Recent research has been directed to intensify the overall gas-to-liquid processes in terms of both reactor engineering and catalyst engineering (Sartipi *et al.*, 2013a). Reactor configuration is very promising to maximize the FTS efficiency by increasing the mass and heat transport properties of the process. On the other hand, studies are focused on formulating a catalyst that can couple FTS with hydrocarbon product upgrading reaction such as hydrocracking and isomerization (Sartipi *et al.*, 2013a). Below are some companies that have invested and devoted their work in developing the FTS technology and catalyst.

British Petroleum (BP) has been actively developing the Fischer-Tropsch (FT) Technology since 1981 and has invested about \$500 million to date (BP, 2013). In 1996, BP entered into collaboration with Johnson-Matthey Davy Technologies (JM Davy) to commercialize a fixed-bed FT process based on a BP cobalt-based catalyst (BP, 2013). They (BP & JM Davy) also developed a process, using a commercially available catalyst, to upgrade the products from the FT process to final products such as synthetic crude, diesel, kerosene and naphtha. According to BP (2013), they plan to continue to develop the FT technology by enhancing its performance via process and catalyst improvements and have programmes in place to test out new concepts and expect to continually incorporate further performance enhancement over time.

Zeolyst international, which is a global leader in zeolite catalyst production for petrochemical, refining and chemical industries, has made a commitment to Research and Development (R&D) with three fully equipped centers, each dedicated to a specific research area (Zeolyst, 2014). Shell Technology Centre, is a research Centre based in the Netherlands and focuses on catalyst development and detailed catalytic performance testing materials and other exploratory investigations. Philadelphia Quartz (PQ) corporation research and development centre in Pennsylvania deals with material modification, scale-up and new applications. Lastly Shell Technology center in Houston, Texas, USA also deals with catalyst development and performance of catalytic testing on materials (Zeolyst, 2014), other research development has been focused on various feedstock, reactor design and catalyst. Many oil companies such as Shell oil, Chevron (Texaco), and ExxonMobil have been conducting research that focus on the development of slurry-phase reactor technology (NETL, 2011) and have built and operated

several pilot plants in conjunction with the National Energy Technology Laboratory (NETL). One of their pilot plants is based in Laporte, Texas.

2.3. Synthetic Gas and Catalyst for Fischer-Tropsch Synthesis

To produce syngas, gasification or pyrolysis is applied to carbonaceous materials like coal, natural gas, waste and biomass (Hu *et al.*, 2012; Peres *et al.*, 2013), these materials serve as the feed to these processes and syngas is captured as the product.

2.3.1. Gasification and Pyrolysis

Gasification is a process that can be used to convert carbonaceous feedstock into a gas mixture which mostly contains carbon monoxide, hydrogen, carbon dioxide, nitrogen, and methane (Subiranas, 2009; Hu *et al.*, 2012). Various waste and biomass feedstock such as wood, used tyres, agricultural and municipal waste can be gasified to produce bio-syngas (Peres *et al.*, 2013; Hu *et al.*, 2012a; Yoon & Lee, 2012) and each type of feedstock possesses different properties. Understanding the types, sources and basic properties of biomass and waste, can serve as a foundation in using the materials in gasification technology. According to Hu *et al.*, (2012), a pre-treatment step of the feedstock before gasification is necessary, this step includes screening, size reduction and drying.

In most gasifiers, the feed materials have to withstand the gasifying agent flow rate with an appropriate size and waste. The feed particle size is often in the range of 20-80 mm (Hu *et al.*, 2012), while drying of the feed material, biomass in particular improves the efficiency of the gasifier. However, drying of the feed results in hydrogen reduction in the gas product, which is unfavorable in the subsequent Fischer-Tropsch synthesis step. The moisture content of the biomass feedstock can be reduced to about 10-20 % through drying (Hu *et al.*, 2012). Gasification process can employ different gasification agents such as air, oxygen rich air and /or steam, as well as various operating conditions (Subiranas, 2009; Hu *et al.*, 2012).

Gasifiers can be designed with different hydrodynamics, this includes the updraft fixed bed gasifier, downdraft fixed bed gasifier, and fluidized-bed gasifier which are widely used. In the updraft bed gasifier the feed is introduced at the top of the gasifier and falls downwards while the gasifying agent is fed at the bottom and flows upwards in the gasifier. The combustion happens at the bottom of the bed, while the gas product is released out of the gasifier at a temperature

around 500 °C (Hu *et al.*, 2012). In the downdraft fixed bed gasifier, both the carbon material feed and the gasifying agent moves downwards and the syngas product exit the process at a high temperature of about 800 °C (Hu *et al.*, 2012). In fluidized bed gasifier, the feed material is fed at the bottom of the gasifier and then fluidized using air, oxygen or any preferred gasifying agent. Such kind of gasifier can increase the reaction rate and conversion by enhancing the heat distribution during the gasification process (Hu *et al.*, 2012). Besides gasification, pyrolysis of carbonaceous materials can be applied in order to produce syngas.

Pyrolysis is a process involving direct thermal decomposition of the feed material in the absence of oxygen at a moderate temperature range of about 400 – 800 °C (Hu *et al.*, 2012). The products from this process are mainly gas, liquid and solid char, while their proportion and composition depends on the pyrolysis method employed and properties of the feed material (Hu *et al.*, 2012).

2.3.2. FTS Catalyst

According to All *et al.*, (1995) numerous studies on Fischer-Tropsch commercial or conventional catalyst such as Co, Ni, Fe and Pd supported on SiO₂, Al₂O₃ and TiO₂ have been studied. These catalysts may be designed to include promoters such as Zirconium (All *et al.*, 1995), Ruthenium (Kangvansura *et al.*, 2013), Zinc-Oxide (Dagle *et al.*, 2014) and Manganese (Liu *et al.*, 2009), to facilitate the active-metal reduction, preferably cobalt and interact with the support, thereby generating a high active metal surface sites to participate in the FTS reaction. However cobalt phase distribution changes during on stream reaction because the cobalt catalyst agglomerates and sinters when exposed to high temperatures.

Thus different supports have been used in order to disperse the Co metal particles and reduce sintering while improving stability and activity of the cobalt catalyst, of which the product selectivities are closely related to the state of the metal and type of the catalyst support. Sandra Bessell, (1993), studied the effect of catalyst support on the cobalt-based catalyst; the support material focus was on kieselguhr, silica, alumina and four different zeolites including ZSM-5 were also used. These supported catalysts were examined for their activities and product selectivities of which it was concluded that zeolites supports are more preferred for gasoline production due to their acidic sites and ability to withstand high temperature. In addition, zeolite supports offer high surface as opposed to kieselguhr, silica, and alumina. These types of catalyst

with both metallic sites and acidic sites are hybrid-catalysts commonly known as bi-functional catalyst (Kang *et al.*, 2014).

Bi-functional catalyst is prepared with two components, one with acid sites, as the acidic component and the other with metal sites, as the metallic component (Oar-arteta *et al.*, 2014). The use of H-ZSM-5 zeolite, as an acidic site in the FT catalyst has been noted to improve both selectivity and quality of the products. However, the metallic component of the bi-functional catalyst can be deactivated due to coke deposition (Oar-arteta *et al.* 2014). In addition and according to Pour *et al.*, (2009) the zeolite acidity can decrease as a result of transformation of active surface carbon species and or active iron carbide to inactive carbon or carbide forms which causes fouling or poisoning on the catalyst surface. Deposition of coke and transformation of active carbide forms to inactive phase can be increased by operating at high temperatures (Oar-arteta *et al.*, 2014) and it was found that coke formation on the H-ZSM-5 zeolite enhances the selectivity of certain products such as *p*-diethyl-benzene and *p*-xylene (Pour *et al.*, 2009) which will be unfavorable if gasoline and diesel range products are targeted.

Cobalt and Iron are the two metals that are industrially employed as commercial FTS catalyst, and both are suitable to catalyze FTS reactions at low temperature with cobalt being more preferred over Iron (Sartipi *et al.*, 2013a). Cobalt and Iron are proposed as the metallic component (Sartipi *et al.*, 2013a) while zeolites are proposed as the acidic component in order to promote hydrolysis reaction at LTFT system (Oar-arteta *et al.*, 2014). Sartipi *et al.*, (2013a) studied two configuration of cobalt catalyst as the metallic component on H-ZSM-5, of which one is cobalt supported on the H-ZSM-5 (see Bessell, 1993; Cheng *et al.*, 2012) and the other, the H-ZSM-5 is coated with cobalt (see Huang *et al.*, 2011; Li *et al.*, 2012). In their studies the cobalt supported on H-ZSM-5 was determined to be more effective for direct production of liquid fuel when compared to H-ZSM-5 coated with cobalt catalyst (Sartipi *et al.*, 2013a).

In this research, the cobalt supported on H-ZSM-5 configuration was employed and utilized as the bi-functional catalyst, this catalyst was synthesized and its performance studied for the direct conversion of liquid fuel via the Fischer-Tropsch Synthesis. In addition of operating conditions and CO₂ co-feeding on the performance of the catalyst was studied.

2.3.3. Synthesis of Fischer-Tropsch Catalyst

This section outlines the synthesis of Co-based catalyst on different supports that can be used in FTS, with resulting different Cobalt weight percentage (wt. %) for each support.

a) Synthesis of Co/SiO₂

Guo *et al.*, (2013), prepared a Co-based catalyst supported on SiO₂ by the impregnation method, with an expected theoretical loading of about 20 wt. % of the Cobalt metal. Cobalt (II) nitrate Hexahydrate was dissolved in 5 ml of deionized water and 4 g of the support was impregnated with the solution. After aging for 12 hours, the samples were dried in a vacuum oven at 110 °C for 12 hrs, thereafter calcined at 550 °C for 6 h with a heating rate of 2 °C/min.

b) Synthesis of Co/Al₂O₃

To prepare Co/Al₂O₃ FTS catalyst, Zhang et al., (2007) used incipient wetness impregnation method of a cobalt solution on the support. Commercial γ -Al₂O₃ was used as the support to prepare the catalyst and preheated at 500 °C for 2 hrs, in the presence of air. Cobalt nitrate solution was impregnated on the preheated support thereafter calcined at 400 °C for 6 hrs, to obtain Co/Al₂O₃ catalyst with 12 wt. % of metallic cobalt as the final FTS catalyst.

c) Synthesis of Co/H-ZSM-5

Sartipi *et al.*, (2013b) used a commercial ammonium form of zeolite (ZSM-5) to prepare Co/HZSM-5. The ZSM-5 was calcined at 550 °C for 5hrs to obtain H-ZSM-5, before impregnation the support samples were dried overnight for 12 hrs at 120 °C. Cobalt solution was prepared by dissolving Cobalt (II) Nitrate hexahydrate in deionized water, the zeolite supports were then impregnated by the cobalt solution using incipient wetness impregnation method. The samples were kept in a desiccator overnight, thereafter dried for 12 hrs at 120 °C to remove moisture, followed by calcination at 400 °C for 2 hrs to form Co/H-ZSM -5 catalyst with 10 wt. % of cobalt metal.

Besides the incipient-wetness impregnation method for loading the metal to the zeolite, Mohanty *et al.*, (2011) used the co-precipitation method, and the resulting metal solid was then mixed with the zeolite, then pelletized and crushed to desired particle size.

In this research, calcination of the ammonium form of ZSM-5 to H-form followed by incipient-wetness impregnation method of the cobalt (II) nitrate solution was employed as outlined in

Sartipi *et al.*, (2013b), For the commercial Co/SiO₂ catalyst , a modified version of the synthesis method reported in Guo *et al.*, (2013) was adopted.

2.4. Effect of Operating Conditions on Catalyst Performance

Marvast *et al.*, (2005) conducted a Fischer-Tropsch reaction in a fixed bed reactor packed with a bifunctional Fe/H-ZSM-5 catalyst to produce a range of gasoline products. The optimum conditions were determined to be 300 °C, 17 bar with a gas feed ratio of H₂/CO = 0.96. The high temperature was selected due to the fact that at low temperature, the acidic sites of the catalyst are not completely active (Marvast *et al.*, 2005) and Iron is more preferable at higher temperatures. In support of the use of high temperature, Egiebor *et al.*, (1984) stated that as the temperature is increased the degree for the branching and aroma-city of the products is increased, resulting to an enhanced octane number products. However, increasing the H₂/CO ratio would result in temperature run off in the reactor, resulting in the production of coke, which becomes deposited on the catalyst surface (Marvast *et al.*, 2005). While Oar-arteta *et al.*, (2014) and Pour *et al.*, (2009) discussed coke deposition as a cause for the loss of catalyst activity and selectivity, some authors (Botes, 2005; Rao & Gormley, 1990) claim that more rapid loss is due to the potassium migration away from the Fe catalyst to the H-ZSM-5 zeolite, resulting in the decrease of the CO conversion and a shift towards a more lighter FT products such as methane (Shah, 2011).

In this research, the Fischer-Tropsch synthesis was conducted in a fixed-bed reactor (FIXBR) packed with a bi-functional Co/H-ZSM-5 catalyst to produce liquid fuel. The Fischer-Tropsch process was conducted at LTFT process, thus a reaction temperature of 220 °C and 250 °C with a pressure range of 2-20 bar were used. Effect of these operating variables and CO₂ co-feeding on the catalyst performance was also evaluated.

2.5. Characterization of FTS Catalysts

Various catalyst characterization techniques can be applied depending on the properties of the material under study. This includes physical and chemical properties in an atomic or molecular dimension of the material. Through characterization, material crystallinity, morphology, adsorption and temperature behavior can be studied at different conditions.

For example, Wang *et al.*, (2004) used a computer-automated powder X-Ray Diffraction (XRD) analysis with Cu-K α radiation to identify crystallinity and various phases present within the Cobalt-Zeolite catalyst. Similarly Kang *et al.*, (2014) used an XRD equipment equipped with Cu-K α radiation, while Sartipi *et al.*, (2013b) used a monochromatic Co-K α radiation to determine the crystallinity of the zeolite supported cobalt catalyst.

To determine the zeolite acidity, Kang *et al.*, (2014) and Sartipi *et al.*, (2013b) used a Temperature-Programmed Ammonia desorption (NH₃-TPD) analysis, while Wang *et al.*, (2004) used a Fourier-Transform-Infrared-Spectroscopy (FTIR) analysis. For thermal analysis, thus how the catalyst mass changes with increasing temperature, Sartipi *et al.*, (2013b) used a Temperature-Gravimetric Analysis (TGA) method, while Wang *et al.*, (2004) used a Thermogravimetric-Differential-Thermal Analysis (TG-DTA) and Kang *et al.*, (2014) did not study catalyst thermal properties.

Brunauer–Emmett–Teller (BET) surface area, pore size and volume were determined by N₂-adsorption isotherms at a temperature of 77 K by both authors listed above. To define reducibility conditions of the zeolite supported metal-oxide, Kang *et al.*, (2014) and Sartipi *et al.*, (2013b) used a Temperature-Programmed-Reduction (TPR) analysis in a hydrogen rich environment. To determine the morphology of the catalyst, Wang *et al.*, (2004) used a Scanning-Electron-Microscopy (SEM). For surface metal, carbon species and electron states of the spent catalyst, Kang *et al.*, (2014) used X-Ray Photoelectron Spectroscopy (XPS), and for elemental analysis Inductively-Coupled-Plasma-Optical-Emission-Spectroscopy (ICP-OES) was utilized by Sartipi *et al.*, (2013b). In addition morphological, compositional and crystallographic information by utilizing material electron energies was, determined by Transmission-Electron-Microscopy (TEM) using a carbon coated Cu-grid (Sartipi *et al.*, 2013b).

For this research, all characterization techniques used by Sartipi *et al.*, (2013b) were employed excluding elemental analysis by ICP-OES, of which was replaced by using an Energy-Dispersion-Spectroscopy (EDS) to determine the elemental composition of the catalytic material.

2.6. Conventional and Synthetic Diesel Fuel

Diesel fuel and other petroleum products are manufactured, traditionally by refining crude oil. However these products can also be produced synthetically from various carbon containing

materials such as coal, biomass, natural or synthetic gas through the FTS process (Larsson, 2007; Riazi, 2005). Conventional Diesel can be produced from crude oil through catalytic cracking or from the Fischer-Tropsch process through coal gasification and Gas-to-Liquids process. Diesel fuel consists of carbon numbers between C₁₁ to C₁₆ and has a boiling point range of about 205 °C to 290 °C (Riazi, 2005). The main use of diesel fuel is for transportation such as rail, shipping and on-road vehicles such as trucks and buses. Table 2.5 shows the comparison of diesel produced via Fischer-Tropsch synthesis to petroleum derived diesel (conventional diesel).

Table 2.5: Specification of FT-Diesel in comparison to conventional diesel, adapted from Laohalidanond *et al.*, 2006)

Fuel Specifications	FT-Diesel	Conventional Diesel
Chemical Formula	Paraffin	C ₁₂ H ₂₆
Molecular Weight (kg/Kmol)	—	170-200
cetane number	> 74	50
Density (kg/l) @ 15 °C	0.78	0.84
Lower heating value (MJ/kg) @ 15 °C	44	42.7
Lower heating value (MJ/l) @ 15 °C	34.3	35.7
Oxygen content (%wt)	≈ 0	0-0.6
Kinetmatic viscosity (mm ² /sec) @ 20 °C	3.57	4
Flash Point (°C)	72	77
Sulphur content (%wt)	< 0.0001	< 0.25

Advantages of synthetic FT-diesel are that they are high quality and ultra clean transportation fuel with very low sulphur content and aromatic compounds (Laohalidanond *et al.*, 2006; Larsson, 2007; States & Agency, 1998). In addition, the FT-diesel can be directly used in existing automobiles and machinery without any adaptations or modification (Laohalidanond *et al.*, 2006).

From the economic point of view, Laohalidanond *et al.*, (2006) stated that, synthetic diesel can compete with conventional diesel in the near future, because of the high crude oil prices. Production cost in Rands (R), of FT-diesel is about R4.42-6.41 per litre whereas the crude oil price is about R5.45 per litre and is predicted that the crude oil price might reach R7.43 per litre in the near future (Laohalidanond *et al.*, 2006). In addition, Larsson (2007) mentioned that for synthetic fuels to be more competitive with petroleum-based fuels, the price of crude oil must be

relatively high, and in countries like Sweden, in which there is a high availability of biomass, it is possible to produce bio-fuels in large quantities.

2.7. Summary and Future Outlook

With regard to Fischer-Tropsch Technology, it is possible to economically justify an investment, but in order to do so there must be a considerable difference in the price of carbon sources used as the feed material and the price of crude oil. Presence of cheap crude oil headed interest in investment in Fischer-Tropsch process. However according to De Klerk & Furimsky (2011), future interest in FTS will most likely be governed by either energy security or economy.

Ambitious targets set by politicians and Environment regulators, to substitute crude oil with renewable energy have stimulated research interest in upgrading and refining of biomass. Biomass refining is currently being studied and as a results attention has been focused on the catalysis of oxygenated conversion. This is expected to give rise in advanced catalyst development and results in benefits for the understanding of the Fischer Tropsch refining catalysis.

In order to make predictions about the future of Fischer-Tropsch syn-crude catalyst, it is useful to look into the past. There are about three aspects to consider, namely, development in catalysis, refining and Fischer-Tropsch Technology. These areas need to be developed simultaneously but not without some interdependence.

Dancuart & Steynberg (2007) and Subiranas (2009) suggested the use of Co-based catalyst at low-temperature Fischer Tropsch Synthesis over the use of a Fe-based catalyst; due to its selectivity, activity and that it produces a wider range of products at low temperature than at high temperature Fischer-Tropsch (Sartipi *et al.*, 2013a; Shah, 2011). Coupling the Fischer-Tropsch active metal (cobalt) with zeolites can increase the yield of diesel and gasoline above 30 and 40 %, respectively (Bessell, 1993). These could enable the possibility to overcome the Anderson-Schultz-Flory polymerization kinetics which in turn results in desired hydrocarbon products.

Companies such as Shell, BP, Johnson Davvy Technologies and Zeolyst International, have channeled their resources to developing and/or modifying the FTS technology including development of active metal catalyst. Currently, different catalyst and supports are being studied and investigated to increase the yield of liquid fuel via FTS.

In this research Co/H-ZSM-5 bi-functional catalyst was synthesized, characterized and its performance evaluated and compared to a commercial Co-based catalyst under similar operating conditions. In addition the effect of the operating variables, CO₂ co-feeding and different H₂/CO ratio, on the performance of the catalyst was studied as well. The results of the investigation revealed for the first time the effect of CO₂ co-feeding on the performance of Co/H-ZSM-5 catalyst.

2.8. References

- All S, Chen B, Goodwin Jr. J.G., 1995, Zr Promotion of Co/SiO₂ for Fischer-Tropsch Synthesis. *Journal of Catalysis*, 157(1), pp.35–41.
- Bessell S, 1993, Support effects in cobalt-based Fischer-Tropsch catalysis, *Applied catalysis A: General*, 96, pp.253–268.
- Botes F.G, 2005, The effect of a higher operating temperature on the Fischer-Tropsch/ HZSM-5 bifunctional process. *Applied Catalysis A: General*, 284(1-2), pp.21–29.
- BP, 2013. BP Fischer-Tropsch Technology. Available at: <http://www.bp.com/en/global/corporate/press/press-releases/bp-and-davy-select-three-leading-epc-contractors-for-fischer-tropsch-deployment.html> [Accessed August 5, 2014].
- Cheng K, Kang J, Huang S, You Z, Zhang Q, Ding J, Hua W, Lou Y, Deng W, Wang Y, 2012, Mesoporous beta zeolite-supported ruthenium nanoparticles for selective conversion of synthesis gas to C₅-C₁₁ isoparaffins. *ACS Catalysis*, 2(3), pp.441–449.
- Dagle R.A, Lizarazo-Adarme J.A, Dagle V.L, Gray M.J, White J.F, King D.L, Palo D.R, 2014, Syngas conversion to gasoline-range hydrocarbons over Pd/ZnO/Al₂O₃ and ZSM-5 composite catalyst system. *Fuel Processing Technology*, 123, pp.65–74. Available at: <http://dx.doi.org/10.1016/j.fuproc.2014.01.041>.
- Dancuart L.P, Steynberg A.P., 2007, Fischer-Tropsch based GTL technology: a new process? *Studies in Surface Science and Catalysis*, 163, pp.379–399.
- Davis B.H, 2003. Fischer-Tropsch Synthesis : Overview of Reactor Development and Future Potentialities. , *American Chemical Society, Division of Fuel Chemistry*, Volume 48, Issue

2, pp.787–790.

De Klerk A, 2011, Part I Introduction. In *Fischer-Tropsch Refining*. Wiley-VCH Verlag GmbH & Co, pp. 1–20.

De Klerk A, Furimsky E, 2011, Fischer – Tropsch Syncrude ”, *Platinum Metals Review*, Vol. 55 (4), pp.263–267.

Egiebor N.O, Ungar K, Wojciechowski B, 1984, A classification of fischer–tropsch synthesis product distributions, *The Canadian Journal of Chemical Engineering*, 62(3), pp.425–430.

Fornasari G, La Torreta T.M.G, Vaccari A, Bednarova S, Jiru P, Tvaruzkova Z, 1991, Fischer-Tropsch Synthesis On Zeolite Supported Cobalt Catalysts, *Natural Gas Conversion* , pp.333–339.

Golodets G.I, Kazachkov S.G, Chaschenikova I.T, Vorotyntsev V.M, 1989, High-Pressure Fischer-Tropsch Synthesis On A Cobalt-Titanium Dioxide Catalyst , *Petro. Chem. U.S.S.R*, Vol 29 (2), pp.369–373.

Guo C, Wu Y, Zhan J, 2013. Study on bimodal mesoporous Co/SiO₂ catalysts for the Fischer-Tropsch synthesis. *Reaction Kinetics, Mechanisms and Catalysis*, 109(2), pp.497–508.

Hassanpour S, Taghizadeh M, Yaripour F, 2010. Preparation, characterization, and activity evaluation of H-ZSM-5 catalysts in vapor-phase methanol dehydration to dimethyl ether. *Industrial and Engineering Chemistry Research*, 49(9), pp.4063–4069.

Hu J, Yu F, Lu Y, 2012, Application of Fischer–Tropsch Synthesis in Biomass to Liquid Conversion. *Catalysts*, 2(2), pp.303–326.

Huang X, Hou B, Wang J, Li D, Jia L, Chen J, Sun Y, 2011, CoZr / H-ZSM-5 hybrid catalysts for synthesis of gasoline-range isoparaffins from syngas. “*Applied Catalysis A, General*”, 408(1-2), pp.38–46. Available at: <http://dx.doi.org/10.1016/j.apcata.2011.09.004>.

Kang SH, Ryu JH, Kim JH, Kim HS, Lee CG, LEE YJ, Jun KW, 2014, Fischer-Tropsch Synthesis of the Promoted Co / ZSM-5 Hybrid Catalysts for the Production of Gasoline Range Hydrocarbons, *Modern Research in Catalysis* (3), pp.99–106.

- Kangvansura P, Poo-arporn Y, Schulz H, Worayingyong A, 2013, The Effect of Promoters on Reduction of Ru / ZrO₂ / Co / SiO₂ Catalyst for Fischer-Tropsch Synthesis as Studied by in situ XANES, *CTSI-Cleantech* (3), pp.310–313.
- Kreutz T.G, Larson E.D, Liu G, Williams R.H, 2008. Fischer-Tropsch Fuels from Coal and Biomass. *25th Annual International Pittsburgh Coal Conference*, Princeton Environmental Institute, Princeton University, Pittsburgh Pennsylvania, 29 Sept-2 Oct, pp.1–81.
- Laohalidanond K, Heil J, Wirtgen C, 2006, the Production of Synthetic Diesel From Biomass. *Agricultural Economics*, 6(1), pp.35–45.
- Larsson M, 2007. An Experimental Study of Fischer-Tropsch Fuels in a Diesel Engine, Thesis of Licentiate of Engineering, Department of Applied Mechanics, Chalmers University of Technology.
- Liu Y, Hanaoka T, Miyazawa T, Murata K, Okabe K, Sakanishi K, 2009, Fischer – Tropsch synthesis in slurry-phase reactors over Mn- and Zr-modified Co / SiO₂ catalysts, *Fuel Processing Technology*, 90, pp.901–908.
- Marvast M.A, Sohrabi M, Zarrinpashne S, Baghmisheh G, 2005, Fischer-Tropsch synthesis: Modeling and performance study for Fe-HZSM5 bifunctional catalyst. *Chemical Engineering and Technology*, 28(1), pp.78–86.
- Mitchell L, Gonzalez-Santiago B, Mowat J.P.S, Gunn M.E, Williamson P, Acerbi N, Clarke M.L, Wright P.A, , 2013, Remarkable Lewis acid catalytic performance of the scandium trimesate metal organic framework MIL-100(Sc) for C–C and C–N bond-forming reactions. *Catalysis Science & Technology*, pp.606–617.
- Mohanty P, Pant K.K, Parikh J, Sharma D.K, 2011. Liquid fuel production from syngas using bifunctional CuO-CoO-Cr₂O₃ catalyst mixed with MFI zeolite. *Fuel Processing Technology*, 92(3), pp.600–608. Available at: <http://dx.doi.org/10.1016/j.fuproc.2010.11.017>.
- Narataruksa P, Tungkamani S, Pana-Suppamassadu K, Keeratiwintakorn P, Nivitchanyong S, Hunpinyo P, Sukkathanyawat H, Jiamrittingwong P, Nopparat V, 2012, Conversion enhancement of tubular fixed-bed reactor for Fischer-Tropsch synthesis using static mixer.

- Journal of Natural Gas Chemistry*, 21(4), pp.435–444. Available at:
[http://dx.doi.org/10.1016/S1003-9953\(11\)60388-5](http://dx.doi.org/10.1016/S1003-9953(11)60388-5).
- Oar-arteta L, Gayubo A.G, Vicente J, Erena J, Azkoiti M.J, Olazar M, Bilbao J, 2014, Causes of deactivation of bifunctional catalysts made up of in DME steam reforming., *Applied Catalysis A : General*, 483, pp.76–84.
- Peres A.P.G, Lunelli B, Filho R.M, 2013, Application of Biomass to Hydrogen and Syngas Production, *Chemical Engineering Transactions* , 32(2011), pp.589–594.
- Pour A.L, Zare M, Shahri Kamali S.M, Zamani Y, Alaei M.R, 2009, Catalytic behaviors of bifunctional Fe-HZSM-5 catalyst in Fischer-Tropsch synthesis, *Journal of Natural Gas Science and Engineering*, 1(6), pp.183–189. Available at:
<http://dx.doi.org/10.1016/j.jngse.2009.11.003>.
- Rao V.U.S, Gormley R.J, 1990, Bifunctional catalysis in Syngas Conversion, Elsevier Science Publishers, Pittsburg , pp.207–234.
- Riazi, M.R, 2005, Characterization and Properties of Petroleum Fractions. *ASTM International Standards Worldwide*, 1st edition, pp.1–435.
- Sartipi S, van Dijk J.E., Kapteijn F, 2013a, Applied Catalysis A : General Toward bifunctional catalysts for the direct conversion of syngas to gasoline range hydrocarbons : H-ZSM-5 coated Co versus H-ZSM-5 supported Co. “*Applied Catalysis A, General*”, 456, pp.11–22. Available at: <http://dx.doi.org/10.1016/j.apcata.2013.02.012>.
- Sartipi S, Parashar K, Makkee M, Gascon J, Kapteijn F, 2013b, Breaking the Fischer–Tropsch synthesis selectivity: direct conversion of syngas to gasoline over hierarchical Co/H-ZSM-5 catalysts. *Catalysis Science & Technology*, 3(3), p.572. Available at:
<http://xlink.rsc.org/?DOI=c2cy20744c>.
- Shah R, 2011. *Zeolite-Modified Fischer-Tropsch Synthesis*, Msc Thesis, University of Cape Town, South Africa
- Silva, V.J, Rodrigues J.J, Soares R.R, Napolitano M.N, Rodrigues M.G.F, 2013, Cobalt Supported on Zsm-5 Zeolite Using Kaolin As Silicon and Aluminum Sources for Fischer-

- Tropsch Synthesis. *Brazilian Journal of Petroleum and Gas*, 7(2), pp.83–94. Available at: <http://www.portalabpg.org.br/bjpg/index.php/bjpg/article/view/303>.
- States & Agency, 1998. Conversion of Coal Mine Methane into Synthetic Fuel (C o c m m i s f), United States Environmental Protection Agency, Air and Radiatin 6202J
- Steynberg A. P, Dry M.E, Davis, M.E, 2004, Fischer-Tropsch Technology, Studies in Surface Science and catalysis ,152,Elsevier, p.722. Available at: <http://books.google.com/books?hl=en&lr=&id=gJfVfbd1Bd0C&pgis=1>.
- SubiranasA.M, 2009. *Combining Fischer-Tropsch Synthesis (FTS) and Hydrocarbon Reactions in one Reactor*, Dissertation Universität Karlsruhe (TH), Fakultät für Chemieingenieurwesen und Verfahrenstechnik, Available at: <http://d-nb.info/1013721381/34>.
- Todic B, Olewski T, Nikoacevic N, Bukur D.B, 2013, Modeling of fischer-tropsch product distribution over Fe-based catalyst. *Chemical Engineering Transactions*, 32(2007), pp.793–798.
- Wang B, Gao Q, Gao J, Ji D, Wang X, Suo J, 2004, Synthesis , characterization and catalytic C4 alkene cracking properties of zeolite ZSM-23, *Applied Catalysisd A: General* ,Vol.274, pp.167–172.
- Wu J, Fang Y, Wang Y,Zhang D-K, 2005, Combined coal gasification and methane reforming for production of syngas in a fluidized-bed reactor, *Energy and Fuels*, 19(2), pp.512–516.
- Yoon S.J, Lee, J.G, 2012. Hydrogen-rich syngas production through coal and charcoal gasification using microwave steam and air plasma torch. *International Journal of Hydrogen Energy*, 37(22), pp.17093–17100. Available at: <http://dx.doi.org/10.1016/j.ijhydene.2012.08.054>.
- Zeolyst, 2014, About Zeolyst, Zeolyst International. Available at: <http://www.zeolyst.com/home.aspx> [Accessed August 1, 2014].

CHAPTER 3: EXPERIMENTAL PROCEDURE

3.1. Introduction

In this chapter information about materials and the methods employed in this study is provided. These techniques were used to obtain the results reported in Chapter 4, Chapter 5 and Chapter 6.

For characterization of the catalyst, the techniques used include N₂ Physisorption to obtain the Brunauer-Emmet-Teller analysis (BET) surface area, pore volume and pore size of the catalyst and the support before and after catalyst preparation. An X-ray analysis was conducted using a Bruker D2 phaser equipped with a Lynxeye detector and a Co-K α radiation ($\lambda=1.79026 \text{ \AA}$) at 30 kV, to obtain the diffraction patterns of the catalyst crystallinity, structure and composition. Scanning Electron Microscopy (SEM) coupled with an Energy Dispersion Spectroscopy (EDS) was used to check the morphology and elemental composition of the catalyst and the supports. For thermal properties of the catalyst, Thermal Gravimetric Analysis (TGA) was used.

Lastly but not the least, Transmission Electron Microscopy (TEM) technique was performed to check the distribution of Co within H-ZSM-5. The building of the FIXBR reactor set-up used in this study is presented as well. In addition, the catalyst activation or reduction conditions that have been obtained from the Temperature-Programmed Reduction (TPR) analysis are outlined in detail. The method used to calibrate the Gas Chromatograph used in the analysis of the feed and the product streams from the reactor is explained in detail as well.

3.2. Materials

Cobalt (II) Nitrate-Hexahydrate (Co(NO₃)₂.6H₂O) was purchased from Sigma-Aldrich and used as the source of Cobalt (Co) metal. Ammonium form of Zeolite Socony-Mobil-5 (ZSM-5) was used as the support and calcined to obtain H-form of zeolite (H-ZSM-5). Syngas (mixture of H₂, CO and N₂ as the inert gas), Nitrogen (N₂), Argon (Ar), Hydrogen (H₂) gas and Air were purchased from Afrox (see images Figure C.1 (a) in Appendix C) and used for the Fischer-Tropsch Synthesis reaction. Cobalt-Silicon-dioxide (Co/SiO₂) was prepared and used as the benchmark catalyst.

3.3. Physicochemical Characterization of the Catalyst

3.3.1. N₂ Physisorption

Nitrogen physisorption was performed on about 0.2 g of the catalyst sample to determine the adsorptive properties of the catalyst as well as the surface areas, pore size and volume, the analysis was performed at 77 K by using N₂ as the adsorbate. Nitrogen physisorption experiment was carried out on ZSM-5, H-ZSM-5, Co/H-ZSM-5_1 and Co/H-ZSM-5 samples using Micromeritics TriStar 3000 V6.05 A. The samples were degassed at 150 °C before nitrogen adsorption experiment. The physisorption experiment using Nitrogen were conducted at the conditions shown in Table 3.1.

Table 3.1: N₂ Physisorption Analysis Conditions and Adsorptive Properties

Analysis Conditions		
Temperature:	-195.800 °C	77.35 K
Measurement interval:	120 min	2 hrs.
Adsorptive Properties		
Adsorbate:	Nitrogen	
Maximum manifold pressure:	1050.00 mmHg	
Non-ideality factor:	0.000062	
Density conversion factor:	0.0015468	
Molecular cross-sectional area:	0.162 nm ²	

3.3.2. X-Ray Diffraction (XRD) Analysis

The zeolite support samples namely ZSM-5, H-ZSM-5 and Co/H-ZSM-5 were analyzed by Bruker D2 phaser equipped with a Lynxeye detector at 30 kV. The XRD patterns were obtained by using a Co-K α radiation ($\lambda=1.79026$ Å) in 2 θ region between 10° and 90° with a step size of 0.027 °. The obtained 2 θ degree and intensity results were compared with the diffraction patterns from the International Zeolite Association (IZA) database (Baerlocher *et al.*, 2007) and Powder Diffraction File (PDF) cards from The American Mineralogists Crystal Structure Database (AMCSD) (Downs & Hall-Wallace, 2003) at the same wavelength.

3.3.3. Scanning Electron Microscopy (SEM) & Energy Dispersion Spectroscopy (EDS) Analysis

SEM-EDS analysis was performed by using Carl-Zeiss Sigma Field-Emission-Scanning-Electron-Microscope (FE-SEM), equipped with Oxford X-act Energy-Dispersion-Spectroscopy

(EDS) detector. The system was initially purged with Nitrogen gas for about 10 min to remove air and any other unwanted gases. SEM was used to obtain electron microscopic images of the samples, while EDS is used to determine the elemental composition of the sample. SEM-EDX detectors collect emitted electrons and photons by striking the sample surface with an electron beam and different elements emit electrons of different energies and thus resulting in a microscopic image and an elemental analysis spectrum of the material.

Before analysis, the samples were mounted on discs using a carbon tape, about 0.1 – 0.3 g of each sample was mounted. After mounting, excess amount of the samples was removed by an air dust spray. The samples were then coated with a one-layer-Gold-Palladium (Au-Pd) coating. After coating the samples were kept in closed container to avoid contamination by air. The samples were then analyzed by SEM/EDS less than an hour after coating.

3.3.4. Thermal Gravimetric Analysis (TGA)

Thermogravimetric analysis was performed on TA Instrument V20.9 Build 20 /SDT Q600 equipment using a Universal V4.7A data handling analysis software. About 10 – 11 mg in mass, of the catalyst samples were analyzed for their change in their mass while heated from 25 to 850 °C with a heating rate of 5 °C.min⁻¹ under 100 cm³.min⁻¹ air flow at Standard Temperature and Pressure (STP). This Thermogravimetric method of analysis used was adopted from (Sartipi *et al.*, 2013b), in order to determine the change of mass with respect to time.

3.3.5. Temperature-Programmed Reduction (TPR)

TPR analysis was performed on AutoChem II 2920 V3.05 in a Hydrogen rich environment. The Co/H-ZSM-5 catalyst sample was analyzed by using 5 % ratio of H₂/Ar gas mixture, at a flow of 30 ml/min from 20 °C to 900 °C and a temperature ramp of 8 °C/min. This H₂-TPR method used for the analysis was adopted from Wang *et al.*, (2000).

3.3.6. Transmission-Electron-Microscopy (TEM)

Transmission Electron Microscopy analysis was performed using JEOL 100S FEI spirit 120 kV equipment, originated from Field Electron and Ion (FEI) Corporate USA. This equipment was used to characterize the catalyst samples in order to view the metal location and internal structure morphology of the catalysts. About 0.1 mg of each representative support material and catalyst sample was ultra-sonicated in methanol for five minutes, before placing a drop of the solution in

a copper grid. The Cu-grid containing solution was ventilated and then fed into the TEM chamber for characterizations or analysis. The images were then observed and the magnification was varied using magnification knobs in order to achieve a clear micrograph. After photographing the desired image, the carbon grid was discharged from the equipment and the samples micrograph-images were then analyzed as outlined in section 4.3.7.

3.4. Reactor Design & Catalyst Loading

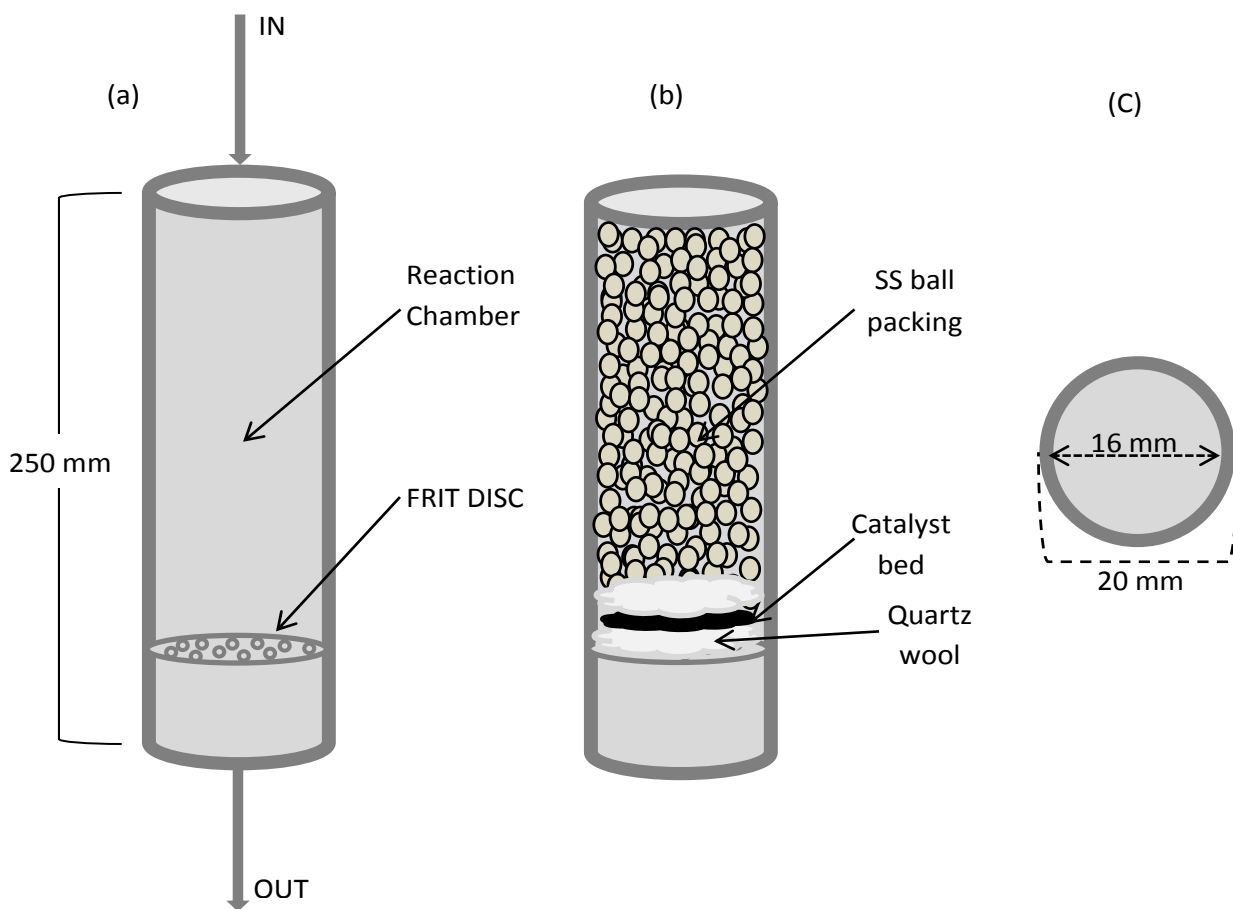


Figure 3.1: Schematic Diagram of Reactor Specifications

3.4.1. Reactor specification

Figure 3.1 depicts the schematic of the reactor configuration used in this study. The FTS reactor used was designed from stainless steel (SS) tubing and Swagelok fittings. The used reactor has a length (l) of 250 mm, internal diameter (ID) of 16 mm and an outer diameter (OD) of 20 mm as seen in Figure 3.1. An SS-1210-6-4 Swagelok stainless steel tube fitting, reducing union, 3/4 in. x 1/4 in. tube outer diameter was fitted to the reactor inlet and outlet which enables assembling

and disassembling of the reactor from the setup to load catalyst. A frit-disc with about 1-2 mm diameter holes was also fitted inside the reactor to support the catalyst and packing and to prevent the gas flowrate and pressure from blowing the catalyst out of the reactor into the tubings, which might result in tube blockages. Stainless steel (SS) ball packing of about 2-5mm was used as the reactor packing, for homogeneous heat conduction in the reactor as well as pre-heating the gas reactants prior in contact with the catalyst bed.

Before catalyst loading, the reactor was cleaned by blowing pressurized-air inside it by using an air-gun. This was done every time when loading the reactor. The SS-balls were cleaned by using an alcohol then drying them in an oven for about 20-30 minutes. After cleaning, the quartz wool was then placed on the frit-disc and ensured that it covers the whole disc surface area. Pre-weighed, 0.5 g of catalyst was loaded inside the reactor and sits on the quartz wool surface and ensured that it covered the whole surface, once the catalyst was placed inside the reactor another layer of quartz wool was placed on top of it; see Figure 3.1 for a schematic diagram. Then the whole reactor was filled with SS-balls with the thermocouple placed in the middle of the reactor and connected to a temperature controller in order to have accurate control of the reaction temperature. Once reactor was loaded, it was connected to the FTS apparatus and then pressurized. The experiment proceeded with the catalyst reduction as outlined in detail in section 3.6, if no leakages were detected.

3.5. Gas Chromatography

For the catalyst evaluation through FTS, online and offline GC analyses were used. For online GC analysis, a pre-calibrated GC equipped with a Thermal Conductivity Detector (TCD) was used to analyze inorganics (H_2 , CO, CO_2 and CH_4) and a GC equipped with a Flame Ionization Detector (FID) was used to analyze the organic (C_1 to C_x) in the feed and the product mixture. The offline GC was used to analyze wax, oil and water. See Figure C.1 (d), (e) and (g) in Appendix C for GC images and Figure C.1 and C.2 for TCD and FID peak signal respectively. Pre-calibration of the TCD was conducted by using syngas when the reactor is at room-temperature (also known as cold-condition) at a predefined pressure. For example if the reaction is to be conducted at a pressure of 8 bar by using a syngas ratio of 1.5 at any temperature, then the TCD would be calibrated at reactor-room-temperature using a syngas ratio of 8 bar and syngas of H_2/CO ratio of 1.5. Same applies for FID calibration only that a calibration gas is used

instead of syngas. For this study a calibration gas mixture of H₂, CO, N₂, CO₂, CH₄, C₂H₄ and C₂H₆ was purchased from Afrox and used for FID calibration. The rest of the calibration procedure such as GC oven temperature and tubing temperature set-point is as reported in section 5.2 in Chapter 5. The specifications of the GC used in this study are shown in Table 3.2.

Table 3.2: GC Properties & Specification

ONLINE GAS CHROMOTOGRAPH	
Detector	Thermal Conductivity Detector (TCD)
Column Specification	Packed, stainless Steel, 11.5m x 1/8"
Stationary Phase	Carboxen-1000, 60/80 mesh
Model	HP, Hewlett-Packard 5890
Detector	Flame Ionized Detector (FID)
Column Specification	Packed, stainless Steel, 2 m x 1/8"
Stationary Phase	Porapaq Q, 80-100 mesh
Model	Packard-Bell, GC model 433
OFFLINE GAS CHROMATOGRAPH	
Detector	Flame Ionized Detector (FID)
Column Specification	30m x 0.53mm x 5µm df
Stationary Phase	Zebtron, ZB-1
Model	Varian 3700

3.6. Catalyst Activation\Reduction

Before commencing with the FTS experiment, activation of the catalyst was performed by using hydrogen gas as the reducing agent. The catalyst activation method used by Sartipi *et al.*, (2013a) was adopted and modified for this project based on Temperature Programmed Reduction analysis results reported in section 4.3.6. Pre-weighed 0.5 g of fresh catalyst was placed inside the fixed bed Reactor (FIXBR) and activated in situ at 30 cm³ STP/min of H₂ gas flow and at 330 °C for 17-20 hrs at 8 bar, followed by cooling down to room temperature under the same H₂ flow. A rate of 2 °C/min was used for both cooling and heating steps.

3.7. Summary

The catalyst was prepared using incipient wetness impregnation method and the physico-chemical characterization of the support and the catalyst was done using SEM equipped with EDS, XRD and TEM. Detailed information about the catalyst loading in the reactor and catalyst

activation (in situ) before the FT reaction has been provided in this chapter. The results obtained from the above mentioned methods are discussed in Chapter 4 to Chapter 6.

3.8. References

- Baerlocher Ch, McCusker L.B, Database of Zeolite Structures: <http://www.iza-structure.org/databases/> , The collection pages are generated "on-the-fly" with programs written and assembled by Grosse-Kunstleve R.W. and Prokic S. The original data correspond to those given in the 4th edition of the Collection of Simulated XRD Powder Patterns for Zeolites by Treacy M.M.J. and Higgins J.B. Data for newly approved framework types have been added by Baerlocher Ch, Downs R.T, Hall-Wallace M, 2003. The American Mineralogist Crystal Structure Database, *American Mineralogists*, (88), pp.247–250.
- Sartipi S, van Dijk J.E., Kapteijn F, 2013a, Applied Catalysis A : General Toward bifunctional catalysts for the direct conversion of syngas to gasoline range hydrocarbons : H-ZSM-5 coated Co versus H-ZSM-5 supported Co. “*Applied Catalysis A, General*”, 456, pp.11–22. Available at: <http://dx.doi.org/10.1016/j.apcata.2013.02.012>.
- Sartipi S, Parashar K, Makkee M, Gascon J, Kapteijn F, 2013b, Breaking the Fischer–Tropsch synthesis selectivity: direct conversion of syngas to gasoline over hierarchical Co/H-ZSM-5 catalysts. *Catalysis Science & Technology*, 3(3), p.572. Available at: <http://xlink.rsc.org/?DOI=c2cy20744c>.
- Wang X, Chen H-Y, Sachtler W.M.H, 2000, Catalytic reduction of NO_x by hydrocarbons over Co / ZSM-5 catalysts prepared with different methods. *Applied Catalysis B: Environment*, Vol. 26, pp227-239

CHAPTER 4: SYNTHESIS AND CHARACTERIZATION OF CATALYST

4.1. Introduction

The results of the synthesis and characterization of the bi-functional catalyst are discussed and compared to literature in this chapter. The chapter starts off by stating the method for synthesis of the bi-functional catalyst. The transformation of the original ammonia form ZSM-5 zeolite to H-ZSM-5 form is also discussed. The characterization methods described in Chapter 3 were to obtain the results discussed in this Chapter.

4.2. Synthesis of the Bi-functional Co/H-ZSM-5 and the traditional Co/SiO₂ Catalyst

Ammonium form of zeolite (ZSM-5) with silicon to aluminium ratio of 40 (Si/Al = 40) was purchased from Zeolyst International in the USA, and then calcined to form the H-form of Zeolite (H-ZSM-5). The H-form of zeolite (H-ZSM-5) was obtained by calcination of the ammonium form of zeolite (ZSM-5), at 550 °C for 5 h in a furnace. The resulting H-ZSM-5 was used to prepare the catalyst.

The H-ZSM-5 support was dried overnight at 120 °C before impregnation. An aqueous solution of Cobalt (II) nitrate hexahydrate ($\text{Co}(\text{NO}_3)_2 \cdot 6\text{H}_2\text{O}$) was prepared using distilled water, thereafter incipient wetness impregnation of the solution on the support was applied, with an expected theoretical cobalt loading of 10 % by weight as stated by Sartipi *et al.*, (2013b). The zeolite impregnated with the solution (Co/H-ZSM-5_1) was kept overnight in a desiccator at room temperature then proceeded by drying at 120 °C for 12 h. The final bi-functional catalyst (Co/H-ZSM-5) was obtained by calcination of Co/H-ZSM-5_1 at 400 °C for 2 h. See Figure 4.1 for catalyst synthesis images, from the zeolite support to final catalyst transformation.

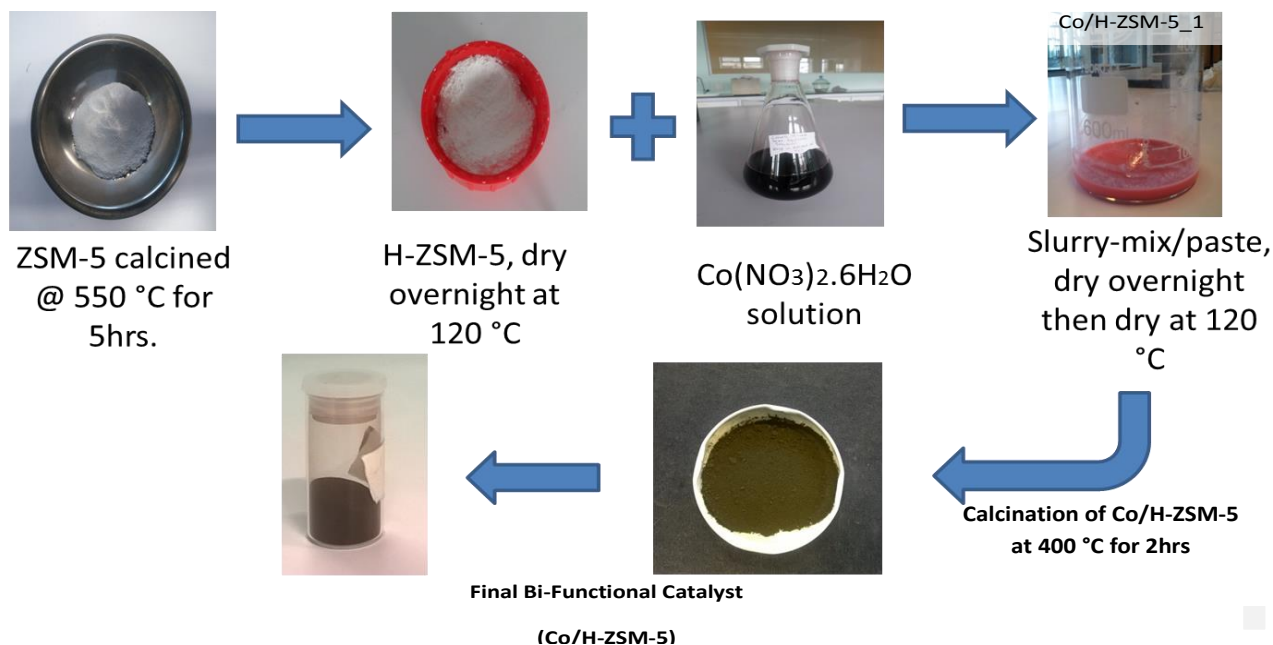


Figure 4.1: Bifunctional catalyst Synthesis procedure

As comparison Co/SiO₂ catalyst was with expected theoretical cobalt loading of 10 %. The Silicon-Dioxide support (SiO₂ ~99 % of composition) with a particle size of about 1-5 μm was purchased from Sigma Aldrich and was used to prepare Co/SiO₂ as the commercial catalyst. Method of synthesis used was adopted from Guo *et al.*, (2013) and modified. The method has been discussed in section 2.3.3 of this dissertation but a static oven was used instead of a vacuum oven.

4.3. Results and Discussion

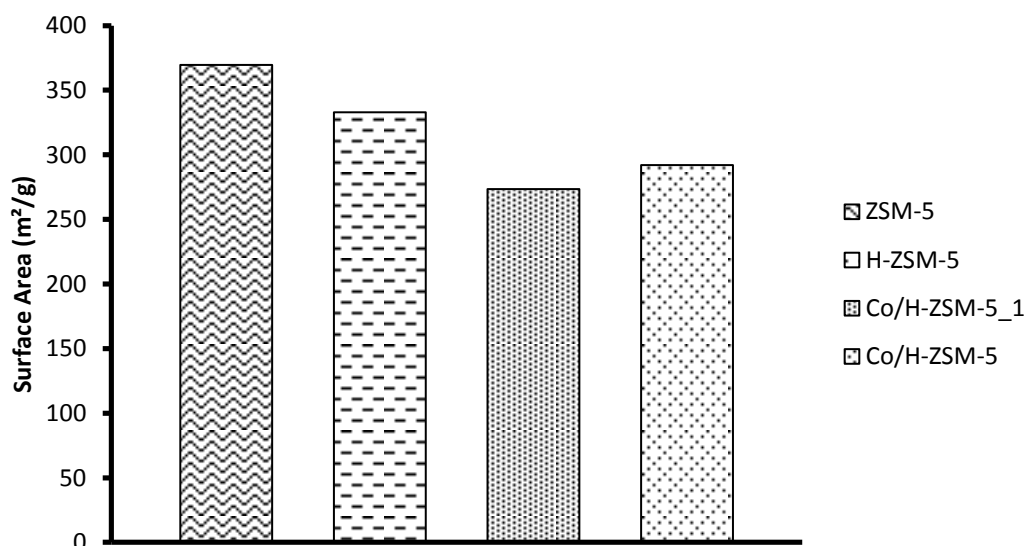
4.3.1. N₂ Physisorption

N₂ physisorption experiment was performed to obtain the adsorptive and surface property of the synthesized catalyst. Table 4.1, shows the difference in the total surface area, pore volume, and pore size of the synthesized zeolite samples, obtained from N₂ physisorption at 77 K, these results are also shown in Figure 4.2 to 4.4.

Table 4.1: Textural Properties of zeolite Samples

sample	Surface Area (m ² /g)	Pore Volume (cm ³ /g)	Pore Size (nm)
ZSM-5	369.543	0.24352	2.90199
H-ZSM-5	333.093	0.23125	3.03364
Co/H-ZSM-5_1	273.455	0.18846	2.95844
Co/H-ZSM-5	292.250	0.18846	2.82825

Zeolite as a fine powder is expected to have a higher total surface area, because fine or micro-porous solids can occupy more area of a surface. Sartipi *et al.*, (2013b), obtained the total surface area of zeolite to be in the range of 52 – 414 m²/g, with H-ZSM-5 having the least surface area of 52 m²/g, but from Table 4.1, the surface area of the synthesized zeolite supports are in the range of 273-369 m²/g with H-ZSM-5 having the lowest surface area of about 333 m²/g. These results are clearly shown in Figure 4.2.

**Figure 4.2: Surface Areas of the Support and the catalyst**

The significant difference between the surface area obtained by Sartipi *et al.* (2013b) and the synthesized zeolite supports as seen in Table 4.1 and/or Figure 4.2, could probably be due to the model in which they were obtained from, Sartipi *et al.* (2013b) used the t-plot model and for the synthesized zeolite samples and the BET model was used to determine the surface area.

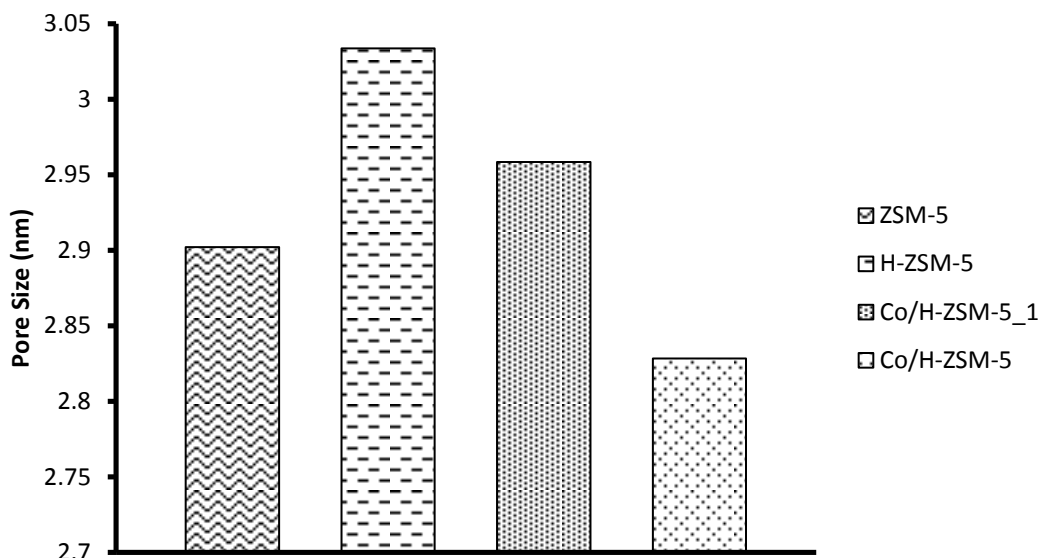


Figure 4.3: Pore size of the support and the catalyst

From Table 4.1 and Figure 4.3, the obtained pore sizes of the synthesized samples are in the range of 2.8 - 3 nm, while that obtained by Sartipi *et al.* (2013b) was in the range of about 4-8 nm. The difference in the pore volume could be due to the fact that Sartipi *et al.* (2013b) performed a desilication process on the support to remove silica, thereby changing the zeolite from micro-porous to meso-porous but no desilication was performed. According to Che & Védrine (2012), micro-porous solid possess a pore size of about 0.4 - 2 nm while meso-porous solids have pore sizes ranging from 2 -50 nm. From Table 4.1, it can be concluded that the synthesized zeolite samples are meso-porous, even though no desilication took place.

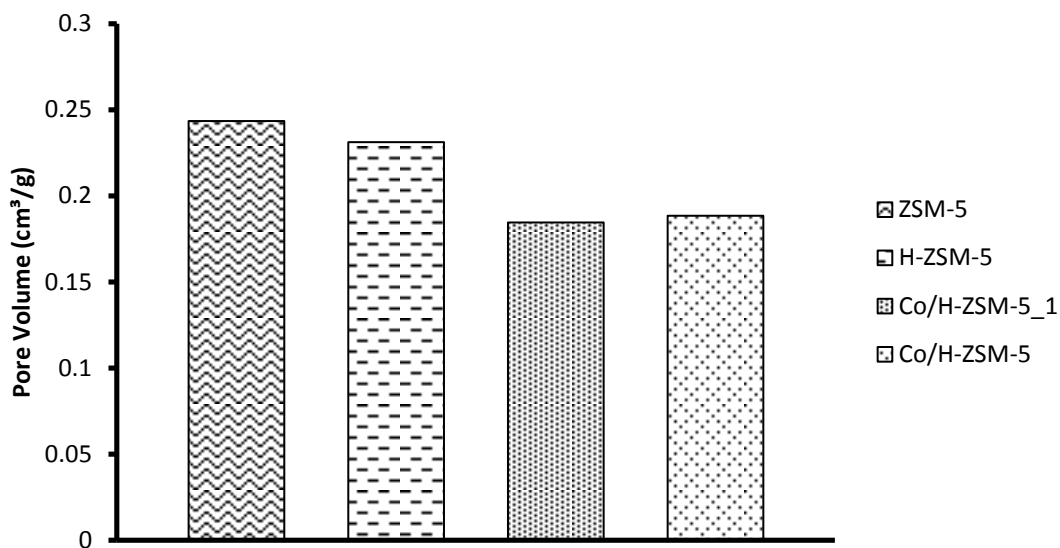


Figure 4.4: Pore Volume of the support and the catalyst

Calcination of ammonium form of zeolite (ZSM-5) at 550 °C, to form H-ZSM-5 resulted in an insignificant change in the pore volume of ZSM-5 to H-ZSM-5; same applies to calcination of Co/H-ZSM-5_1 at 400 °C to form Co/H-ZSM-5 final catalyst. However an enormous change in the pore volume that can be discussed in detail is between H-ZSM-5 support and Co/H-ZSM-5 catalyst. The H-form of zeolite (H-ZSM-5) had a pore volume of 0.231 cm³/g initially, before impregnation of the cobalt metal, while the final catalyst, Co/H-ZSM-5 had a pore volume of about 0.188 cm³/g as it can be seen from Table 4.1 and Figure 4.4. From this it can be anticipated that the decrease in the pore volume could be due to the Cobalt that was impregnated within the H-ZSM-5 zeolite support. In comparison to the pore volume in Table 4.1 and Figure 4.4, Sartipi *et al.* (2013b), obtained a pore volume which is in the range of 0.08 – 1.08 cm³/g, this difference could be due to desilication that was performed by Sartipi.

4.3.2. XRD Analysis

Figure 4.5, depicts the diffraction patterns of a simulated and synthesized zeolite samples. The simulated ZSM-5 and H-ZSM-5 diffraction pattern were obtained online from the International Zeolite Association Database (IZA). These patterns were used as a reference point for comparison with the obtained diffraction pattern from the XRD analysis of the zeolite materials under study i.e. ZSM-5, H-ZSM-5 and Co/H-ZSM-5. Other diffraction patterns, for the main elements that constitute zeolites such as, Silicon, Aluminium, Oxygen and the impregnated cobalt were also obtained online from The American Mineralogists Crystal Structure Database (AMCS) (Downs & Hall-Wallace, 2003). The diffraction pattern of the synthesized and analyzed H-ZSM-5 zeolite support corresponds well with that of the simulated H-ZSM-5 from the IZA database; same applies for ZSM-5 zeolite. The higher intensity peaks that are observed between 10 – 40 ° shows the crystallinity of ZSM-5, H-ZSM-5 and Co/H-ZSM-5 samples, at this point the samples are considered to be highly crystalline which might be due to silicon and aluminium present in this 2θ region.

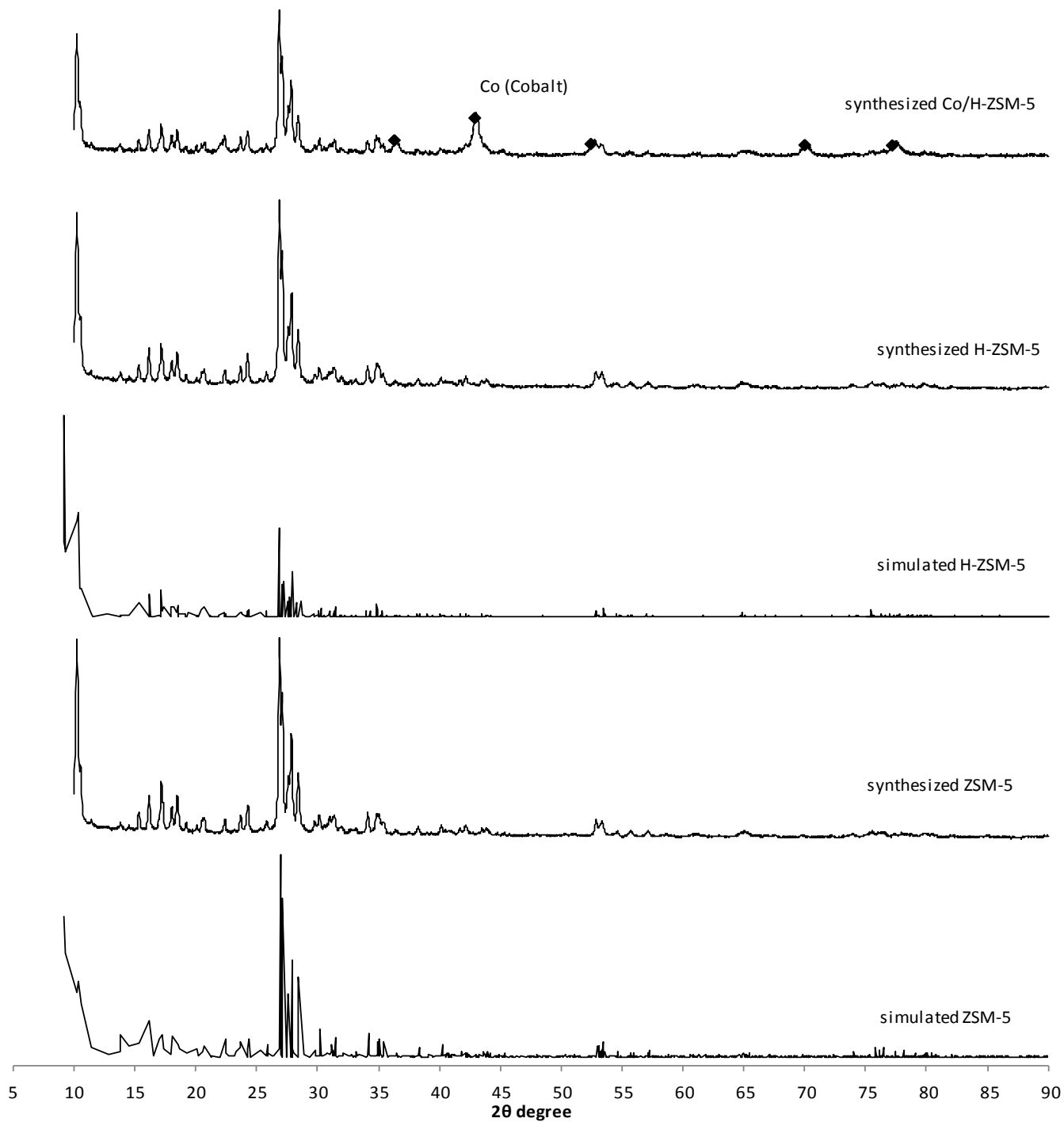


Figure 4.5: XRD Patterns of the Support and Synthesized Catalyst

According to Lu *et al.* (2003), ZSM-5 is known to have an MFI morphology and orthorhombic structure. Orthorhombic crystal structures possess Simple Cubic (SC), Body-Centred (BC) and Face Centred (FC) lattice symmetry (Smith, 2012; Che & Védrine, 2012). Applying the Bragg's law and Miller indices on the synthesized ZSM-5 peaks in Figure 4.5, resulted in an SC, BC and FC crystal systems of the synthesized zeolite support samples. Almost all of the ZSM-5 diffraction peaks are SC, some are either BC or FC. Having that stated, few of the diffraction peaks possess SC, BC and FC structure simultaneously. For example, the peak diffracted at $2\theta = 26.878^\circ$ which is the peak with the highest intensity in the synthesized ZSM-5 diffraction pattern in Figure 4.5, is both SC, BC and FC, and of all the studied ZSM-5 diffraction peaks, only 9 peaks had this property.

The presence of elemental constituent of the synthesized samples in Figure 4.5, was determined by comparing the diffraction peaks at each angle with an elemental PDF card obtained from AMCS database, provided the elements of the samples are known. Both the samples were found to consist of Silicon, Aluminium, Oxygen, Hydrogen, and Nitrogen elements. The quantity or composition of these elements was determined by a Scanning Electron Microscopy analysis coupled with Energy Dispersion X-ray (SEM/EDX) or Energy Dispersion Spectroscopy (SEM/EDS).

The presence of cobalt metal in Co/H-ZSM-5 is labelled by the black-diamond marker, as depicted in Figure 4.5. At an X-ray angle of 36.4 , 42.99 , 70.01 , and 77.51° there are no peaks diffracted for H-ZSM-5 sample, however after incipient wetness impregnation of the cobalt solution on H-ZSM-5, drying and calcination at 400°C for 2 h, the resulting catalyst (Co/H-ZSM-5) had peaks diffracted at the same angles, which proves that cobalt had been successfully impregnated in the zeolite support. In support of this, cobalt metal XRD database from the American Mineralogists Crystal Structure Database by Downs & Hall-Wallace was used, and it was expected to find cobalt at the same 2θ degrees as stated above. However at an angle of 52.73° the cobalt peak overlapped with a peak of another element. By using the Bragg's equation and the Miller indices of elements that constituents H-ZSM-5, it was noticed that the cobalt peak at 52.37° might have overlapped with an oxygen peak at the same X-ray angle. It is well known that cobalt metal would prefer oxygen over hydrogen, and the reaction of cobalt and oxygen is a

redox reaction in which the Cobalt is the oxidizing agent and oxygen will be the reducing agent, resulting in the formation of Cobalt (II)-Oxide.

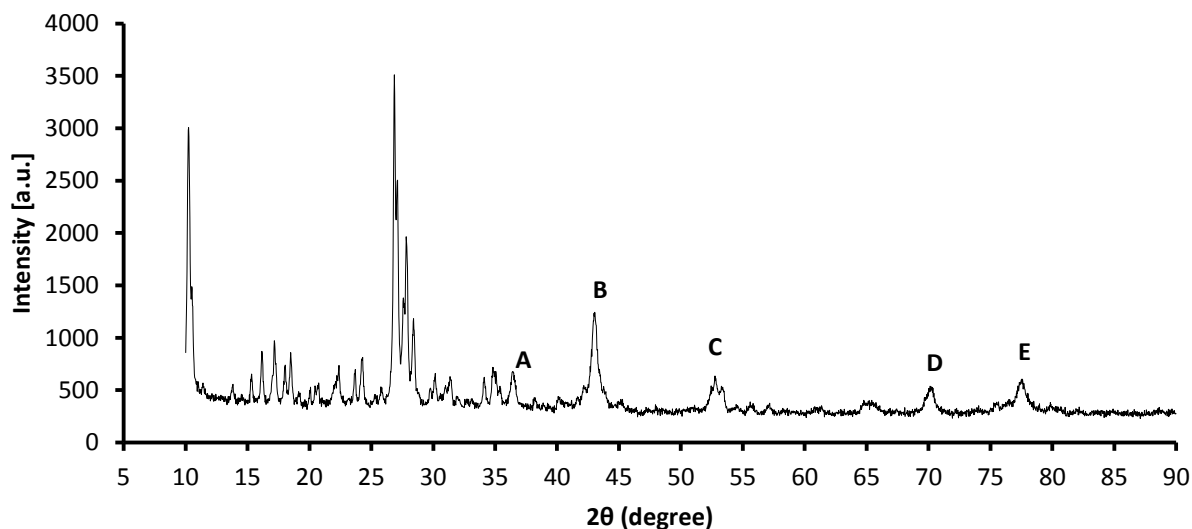


Figure 4.6: XRD Patterns of Co/H-ZSM-5 final catalyst

Figure 4.6, gives emphasized discussion on the simulated Co/H-ZSM-5 depicted in Figure 4.5. Other diffraction peaks of synthesized Co/H-ZSM-5 were observed at different X-ray angle when compared to synthesized H-ZSM-5 diffraction peaks in Figure 4.5, these peaks are labelled A-E. Reason arising to these peaks could be due to the presence of Cobalt that has been impregnated on the zeolite support as stated above. However the Crystal Structure of these peaks and their Miller indices are discussed in this section. Figure 4.6 is amplified in Table 4.2.

Table 4.2: Miller Indices and spacing of adjacent planes of cobalt metal

	Miller indices (hkl)	Spacing, d (Å)	Lattice System
A	100	2.460	SC,BC
B	100	2.099	SC
C	101	1.732	SC
D	111	1.337	SC, FC
E	002	1.229	SC, BC ,FC

From Table 4.2, it can be observed that the plane spacing increases from left to right on the labelled, A-E, diffraction peaks. The Miller indices obtained for peak A-E, and the spacing

between them (as seen in Table 4.2) corresponds to that of Cobalt metal diffraction peaks obtained from The American Mineralogists Crystal Structure Database (Downs & Hall-Wallace 2003). Therefore the labelled diffraction peaks in Figure 4.6, might be Cobalt metal that has attached itself to the H-ZSM-5 zeolite support after impregnation and calcination.

However, the Miller indices (111) obtained from peak (D), does not relate to any of the cobalt Miller indices from the Cobalt database, but at an X-ray angle when 2θ is between $70-75^\circ$ a Cobalt peak should be observed, so this brings to the conclusion that at peak D, the cobalt diffraction peak might have overlapped with a diffraction peak of other element(s) hence resulting in the Miller indices of (111), this element was determined to be oxygen, hence forming Cobalt-Oxide as stated above.

According to Bergström, (2013) and Wu, (2012), Cobalt is a Hexagonal-Closed-Pack (hcp) structure and becomes transformed to Face-Centred Cubic (FCC) at temperatures above 425°C . Since Co/H-ZSM-5 was obtained after calcination (at 400°C for 2hrs) of the impregnated zeolite sample with cobalt (II) hexahydrate solution, it is expected to have an FCC crystal structure; this can be supported by the results obtained in Table 4.2, with an emphasis on peak D and E.

4.3.3. SEM Analysis

Figure 4.7, depicts the micrographs of ammonium form of zeolite (ZSM-5) and H-form of zeolite (H-ZSM-5). In (a) the ZSM-5 sample image was captured at a scale of $10\ \mu\text{m}$ and 2000X magnification at signal of 10 kV and (b) at a scale of $1\ \mu\text{m}$. From Figure 4.7(a) and 4.7(b), the zeolite samples particle morphology was found to be, irregular-rounded and aggregated, thus no or little presence of voids in between the solid particles, this can be seen clearly in (b). The texture of both ZSM-5 and H-ZSM-5 is not smooth, or rather it is observed as a rough particle surface. Looking at (a) and (b) of Figure 4.7, it can be seen that (b) has more spread out, brighter contrast areas; one of the regions is circled and marked with an (X). The difference in contrast and brightness in (a) and (b) is due to the presence of Hydrogen ions (H^+) present in H-ZSM-5. The equipment used for EDX/EDS analysis does not detect electronegativities of lighter elements (in weight) like Hydrogen and Helium, which is a detector equipment limitation, however their existence can be confirmed by the change in contrast of the sample by becoming more brighter as seen in Figure 4.7(b), thus H-ZSM-5 contains Hydrogen ion which is observed by bright contrast of the sample image and hence the name H-form of zeolite (H-ZSM-5).

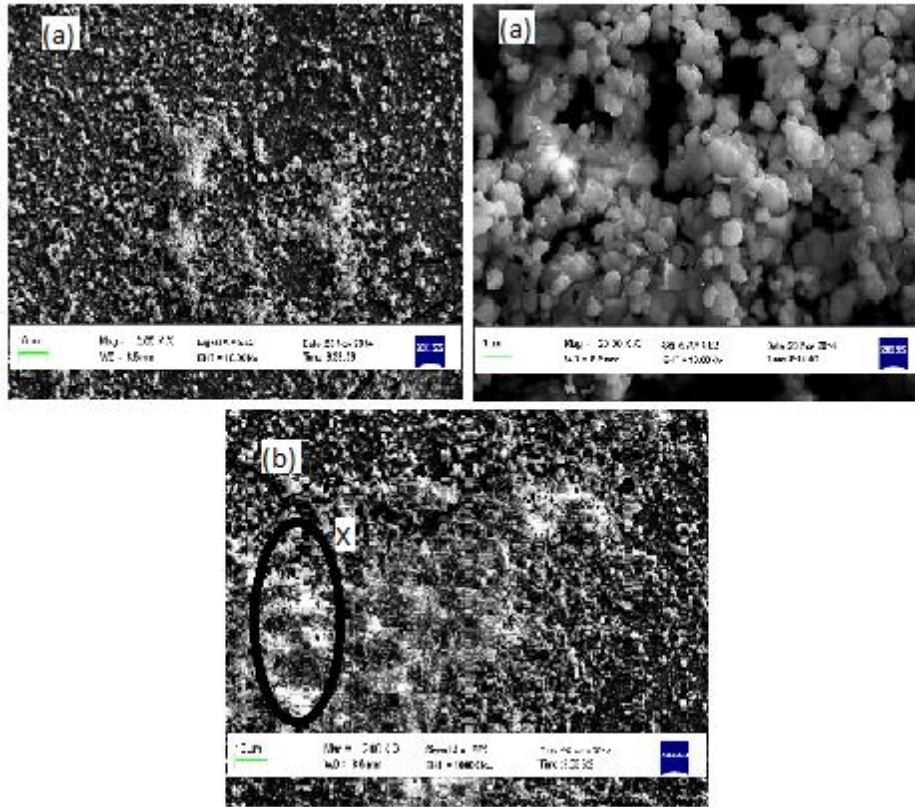


Figure 4.7: SEM image for (a) ZSM-5 and (b) H-ZSM-5

Figure 4.8 below, depicts micro-images of Co/H-ZSM-5 at 1000X magnification (2 μm scale) and at 2000X magnification (1 μm scale) for (a) and (b) respectively at a signal of 10kV. The presence of Hydrogen in the H-form of zeolite continues to be observed in the micro-images in Figure 4.8, due to high contrast and brightness. The morphology of the Co/H-ZSM-5 catalyst is irregular-rounded possessing a sphere like particles and a rough particle surface texture due to metallic nature of Cobalt as depicted in the below Figure 4.8(b). Similar to H-ZSM-5 zeolite support (Figure 4.7(b)), high level of agglomeration was also observed for Co/H-ZSM-5 catalyst as shown in Figure 4.7(b). Kangvansura *et al.*, (2013) described this cobalt-catalyst agglomeration and sintering as the results of cobalt being exposed to high temperatures, in this research, this was done during the catalyst calcination at a temperature of 400 $^{\circ}\text{C}$ as outlined in the catalyst synthesis section 4.2.

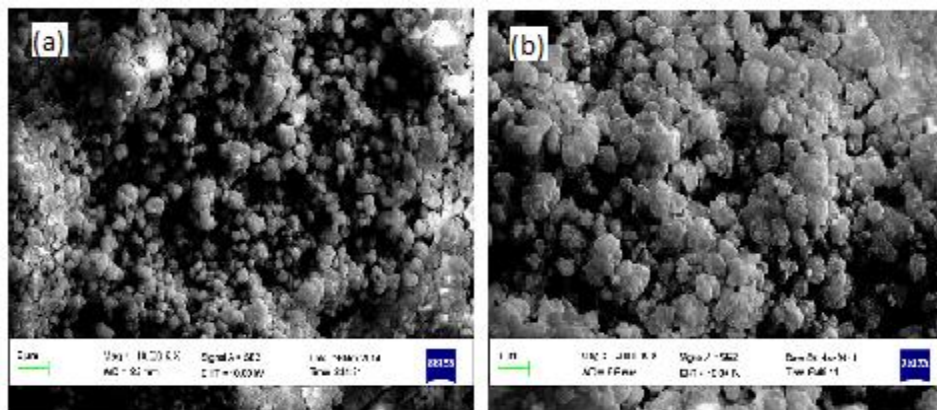


Figure 4.8: SEM Image for Co/H-ZSM-5

4.3.4. EDS Analysis

Figure 4.9, shows a spectrum (a) of elemental composition of ZSM-5 as well as a micro-image (b) of the area in which the elemental analysis was obtained, the results are also shown in tabulated form (c) depicting the elements present and their composition in weight percentage. Zeolites can be natural or produced synthetically and are known to be Alumino-Silicate materials, thus they contain high levels of aluminium and silicon at different ratios depending on their applications as well as other elements such as Oxygen (O), Hydrogen (H) and Sodium (Na) and Hydrogen could not be determined due to the detector limitation as mentioned above.

From Figure 4.9 (c) the ratio of Si/Al was found to be $\pm 40\%$ as this was the ratio of the ammonium form of ZSM-5 as produced by the supplier. It can also be seen from Figure 4.9 (a) that no other elements are present in the zeolite sample, since the detector did not detect any electronegative signal of other elements beyond 4kV, which implies that the sample is pure and no contamination of known elements. The same spectrum and elemental composition results are expected for H-ZSM-5, since the composition of Hydrogen ion could not be determined. The presence of Gold (Au) that is reflected in the spectrum is due to the Pd-Au coating applied during sample preparation (see section 3.3.3. in Chapter 3), and the capability of the detector to detect Au was not suppressed during the time of analysis.

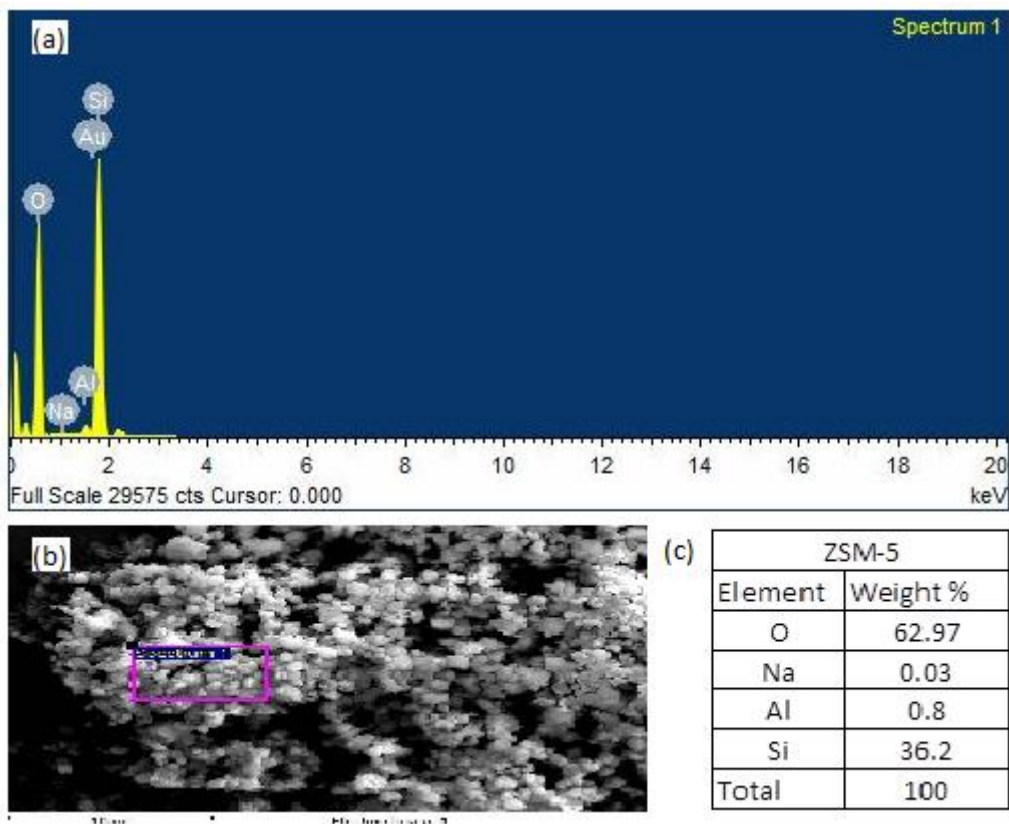


Figure 4.9: Elemental Composition of ZSM-5

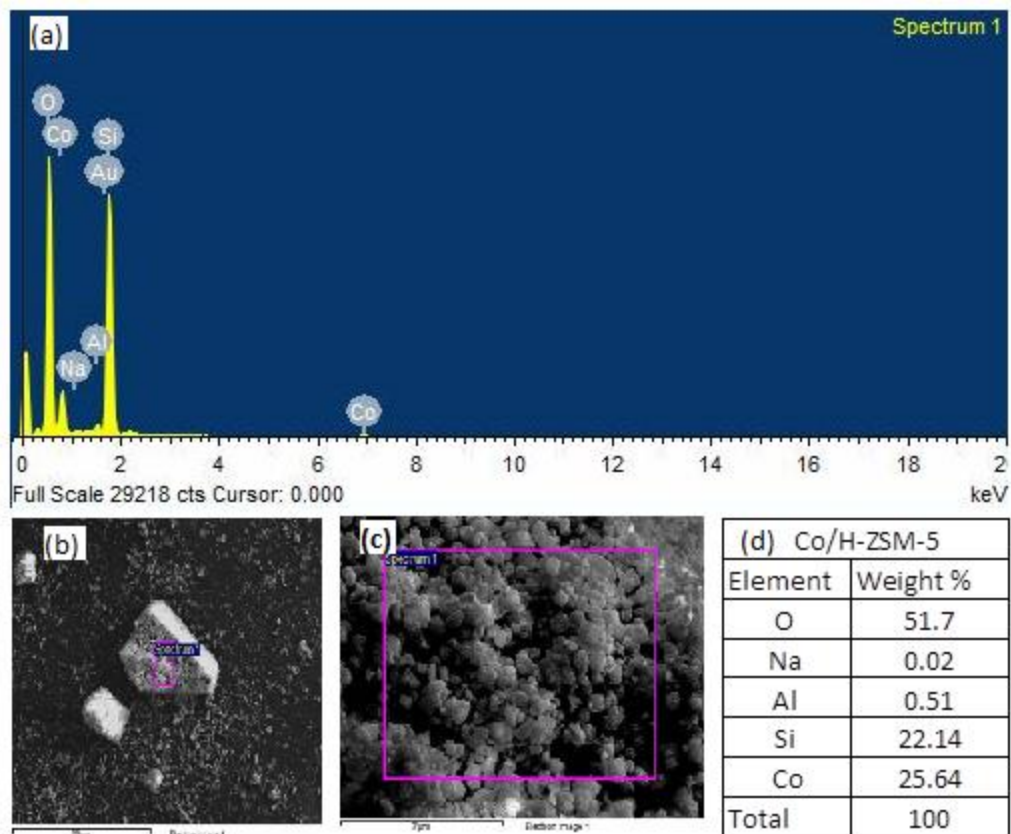


Figure 4. 10: Elemental Composition of Co/H-ZSM-5

A spectrum that consists of all the elements present in Co/H-ZSM-5 catalyst sample and the micro-image area in which the spectrum was obtained as well is shown in Figure 4.10 (a)-(d). Cobalt has an electronegativity of about 1.88 and was detected at about 0.8 kV and 7 kV as it can be seen in the spectrum Figure 4.10(a). Although the method used and adopted from Sartipi *et al.*, (2013b) for incipient wetness impregnation of the cobalt-solution on the zeolite support reported about 10 % weight of Cobalt in the final catalyst, it can be seen from Figure 4.9 (d) the obtained Cobalt composition is 25 % by weight which is two times more, as reported by Sartipi *et al.*, (2013b). This is because of a two step-impregnation that Sartipi *et al.*, (2013b) suggested for microporous materials such as H-ZSM-5 which was employed in this study, however it results in two times the cobalt-metal composition he obtained. Having that mentioned, it can be concluded that the cobalt-metal was successfully impregnated in the zeolite support. The presence of Au is due to Pd-Au coating used during sample preparation; see section 3.3.3 in Chapter 3 for detailed discussion on sample preparation. No any other known metals are present or contaminants, hence the sample spectrum is clear of any other elements.

4.3.5. TGA Analysis

Figure 4.11, depicts the change in mass (in weight %), of zeolite supports and catalyst with respect to temperature in degree Celsius. It can be observed from Figure 4.11, that at temperatures below 200 °C, a rapid loss in mass occurred for all the samples, resulting in a steep slope of the thermal-curve. This rapid loss in mass is about 5-7 % of the initial sample mass. At a temperature of 150 °C, a mass of 93, 94 and 95 % (wt.) was recorded for H-ZSM-5, ZSM-5 and Co/H-ZSM-5 respectively. These recorded mass (wt. %) correspond to 7 wt. % mass loss for H-ZSM-5, 6 wt. % mass loss for ZSM-5 and Co/H-ZSM-5 had a mass loss of 5 wt. % from an initial mass, which was about 11 mg for each of the sample. As the temperature was increased the sample mass continued do decrease, however at temperatures above 200 °C, a moderate decrease in mass continually occurred, and is observed by a gentle slope at high temperatures. In general H-ZSM-5 lost the most mass while Co/H-ZSM-5 lost the least mass, this can be due to the fact that the presence of metal species (Cobalt) increased Co/H-ZSM-5 stability, and ZMS-5 lost a moderate mass. The samples lost about 2 % of mass from 150 °C to 850 °C. But in overall about 10 wt. % in mass of each of the samples was lost from 0 °C until completion of the analysis.

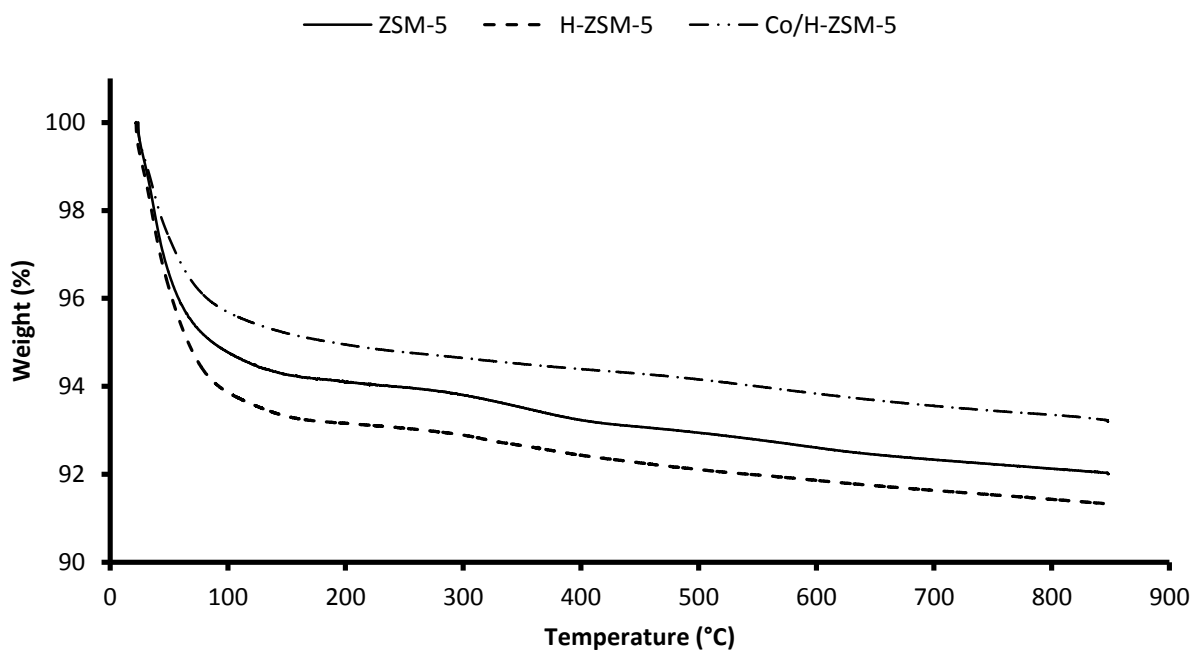


Figure 4.11: Change in Sample mass with Temperature

The graphs in Figure 4.11, are plotted with a temperature profile against time as the independent variable, this is depicted in Figure 4.12. The temperature profile is a smooth straight line due to a constant heating rate of 5 °C/ min. All the zeolite samples were heated from room temperature to 850 °C in Air flow. The temperature profile cuts the thermal-curve at point A, B and C for Co/H-ZSM-5, ZSM-5 and H-ZSM-5 respectively. These points at which the temperature profile cuts the thermal-curves are considered as the optimum points. In regard to TGA, an optimum point is a point in which a sample will lose the least mass, at a certain temperature at a given time, and any change in either time or temperature will result in different conditions and mass loss.

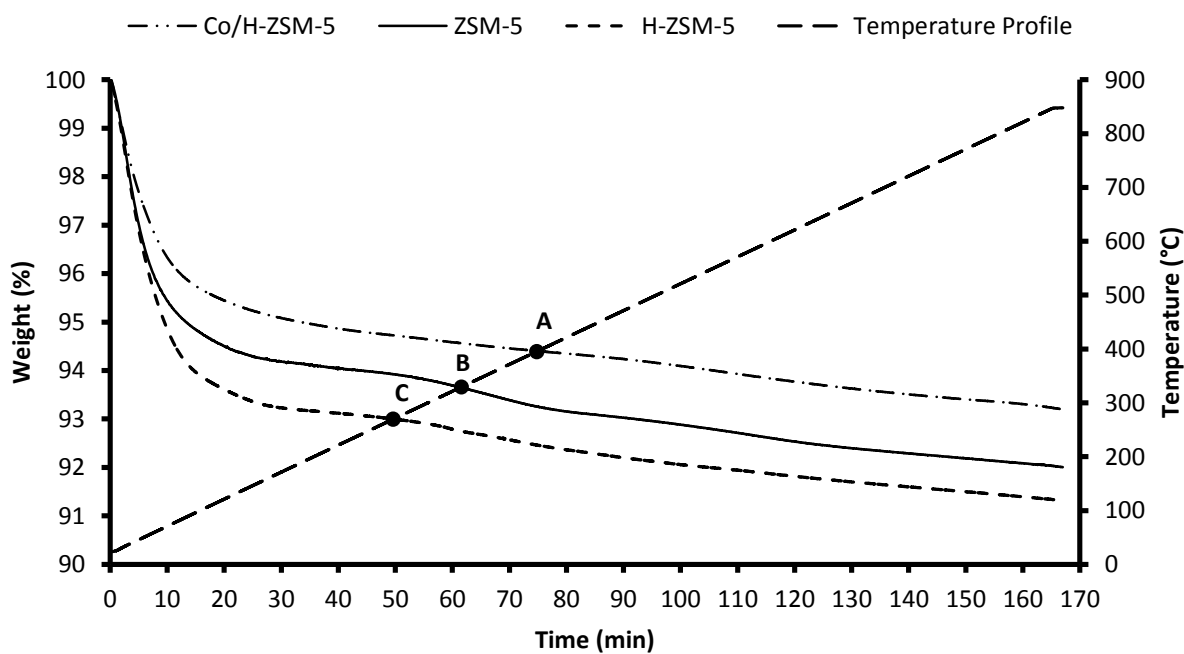


Figure 4.12: Optimum Sample Decomposition Conditions

Table 4.3, shows the conditions of the optimum point of decomposition due to combustion of the zeolite samples in air. From Table 4.3, it can be seen that the difference in time of the optimum point is about 10 min between samples, this difference correspond to about 50 °C temperature difference and 1 wt. % of the mass lost. The zeolite samples under study are expected to lose mass in the form of evaporation, chemical reaction and through decomposition. Products that are expected to form from the zeolites samples when combusted in air are $(NH_4)_2O$, H_2O , Na_2O in gas form; release of other species is also possible. Hence due to these physical and chemical actions the samples have lost mass.

Table 4.3: Sample Optimum Decomposition Point

Point	Time (min)	Mass (wt %)	Temperature (°C)	Mass Loss (wt %)
A	75	94.5	395	5.5
B	62	93.7	329	6.3
C	50	92.9	270	7.1

4.3.6. TPR Analysis

Figure 4.13, depicts the catalyst H_2 -TPR profile of Co/H-ZSM-5. The TPR was performed in 5 % of H_2/Ar from 20 to 900 °C. The onset for Co/H-ZSM-5 starts at about 180 °C and the reduction ends at about 650 °C after peaking at A,B,C and D, resulting in a broader overall peak. These observed peaks will be further discussed by the reactions below and Table 4.4. After final calcination during catalyst synthesis, the Cobalt metal exists which confirms the XRD analysis outlined in section 4.3.2, and hence reduction is required to obtain the active elemental Cobalt supported on the zeolite.

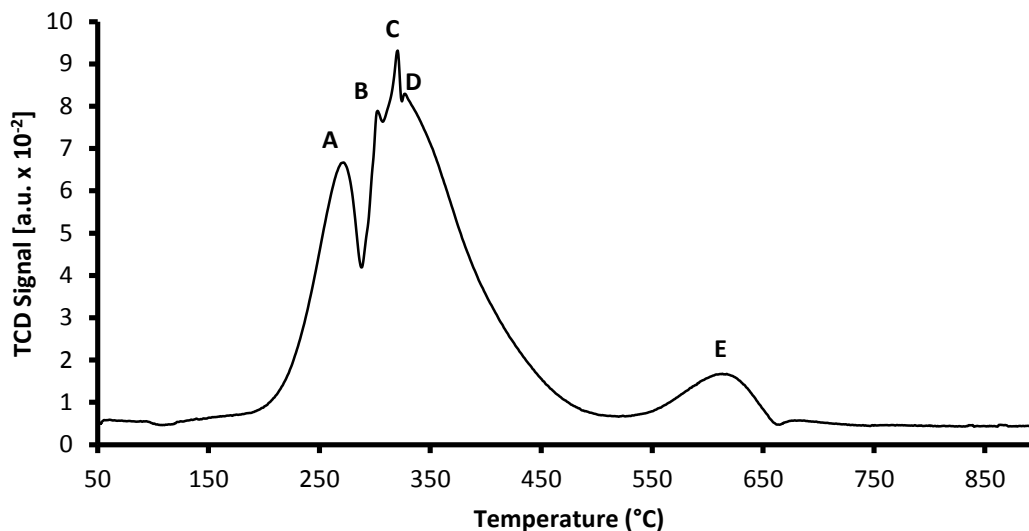


Figure 4.13: Co/H-ZSM-5 catalyst TPR profile

The following reactions represent the steps or paths of the Cobalt-Oxide to elemental Cobalt ($\text{Co}_3\text{O}_4 \rightarrow \text{CoO} \rightarrow \text{Co}$) in the presence of hydrogen as the reducing agent.

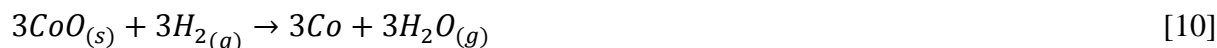
Reaction at A to B:



The tetra-Oxide form of Cobalt is reduced to Cobalt-Oxide with a hydrogen consumption of 0.33 mole ratio ($\text{H}_2/\text{Co} = 0.334$), which is the degree of reduction (33 %) at this stage, and is calculated using the following equation (Wang *et al.*, 2005).

$$\begin{aligned} \text{Degree of Reduction (\%)} &= \frac{\text{Moles of H}_2 \text{ consumed}}{\text{initially moles of Co}^{2+}} \times 100 \\ &= \frac{2(1)}{3(2)} \times 100 = 33.33\% \end{aligned}$$

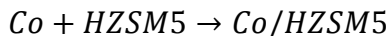
Reaction at B to C:



The Cobalt-Oxide is then reduced to elemental Cobalt with a 100 % degree of reduction, thus $\text{H}_2/\text{Co} = 1$, at this stage the cobalt-oxide was fully reduced to metallic cobalt. In overall the

reduction of Co_3O_2 to elemental Co requires about 133 % of hydrogen consumption, which is in excess by 33 %. However since another species was also reduced at about 600 °C (Peak E) then the overall hydrogen consumption is expected to be above 133 %.

Peak C to D:



This is not a reaction of Cobalt and the zeolite, but rather an indication that the cobalt then attached itself to the zeolite in its elemental form. At this peaks, it is where the Cobalt in its pure form interacts with the support

Table 4.4: Element Peak Reduction Temperature

Reduction Peak	Temperature (°C)	Element
A	272	Co_3O_4
B	302	CoO
C	320	Co
D	327	Co/H-ZSM-5
E	617	Al_2O_3

At peak labelled A, tri-Cobalt-tetra-oxide is reduced to Cobalt (II) Oxide at a temperature of about 272 °C, as it can be seen from Figure 4.13 and Table 4.4. The Cobalt (II) Oxide is then reduced at 302 °C to elemental Cobalt, which is then fully reduced at 320 °C shown by Peak C. At peak D the elemental Cobalt binds itself to the Zeolite support, forming Co/H-ZSM-5 at peak D. Hydrogen was highly consumed throughout the reduction process (180-650 °C), the broad hydrogen consumption at high temperatures results in high oxidation states of the cobalt metal and hence strong interaction of the cobalt metal with the support this can also be attributed to the overlapping of peak C and D (Wang *et al.*, 2005; Martens *et al.*, 1986; Galvagno *et al.*, 1984). Wang *et al.*, (2005) also mentioned that the high interaction of metal-support, a high reduction temperature and high oxidation states of metals is also due to high acidity of the support materials, and this is expected since zeolites are acidic-materials. From the reduction profile, another species has been observed to be reduced, this might be a form of aluminium oxide, since zeolite is known as an aluminous-silicate material, and since no impurities were detected by the EDS analysis (section 4.3.4), this brings to the conclusion that at temperatures of about 500 °C,

peak E is a result of Aluminium-oxide reduction, since most catalyst supported on Aluminium-oxide are reduced at temperatures above 500 °C (see Li & Chen, 1995; Vermaire, 1989; Álvarez-Galván *et al.*, 2003).

4.3.7. TEM Analysis

From the micrograph in Figure 4.14, the morphology of the catalyst is fairly uniform with an irregular circular shape with a diameter of about $2.5 \pm 0.5 \mu\text{m}$. The morphology of the catalyst was also confirmed by the SEM analysis as discussed in section 4.3.3. Figure 4.14(a) depicts the H-ZSM-5 zeolite support before impregnation with the cobalt precursor, while Figure 4.14(b) shows the finished catalyst with Co_3O_4 embedded within the support as shown with the red arrows. By using the scale on the micrographs the metal grains have been discovered to be in the range of about $8 \pm 3 \text{ nm}$. It can be observed from Figure 4.14(b) that the cobalt metal particles were successfully imbedded into a single H-ZSM-5 crystal and fully dispersed throughout the support. Mohanty *et al.*, (2011) obtained a metal grain diameter in the range of 15-30 nm, this might be due to the reason that copper and chromium was also used as promoters in the catalyst hence the overall metal grain was obtained to be higher. On the other hand, Sartipi *et al.*, (2013b) obtained a metal grain diameter of about 17 nm; this could be due to desilication of the zeolite that was performed. The metal particles are located closer to the support surface, with their outer-surface being covered by poor-crystallized-oxide-layer of which Mohanty *et al.*, (2011) described it as an oxide-layer that serves to protect the metal from rapid oxidation in the presence of hydrogen at higher temperature. This phenomenon was confirmed by the TPR analysis (section 4.3.6) in which the Co_3O_4 was reduced to metallic-cobalt in a 2 step reaction (see Eq. (9) and (10)) at temperatures between 250-350 °C. This tendency has been attributed to the zeolite composition (Mohanty *et al.*, 2011) hence the use of different zeolite composite material combination will offer different reduction temperature.

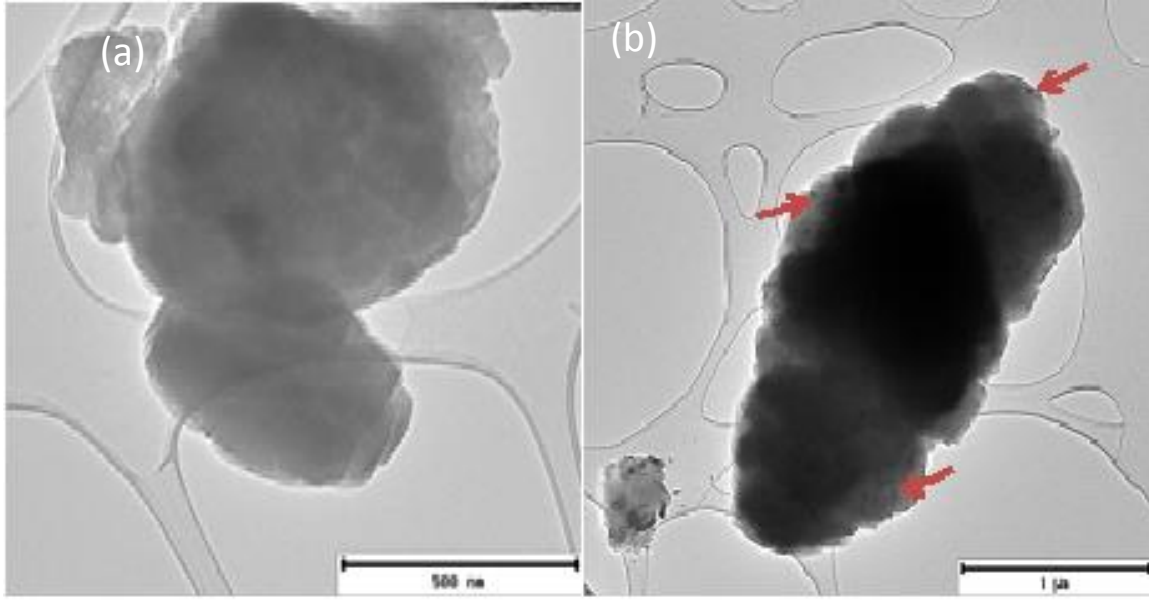


Figure 4.14: TEM images of (a) H-ZSM-5 support and (b) Co/H-ZSM-5 bi-functional catalyst

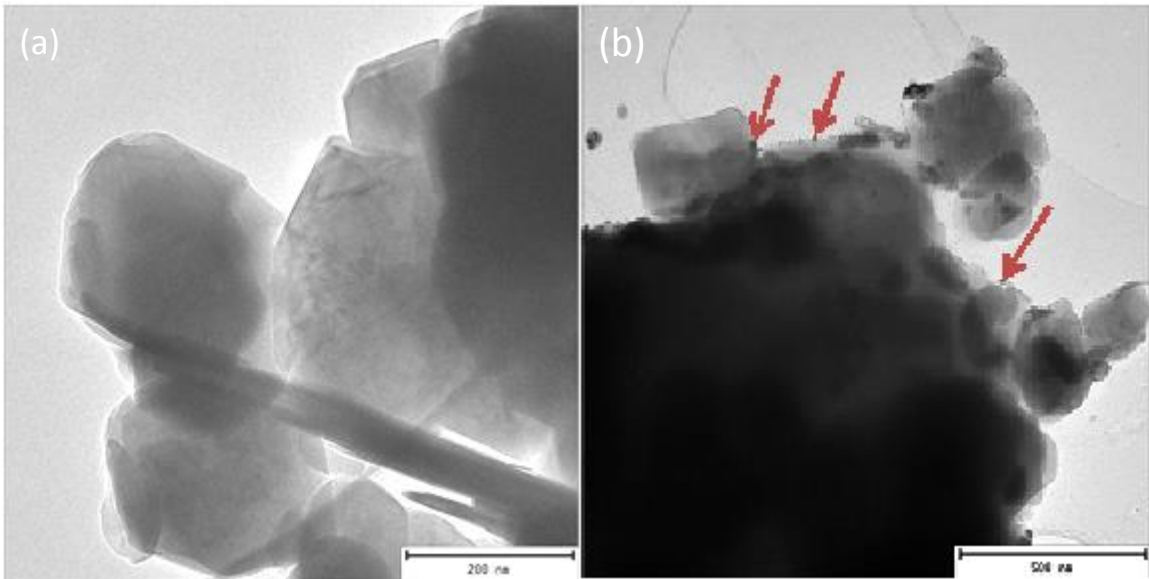


Figure 4.15: TEM images of (a) SiO₂ support and (b) Co/SiO₂ commercial catalyst

Similar to Figure 4.14, Figure 4.15 also depicts the metal-free support (a) and the finished commercial catalyst with the cobalt-metal being successfully embedded and dispersed within the support (b). According to Figure 4.15, the Co metal particles were widely-dispersed across the amorphous silica-oxide support. This metal dispersion (in Figure 4.15 (b)) is an improvement as compared to the zeolite support (compare Figure 4.14 (b) and Figure 4.15 (b)), in which the metal particles are clustered across the H-ZSM-5 support. However a high concentration can be

observed between the H-ZSM-5 and SiO₂ supported catalyst as shown in both Figure 4.14 (b) and Figure 4.15 (b). For Co/SiO₂, Sartipi *et al.*, (2014) obtained Co crystallite particle size of 16 nm, and for the zeolite the Co crystallite size was in the range of 10-13 nm. Ernest *et al.*, (1998) obtained the cobalt particles in Co/SiO₂ to be in the range of 8-35 nm. From Figure 4.15 (b), the Co metal particles in Co/SiO₂ was determined to be 15 ± 0.5 nm which agrees well with values reported by Ernest, (1998) and Sartipi`s, (2014).

4.4. Summary

In this Chapter, synthesis and characterization of the two catalyst employed in this study have been discussed elaborately. The synthesized bi-functional catalyst had a surface area of 292 m²/g, a pore volume of about 0.189 cm³/g and a pore diameter of 2.828 nm. From the thermal decomposition, Co/H-ZSM-5 was found to be more stable due to the presence of the Cobalt-metal resulting in the least loss of mass when compared to ZSM-5 and HZSM-5. The resulting reduction conditions were obtained to be in the range of 320-350 °C. The Cobalt-oxide was found to be located close to the surface of the support with a diameter of 8 ± 3 nm in Co/H-ZSM-5 catalyst while for CO/SiO₂ catalyst the metal grains were obtained to be in the range 15 ± 0.5 nm. The synthesized bi-functional catalyst was then tested in FT synthesis using a simulated syngas mixture from waste tyres under different process conditions and the performance of the bifunctional catalyst was compared to that of the commercial catalyst, Co/SiO₂. Results of these tests and comparison are presented in Chapter 5 and Chapter 6 of this dissertation.

4.5. References

Álvarez-Galván M.C, Pena O`Shea V.A, Fierro J.L.G, Arias P.L, 2003, Alumina-supported manganese- and manganese-palladium oxide catalysts for VOCs combustion. *Catalysis Communications*, 4(5), pp.223–228.

Bergström J, 2013, Oxidation of Cobalt Nanocrystals: Investigation of the Role of Nanocrystallinity. Self-Ordering and Nanocrystal Size, Masters of Science Thesis in the Master`s Degree Program, Materials Chemistry and Nanotechnology, Department of Chemical and Biological Engineering, Chalmer University of Technology

Che M, Védrine J.C (ed.), 2012, Characterization of Solid Materials and Heterogeneous Catalyst- From structure to Surface Reactivity, Volume 2, Wiley-VCH Verlag GmbH &

CO. KGaA, Weinheim, Germany

- Downs, R. & Hall-Wallace, M., 2003. The American Mineralogist Crystal Structure Database., *American Mineralogists*, (88), pp.247–250.
- Ernest B, Besaddik A, Hiaine L, Chaumete P, 1998, Study on a Cobalt Silica Catalyst during Reduction and Fischer-Tropsch Reaction: In situ EXAFS compared to XPS and XRD. *Catalysis Today*, 39, pp.329–341.
- Galvagno S, Crisafulli C, Maggiore R, Tauszik G.R, Giannetto A, 1984, Temperature-programmed reduction. Metal-support interaction on supported monometallic Ru and Cu Catalysts, *Journal Of Thermal Analysis* ,Vol. 30, pp.611–618.
- Kangvansura P, Poo-arporn Y, Schulz H, Worayingyong A, 2013, The Effect of Promoters on Reduction of Ru / ZrO₂ / Co / SiO₂ Catalyst for Fischer- Tropsch Synthesis as Studied by in situ XANES, CTSI-Cleantech (3), pp.310–313.
- Li C, Chen Y.-W, 1995. Temperature-programmed-reduction studies of nickel oxide/alumina catalysts: effects of the preparation method. *Thermochimica Acta*, 256(2), pp.457–465.
- Lu R, Tangbo H, Wang Q, Xiang S, 2003, Properties and Characterization of Modified HZSM-5 zeolites. *Journal of Natural Gas Chemistry*, 12, pp.56–62. Available at: <http://www.jngc.org/EN/article/downloadArticleFile.do?attachType=PDF&id=8458>.
- Martens J.H. A, van 't Blik H.F.J, Prins R, 1986, Characterization of supported cobalt and cobalt-rhodium catalysts II. Temperature-Programmed Reduction (TPR) and Oxidation (TPO) of Co/TiO₂ and Co -Rh/TiO₂. *Journal of Catalysis*, 97(1), pp.200–209. Available at: <http://www.sciencedirect.com/science/article/pii/0021951786900503>.
- Sartipi S, Parashar K, Makkee M, Gascon J, Kapteijn F, 2013b, Breaking the Fischer–Tropsch synthesis selectivity: direct conversion of syngas to gasoline over hierarchical Co/H-ZSM-5 catalysts. *Catalysis Science & Technology*, 3(3), p.572. Available at: <http://xlink.rsc.org/?DOI=c2cy20744c>.
- Sartipi S, Alberts M, Santos V.P, Nasalevich M, Gascon J, Kapteijn F, 2014, Insights into the Catalytic Performance of Mesoporous H-ZSM-5-Supported Cobalt in Fischer – Tropsch Synthesis, *ChemCatChem, ChemPubSoc , Europe*, pp.142–151.

- Smith, E., 2012. *Basic Physical Chemistry-The Route to Understanding*, london, Imperial College Press,.
- Vermaire D.C, van Berge P.C, 1989, The preparation of WO₃/TiO₂ and WO₃/Al₂O₃ and characterization by temperature-programmed reduction. *Journal of Catalysis*, 116(2), pp.309–317. Available at: <http://linkinghub.elsevier.com/retrieve/pii/0021951789900985>.
- Wang W.J, Lin H.Y, Chen Y.W, 2005, Carbon monoxide hydrogenation on cobalt/zeolite catalysts. *Journal of Porous Materials*, 12(1), pp.5–12.
- Wu C-H, 2012, “Low Energy-Consumption Industrial Production of Ultra-Fine Spherical Cobalt Powders” in Energy Conservation, Ahmed A.Z (eds.), InTech Publisher, 149-170

CHAPTER 5: PERFORMANCE EVALUATION OF THE BI-FUNCTIONAL Co/H-ZSM-5 CATALYST DURING FISCHER-TROPSCH SYNTHESIS.

5.1. Introduction

The previous chapters, Chapter 3 and Chapter 4, focused on the synthesis and characterization of the bi-functional Co/H-ZSM-5 catalyst and the commercial Co/SiO₂ catalyst. In this chapter detailed information about the performance evaluation of the bi-functional catalyst and its comparison with that of the Co/SiO₂ catalyst is provided. The description of the experimental set-up and how the experiments were conducted is also provided. These findings from this study are also discussed and compared to results from previous studies. In this Chapter the effect of operating conditions and H₂/CO ratio on the performance of the catalyst is discussed.

This Chapter as well as Chapter 6 will focus on two organic compounds of Hydrocarbons known as olefins and paraffins (See Eq. (2) and Eq. (3) in Chapter 2 section 2.1.3 for associated reaction equation for paraffins and olefins production respectively), which are always products of FTS process in different production rate and proportions. Hydrocarbons produced would be discussed in terms of conversion and selectivity based on their carbon number. Olefins are hydrocarbons with more than one carbon-carbon bonds for example Ethylene (a C₂ compound with double bonds between carbon atoms) which is an Alkene and contains double bonds within the carbon-carbon atoms. Paraffins are saturated straight chains and can also be branched chains of these straight chains, these branched chains are also known as isomers, for example *n*-butane, an alkane which is a straight C₄ chain, has a methyl-propane compound as its isomers also known as an isobutane. Figure 5.1, as an example, depict comparison of Olefins and Paraffin including its isomer.

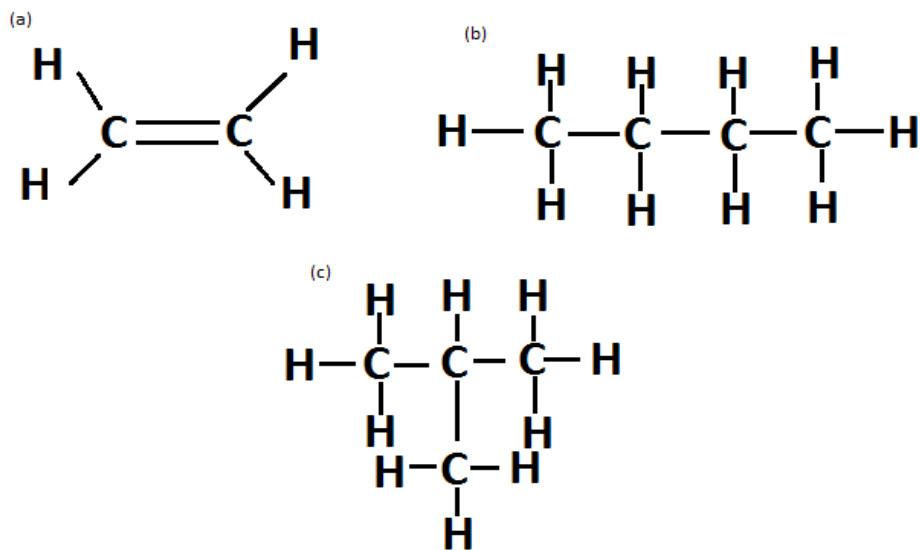


Figure 5.1: Olefin: (a) Ethylene, Paraffin: (b) Butane (c) isobutane which is a Butane isomer

The double bonds can be seen in the above Figure 5.1(a) in an Olefin ethylene molecular structure and a straight molecular structure for *n*-butane in Figure 5.1(b), and a branched molecular structure in Figure 5.1(c) which is the Butane isomer known as Methyl-Propane or isobutane. Method for the estimation and calculation of the conversion and selectivity employed in this study was based on Price (1994); Motchelaho (2011) and Moyo (2012).

5.2. Experimental Procedure for the Evaluation of the Performance of the Catalyst

The catalytic performance of the specific amount of the synthesized bi-functional catalyst (Co/H-ZSM-5) was evaluated by using a fixed bed reactor (FIXBR) at predetermined conditions. The catalytic performance of this bi-functional catalyst (Co/H-ZSM-5) was compared with that of the synthesized Co-based FT catalyst (Co/SiO₂) at similar conditions. Figure 5.2 depicts the experimental set-up used for the FT synthesis to evaluate the performance of the catalyst (also See Figure C.1 in Appendix C for images). The reactor is equipped with two traps, also known as knock-outs. The first trap is used to trap wax (Heavy Hydrocarbons) while the second trap is used to capture oil and water.

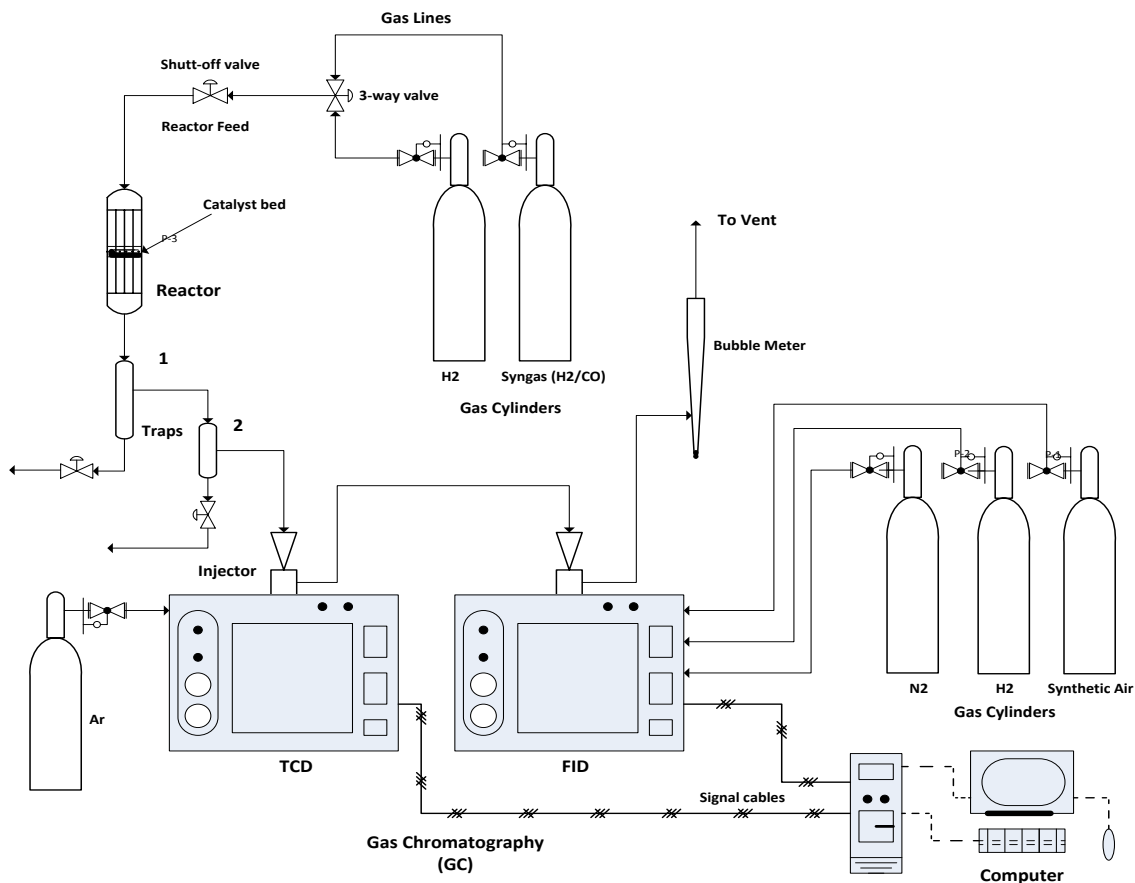


Figure 5.2: Fischer-Tropsch Experimental Setup

The feed and reaction products from the reactor were analyzed with a pre-calibrated online GC and pre-calibrated offline GC as reported in section 3.5 of Chapter 3. The two GCs were equipped with a Flame Ionization Detector (FID) and the other with a Thermal Conductivity Detector (TCD). The Flame Ionization Detector (FID) uses Nitrogen as a carrier gas while the Thermal Conductivity Detector (TCD) uses Argon. Synthetic Air and Hydrogen are also used in the FID to ignite the flame. For reactor feed, a two-way valve is used to switch between hydrogen and synthetic gas during catalyst reduction and reaction runs respectively. Compressed air is also used for pneumatic valves to switch the valves between sampling and cooling to open and shut the GC's oven doors.

Most of the gaseous products (light Hydrocarbons) are analyzed by the online GC's. The GC gas feed lines are heated to 100 °C while the valves and detectors are heated to 100 °C and 220 °C

respectively. The FID-GC gas outlet is connected to a flowmeter which is used to measure the flow of the gases; the flowmeter is connected to a vent to purge out the gases from the system. The GC's were preset to analyze for an hour at an oven temperature of 200 °C and cool down for another hour to room temperature. The GC signals were received by a transmission box which is connected to a computer. The computer analyzes the reaction products and the feed by making use of DataApex Chromatograph software package known as Clarity ® (v. 2.5). This programme enables saving of reaction files and integration of peaks which are a result of the products and the feed material. These peaks can be seen in Appendix C, Figure C.1 for TCD and Figure C.2 for FID when using Clarity ®. From the obtained results, then conversion and selectivity can be calculated at different conditions such as reaction temperature, gas flow and pressure.

5.3. Results and Discussion

In this study, a syngas flow-rate of 1200 GHSV (ml/gcat.hr) (gas hourly space velocity) was considered as a low flow rate, while 2400 GHSV and 3600 GHSV were considered as an intermediate and high flow rate respectively. Conversion discussed in this dissertation is based on CO (Carbon-monoxide) unless stated otherwise. With respect to selectivity, C₂-C₄ carbon numbers are considered as lower hydrocarbons or middle distillates while C₅ and C₆₊ are considered as higher hydrocarbons and methane is referred to as C₁ hydrocarbon throughout this study.

The results in Table 5.1, show that a CO Conversion of 2.64 % was obtained at low flowrate of 1200 GHSV(ml/gcat.hr) while CO conversions of 1.45 % and 1.28 % was obtained at a flow rate of 2400 GHSV and 3600 GHSV respectively. The obtained CO conversion as shown in Table 5.1 is a results of changing syngas flow rate from 1200, 2400 to 3600 GHSV at a constant temperature of 220 °C, a syngas H₂/CO ratio of 1.5 and a pressure of 2 bars, by using a bi-functional, Co/H-ZSM-5 catalyst.

Table 5.1: Effect of flow rate on conversion

H ₂ /CO	GHSV (ml/gcat.hr)	Temperature (° C)	Pressure (bar)	% CO Conversion
1.5	1200	220	2	2.64
	2400			1.45
	3600			1.28

Calleja *et al.*, (1995) reported a CO conversion of 36 % by using a bi-functional Co/H-ZSM-5 catalyst at a low H₂/CO ratio of 1.5; however this was obtained at pressure of 21 bars and temperature of 280 °C, and Tristantini *et al.*, (2007) obtained a CO conversion in the range of 6 to 15 % at higher pressure 20 bar and a temperature of 210 °C. From these findings it was observed that a low flow rate yields a higher conversion and a higher flow rate resulted in a lower conversion (compare CO conversion at different flow rates in Table 5.1). Thus as flow rate is increased the rate at which the reactants are converted to products decreased, this is attributed to change in the residence time of the reactants and the time of contact between the reactants and the catalyst active sites at changing feed flow rates. At low flow rate there is a maximum contact time (high residence time) between the reactants and the catalyst active sites which resulted in a higher conversion. On the other hand a high flow rate resulted in a low conversion due to minimum contact (low residence time) of reactants with the catalyst active sites.

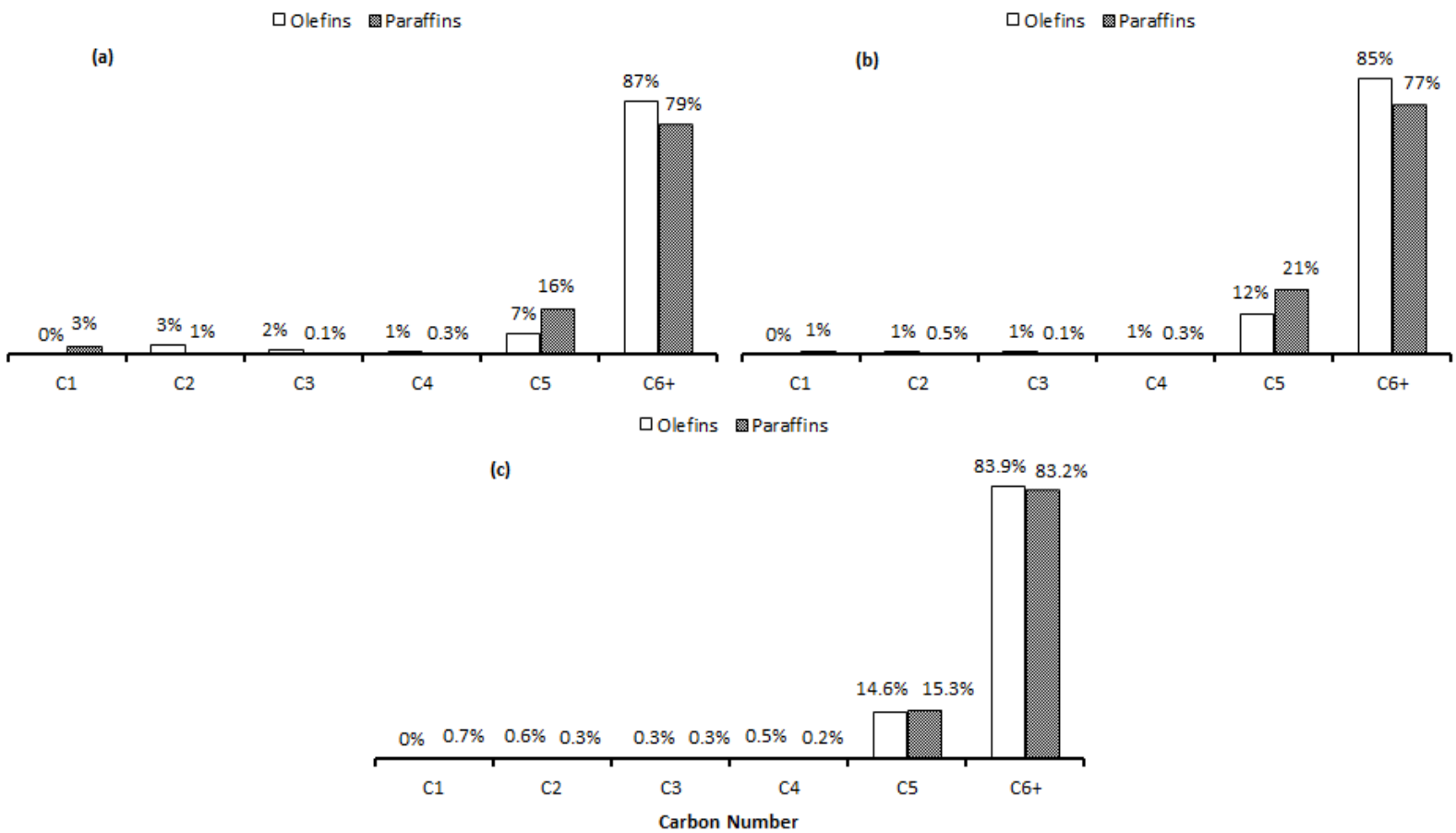


Figure 5.3: Olefin & Paraffin Selectivity at flow rate of (a) 1200 (b) 2400 and (c) 3600 GHSV (ml/gcat.hr)

The effect of feed flow rate on the performance of the catalyst was studied at reaction temperature of 220 °C, H₂/CO ratio of 1.5 and total pressure of 2 bar. Three values of the flow rates were considered, namely, 1200 GHSV, 2400 GHSV and 3600 GHSV. Figure 5.3(a) shows hydrocarbon (HCs) selectivity for 2.64 % conversion and Figure 5.3(b) and Figure 5.3(c) shows HCs selectivity for CO conversion of 1.45 % and CO conversion of 1.28 % respectively. These results were obtained under similar conditions as stated in Table 5.1 by using a bi-functional, Co/H-ZSM-5 catalyst. At all studied gas flow rates, the bi-functional, Co/H-ZSM-5 catalyst was found to be more selective to olefins over paraffins, especially to C₆₊ hydrocarbons. At the lowest flow-rate (1200 GHSV), the selectivity to C₆₊ olefin and paraffin was as 87 % and 79 %, respectively. At the flow rate of 2400 GHSV the selectivity to olefins and paraffins was as 85 % and 77 %, respectively, at conditions stated in Table 5.1. At highest flow-rate (3600 GHSV) the selectivity of the catalyst to C₆₊ was obtained as 83 % per olefin and paraffin hydrocarbons. These results at 2 bars indicate that conversion of syngas to liquid fuels is possible at conditions stated in Table 5.1, by using the bi-functional catalyst, although conversion at these conditions is a big challenge.

Calleja *et al.*, (1995) has reported selectivity of about 35 % to C₆₊ hydrocarbon, with 36 % selectivity to methane and selectivity of 29 % to middle distillates. Tristantini *et al.*, (2007) obtained methane selectivity of about 7 % to 11 % by using a syngas of H₂/CO ratio of 1.5, temperature of 210 °C and pressure of 20 bars. From Figure 5.3, the highest selectivity to C₆₊ olefin (87 %) was obtained at low flow-rate while the highest selectivity to C₆₊ paraffin (83 %) was obtained at a high flow-rate. Higher flow-rate resulted in selectivity to paraffin to increase from 77 % (at 2400 GHSV) to 83 % (at 3600 GHSV), which is attributed to the efficient product separation that occurred at higher flow-rates. From these findings it can be observed that at higher flow-rate, products can be easily distinguished from each other due to less or no overlap of the product signal peaks.

Hydrocarbon of C₅ olefins selectivity increased when flow rate was increased, opposite is the case for C₆₊ olefins. Methane production remained minimal by the bi-functional Co/H-ZSM-5 catalyst, with a selectivity of 3 % obtained at flow rate of 1200 GHSV and < 1 % selectivity per 2800 GHSV and 3600 GHSV syngas flow rate. Middle distillate HCs of C₂ –C₄ olefin and

paraffin was also produced insignificantly (less than 3 % of selectivity) this was observed in Figure 5.3 (a) to (c)

Table 5. 2: Effect of Temperature on conversion at low pressure

H ₂ /CO	GHSV (ml/gcat.hr)	Temperature (° C)	Pressure (bar)	% CO Conversion
1.5	1200	220	2	2.64
		250		4.18

Since a higher conversion was obtained at lower flow rate of 1200 GHSV as reported in Table 5.1, the study was preceded at this flow-rate while changing other process variables (i.e. pressure, temperature and syngas composition). Table 5.2, is a tabulation of CO conversion at 220 °C and 250 °C at a low pressure of 2 bar and H₂/CO ratio of 1.5. It was observed from Table 5.2, that when temperature is increased from 220 °C to 250 °C conversion of CO doubled under these conditions, thus it increased from 2.64 % to 4.18 %, while the flow-rate and pressure remained constant. The corresponding selectivity as a result of the temperature change is depicted in Figure 5.4 for both olefins and paraffin hydrocarbons.

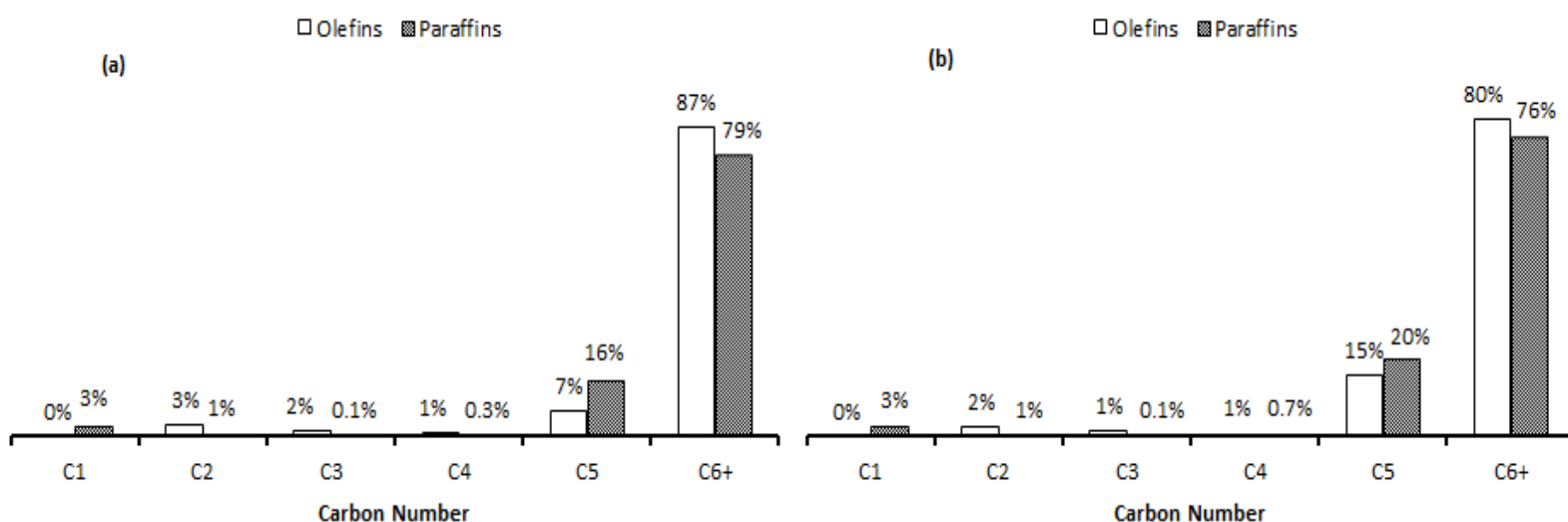


Figure 5.4: Olefin & paraffin Selectivity at low pressure and (a) 220 and (b) 250 degrees

Figure 5.4 depicts selectivity to olefin and paraffin hydrocarbons produced at a temperature of (a) 220 °C and (b) 250 °C, a low pressure of 2 bar and a low flow rate of 1200 GHSV and a 1.5, H₂ to CO syngas ratio. Methane production remained constant resulting in a selectivity of 3 %, also selectivity to middle distillates (C₂-C₄) paraffin was similar at both studied temperatures. Olefin and paraffin of C₆₊ carbon number decreased while temperature was increased from 220 °C to 250 °C. Thus, selectivity to C₆₊ olefin decreased from 87 % to 80 %, while selectivity to C₆₊ paraffin decreased from 79 % to 76 %. This increase in temperature from 220 °C to 250 °C that resulted in a decreased selectivity to C₆₊ hydrocarbons also led to an increase in selectivity to C₅ hydrocarbons.

Selectivity to olefin of C₅ carbon number increased from 7 % to 15 % while selectivity to paraffin increased from 16 % to 20 % of the same carbon number. Selectivity to methane remained the same at both studied temperatures (220 °C and 250 °C, compare Figure 5.4(a) and Figure 5.4(b)) under similar conditions as stated in Table 5.2. These may bring to the conclusion that an increase in temperature at a constant low pressure of 2 bar and a low flow rate of 1200 GHSV, when using bi-functional Co/H-ZSM-5 catalyst has no effect on methane production (compare selectivity to C₁ HC in Figure 5.4(a) and Figure 5.4(b)), but resulted in a more distribution of other hydrocarbon products that were previously produced in less quantity, particularly C₅ hydrocarbons. The next variable that was studied is the effect of higher pressure at the same conditions as stated in Table 5.2.

Table 5.3: Effect of Temperature on conversion at High pressure

H ₂ /CO	GHSV (ml/gcat.hr)	Temperature (° C)	Pressure (bar)	% CO Conversion
1.5	1200	220	15	4.97
		250		7.49

Since the CO conversions reported in Table 5.2 and its corresponding selectivity in Figure 5.4, was based on a low pressure of 2 bars, a higher pressure of 15 bars was studied in comparison to a pressure of 2 bars. The study was conducted at a flow rate of 1200 GHSV and H₂/CO ratio of 1.5 at a temperature of 220 °C and 250 °C. The effect of changing pressure from 2 bars to 15 bars to the catalyst performance was discussed in Table 5.3 and Figure 5.4 and compared to

Table 5.2 and Figure 5.3. It was observed from Table 5.2 and Table 5.3 that at a constant temperature, syngas composition and flow-rate, CO conversion increased with an increase in pressure. At a temperature of 220 °C, CO conversion increased from 2.64 % (in Table 5.2) to 4.97 % (see Table 5.3) when pressure was increased from 2 bars to 15 bars respectively. At a temperature of 250 °C, CO conversion increased from 4.18 % to 7.49 % (compare Table 5.2 and Table 5.3) at a constant flow-rate of 1200 GHSV. Similarly to Table 5.2, an increase in temperature at constant pressure, flow rate and similar syngas composition resulted in an increased in CO conversion (from 2.64 % to 4.18 % reported in Table 5.2). From Table 5.3, CO conversion increased from 4.97 % to 7.49 % when temperature was increased from 220 °C to 250 °C at a higher pressure of 15 bars.

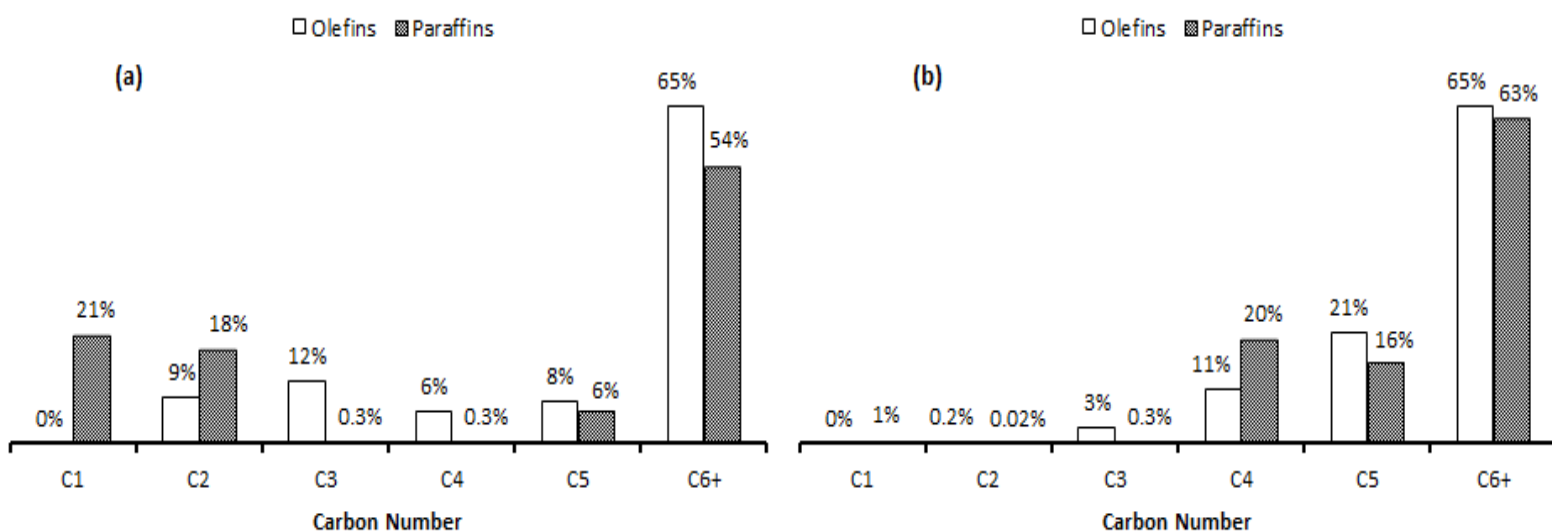


Figure 5.5: Olefin & paraffin Selectivity at High Pressure and (a) 220 and (b) 250 degrees

Although a higher CO conversion was obtained when pressure was increased from 2 bars (see Table 5.2) to 15 bars (see Table 5.3), however in terms of selectivity, a higher pressure resulted in a decreased in selectivity to higher hydrocarbon products, compare Figure 5.4 (when pressure was 2 bar) and Figure 5.5 (when pressure was 15 bar). Thus, the change in pressure from 2 bars to 15 bars resulted in selectivity to C₆₊ olefin to decrease from 87 % (at 220 °C) and 80 % (at 250 °C) to 65 % at per studied temperatures of 220 °C and 250 °C. Similarly to C₆₊ olefin, selectivity to paraffin of C₆₊ HCs decreased from 79 % to 54 % at 220 °C (compare Figure 5.4 (a) and Figure 5.5 (a)), while selectivity to methane increased rapidly from 3 % to 21 % and

again selectivity to C₆₊ paraffin decreased from 76 % to 63 % at a temperature of 250 °C (compare Figure 5.4 (b) and Figure 5.5 (b)). On the other hand, when comparing Figure 5.5(a) and Figure 5.5(b), it was observed that, at constant high pressure of 15 bars, a low flow rate of 1200 GHSV and 1.5 of syngas ratio, increasing temperature from 220 °C to 250 °C resulted in a decreased selectivity to methane from 21 % to 1 %.

At a temperature of 220 °C, selectivity to hydrocarbons of C₂-C₄ olefin was <12 % and selectivity to C₅ olefin was 8 % as depicted by Figure 5.5(a) while selectivity to C₆₊ olefin was obtained to be 65 %. However the effect of increasing temperature from 220 °C to 250 °C had no effect on C₆₊ olefin selectivity, while selectivity to C₆₊ paraffin hydrocarbon, increased from 54 % to 63 %. Similarly, the selectivity to C₄ and C₅ hydrocarbons, increased at changing temperature. Selectivity to C₄ paraffin increased from 0.3 to 20 % and selectivity to C₄ olefin increased to 11 % from 6 %. For C₅ hydrocarbon, olefin selectivity increased from 8 % to 21 % while selectivity too its paraffin counterpart increased from 6 % to 16 %. However, changing the temperature from 220 °C to 250 °C had no effect on the selectivity of the catalyst to C₆₊ olefin. In general, changing the temperature from 220 °C to 250 °C (while keeping other conditions :pressure, H₂/CO ratio and feed flow rate the same) resulted in the reduction of the product from C₁ to C₃ hydrocarbons with a significant increase in the production of C₄ as compared to C₅ hydrocarbons, mainly olefins. For C₆₊ HCs, no effect on olefin was observed but paraffin selectivity increased when temperature was increased. Also a high production of methane and C₂ hydrocarbon was observed at low temperature of 220 °C as opposed to 250 °C under the same pressure, flow rate and syngas composition (compare Figure 5.4 (a) and Figure 5.5 (b)).

Table 5.4: Effect of Pressure on Conversion

H ₂ /CO	GHSV (ml/gcat.hr)	Temperature (° C)	Pressure (bar)	% CO Conversion
1.5	1200	250	2	4.18
			8	4.48
			15	7.49

The discussion based on Table 5.2 and Table 5.3, as well as Figure 5.4 and Figure 5.5, focused on the change of temperature (220 °C to 250 °C) at low (2 bars) and high pressure (15 bars) respectively. Table 5.4 and Figure 5.6, was discussed based on the effect of changing pressure at

a constant high temperature of 250 °C, low flow-rate of 1200 GHSV and a 1.5 H₂ to CO ratio. As the pressure was increased from 2 bar to 8 bar and 15 bars, CO conversion also increased from 4.18 % to 4.48 % and 7.49 % respectively. This occurred at constant flow rate and temperature, with the most significant increase in CO conversion being from, 4.18 to 7.49 % for 8 bar and 15 bars respectively. Rao & Gormley (1990) reported a CO conversion of 47- 53 %, at a high temperature of 280 °C and pressure of 21 bars and H₂/CO ratio of 1, Hence, the results obtained and presented in Table 5.4 are lower than what Rao & Gormley (1990) reported.

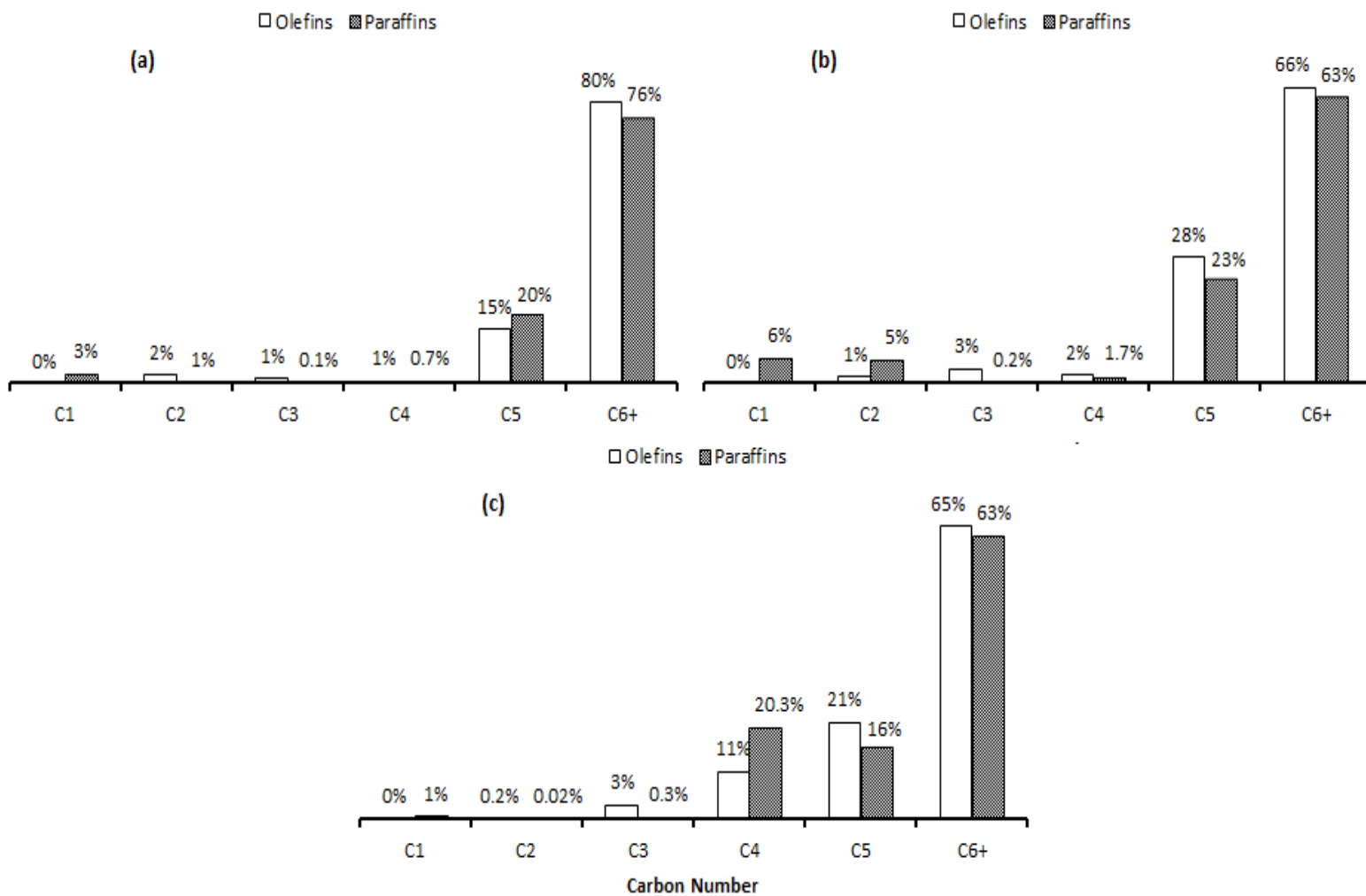


Figure 5.6: Olefin & Paraffin Selectivity at Pressure of (a) 2 bar (b) 8 bar and (c) 15 bar

Hydrocarbon selectivity of different carbon numbers at a reaction pressure of 2, 8 and 15 bars is depicted in Figure 5.6(a), (b) and (c) respectively, this is with respect to CO conversion obtained

from Table 5.4. An increase in pressure from 2 bars to 15 bars at the same flow rate and temperature resulted in a decrease in selectivity of the Co/H-ZSM-5 to C₆₊ hydrocarbon from 80 % to 65 % for olefins and 76 % to 63 % for paraffin. Similar results were obtained for C₆₊ hydrocarbon at 8 bar and 15 bar (66 % olefin and 63 % paraffin), this was shown in Figure 5.6(b) and Figure 5.6(c). Selectivity to C₅ hydrocarbon increased when pressure was increased from 2 bars to 8 bars, and then decreased when pressure was further increased to 15 bars, indicating that, the bi-functional catalyst is more selective to C₅ hydrocarbons at a pressure of 8 bar than at 15 bar, and more selective to C₄ hydrocarbons at a higher pressure of 15 bars. However, the Co/H-ZSM-5 catalyst remained less selectivity to C₁-C₃ hydrocarbons at all pressures with a considerable increase in selectivity at a 8 bars. Selectivity to methane was about 6 % and the bi-functional catalyst achieving 5 % of C₂ paraffin selectivity, while olefin of the same carbon number range remained minimal at < 2 % at all pressures. Rao & Gormley (1990) obtained selectivity of about 51 – 74 % for C₅₊ paraffins and 17 - 26 % for methane with less than 6 % selectivity to middle distillates. In general, as pressure is increased, CO conversion also increased and selectivity to higher hydrocarbons decreased. In addition, as pressure increased the production shifted towards C₄ and C₅ hydrocarbons while lower hydrocarbons remained produced at low rate throughout the reaction at conditions stated in Table 5.4.

Table 5.5: Effect of Syngas Composition on Conversion

H ₂ /CO	GHSV (ml/gcat.hr)	Temperature (° C)	Pressure (bar)	% CO Conversion
1.5	1200	250	15	7.49
2.5				53.77

The results and discussions above were based on the effect of changing process conditions (i.e. flow rate, temperature and pressure) on CO conversion and product distribution. One more aspect to consider is varying the feed composition. In this study, investigation of the effect of varying H₂/CO ratio reveals that increasing the H₂/CO ratio from 1.5 to 2.5, thus more hydrogen was present in the reactant feed than Carbon-monoxide, resulted in an increase of the CO conversion from 7.49 % to 53.77 % when the flow rate, reaction temperature and reaction pressure were kept constant at 1200 GHSV, 250 °C and 15 bars, respectively. Calleja *et al.*, (1995), had reported that an increase in H₂/CO ratio results in an increase in CO conversion and

a decrease in selectivity to C_{6+} hydrocarbons. The CO conversion is directly proportional to the hydrogen concentration in the feed, while the opposite trend is observed for C_{6+} hydrocarbons (Calleja *et al.*, 1995). Expectedly, it was observed from Table 5.5 that as hydrogen was increased in the reactant feed or rather when the H_2/CO ratio was increased from 1.5 to 2.5, CO conversion increased significantly from 7.49 % to 53.77 % at conditions stated in Table 5.5 and selectivity to C_{6+} hydrocarbons decreased from 65 % (olefin) and 63 % (paraffin) to 9 % per olefin and paraffin hydrocarbons (compare Figure 5.7(a) and Figure 5.7(b)). The resulting product distribution associated with these rapid increase in CO conversion due to increased H_2/CO ratio to 2.5 from 1.5, was defined in terms of selectivity, in order to study the effect of increasing H_2/CO ratio, these was shown in Figure 5.7.

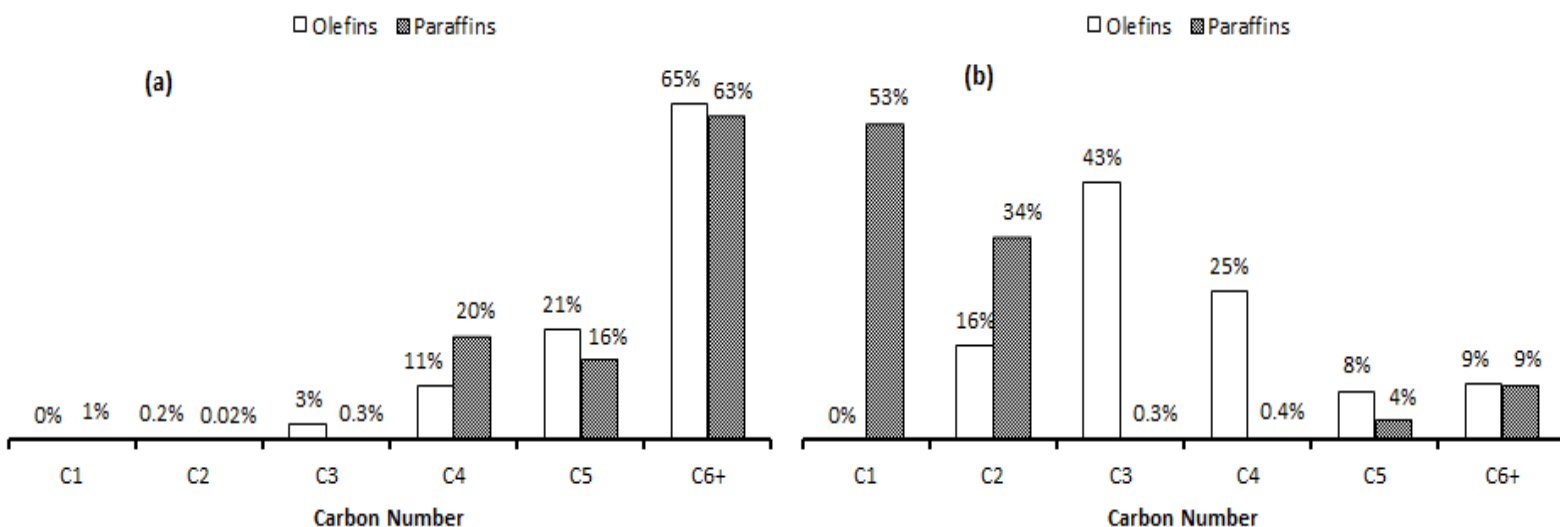


Figure 5.7: Olefin & Paraffin Selectivity at different syngas composition

Product selectivity shown in Figure 5.7(a) corresponds to a CO conversion of 7.49 % of which it was obtained at H_2 to CO ratio of 1.5 while Figure 5.7(b) corresponds to CO conversion of 53.77 % and a H_2/CO ratio of 2.5. It was observed from Figure 5.7 that a CO conversion of 53.8 % is due to the catalyst being more selective to methane and C_2 HCs production under conditions stated in Table 5.5 due to an increased H_2 concentration in the feed. Therefore an increase in H_2 to CO ratio resulted in a rapid increase of methane selectivity from 1 % to 53%, C_2 olefin increased from 0.2 % to 16 % and Co/H-ZSM-5 selectivity to C_2 paraffin also increased from 0.02 % to 34 %. Selectivity to higher hydrocarbon, C_{6+} , dropped from 65 % and 63 % to 9 % per

olefin and paraffin respectively, thus selectivity to olefin and paraffin obtained at a syngas H_2/CO ratio of 2.5 was similar due to increased H_2/CO ratio to 2.5 from 1.5, which is in agreement to reported findings by Calleja *et al.*, (1995).

Selectivity to paraffin of C_3 remained the same at 0.3 % while selectivity to $C_4 - C_{6+}$ paraffin decreased. The decrease in the selectivity to $C_4 - C_{6+}$ paraffin could be attributed to the higher hydrocarbon cut-off at these process conditions as a result of the presence of the zeolite acidic sites. This hydrocarbon cut-off is due to the presence of zeolites acidic sites that has been reported by Dagle *et al.*, (2014) and Mohanty *et al.*, (2011). According to the authors, the hydrocarbon cut-off was due to hydrocracking and hydro-isomerization of the primary Fischer-Tropsch products (mainly higher hydrocarbons). This occurrence breaks the Anderson-Schultz-Flory (ASF) hydrocarbon product distribution, thereby facilitating direct conversion of liquid fuel without the need for further hydro-treatment and limiting the FT product spectrum to $C_4 - C_5$. This phenomenon circumvents the hydrocracking and the hydro-isomerization stages required in the downstream process in refinery when the traditional catalyst is used. When comparing Figure 5.7(a) and Figure 5.7(b) the higher hydrocarbon cut-off occurred from C_4-C_{6+} carbon numbers, this was enhanced by increasing the ratio of H_2/CO ratio from 1.5 to 2.5, hence selectivity to these products dropped dismally.

Therefore, a higher H_2/CO ratio of 2.5 resulted in higher CO conversion and the bi-functional Co/H-ZSM-5 catalyst was more selective to C_1 and C_2 paraffins with more emphasis on methane (53 % of selectivity), at the conditions stated in Table 5.5. Sartipi *et al.*, (2013b) obtained about 26 % of methane selectivity by Co/H-ZSM-5 catalyzed reaction and attributed this high methane selectivity to a higher diffusion of H_2 when compared to CO, which resulted in yields towards middle distillates as evident and depicted in Figure 5.7(b). This brings to the conclusion that at the conditions stated in Table 5.5 (i.e. flow rate of 1200 GHSV, temperature of 250 °C, ratio of 2.5 and pressure of 15 bars) the bi-functional Co/H-ZSM-5 catalyst was less selective to higher paraffin hydrocarbons. This was predicted by Calleja *et al.*, (1995) with respect to the inversely proportion relationship of higher hydrocarbons and H_2 concentration as well as authors like Dagle *et al.*, (2014) and Mohanty *et al.*, (2011) who reported findings of higher hydrocarbon cut-off with respect to the acidic nature of the zeolite support and ASF product distribution. On the

other hand, Sartipi *et al.*, (2013b) attributed the decreased in higher olefin selectivity to high diffusion of H₂ gas molecules on the catalyst surface when compare to gas molecules of CO.

5.4. Comparison of the Bi-functional Catalyst with a Commercial Catalyst: Effect of operating conditions

In this section, the results discussed are based on the comparison of the synthesized bi-functional Co/H-ZSM-5 catalyst with a commercial Co/SiO₂ catalyst under similar process conditions.

Table 5.6: Comparison between Bi-functional and Commercial catalyst

Catalyst	H ₂ /CO	GHSV (ml/gcat.hr)	Temperature (° C)	Pressure (bar)	% CO Conversion
Co/H-ZSM-5	1.5	1200	220	2	2.64
Co/SiO ₂					15.48

Table 5.6, reports on the CO conversion obtained by using synthesized bifunctional Co/H-ZSM-5 and commercial Co/SiO₂ catalyst at a low flow-rate of 1200 GHSV, a temperature of 220 °C and a pressure of 2 bars. Co/H-ZSM-5 is considered as the bi-functional catalyst and Co/SiO₂ as the commercial catalyst. A CO conversion of 2.64 % was obtained by using Co/H-ZSM-5 catalyst; on the contrary a conversion of 15.48 % was obtained by using Co/SiO₂ as shown in Table 5.7. All *et al.*, (1995) has reported a CO average conversion of 3.3 % of which stabilized to 2.7 at steady state by using a Co/SiO₂ catalyst at 220 °C and 1.4 bars and a ratio of Hydrogen to Carbon monoxide of 2, while Yan *et al.*, (2009) had predicted CO conversion less than 1 % at 1 bar, H₂/CO ratio of 1 and temperature of 240 °C for Co/SiO₂ catalyzed reaction. However when comparing these findings to the results reported in Table 5.6, the bi-functional, Co/H-ZSM-5 catalyst is well in agreement with findings by All *et al.*, (1995) and Yan *et al.*, (2009).

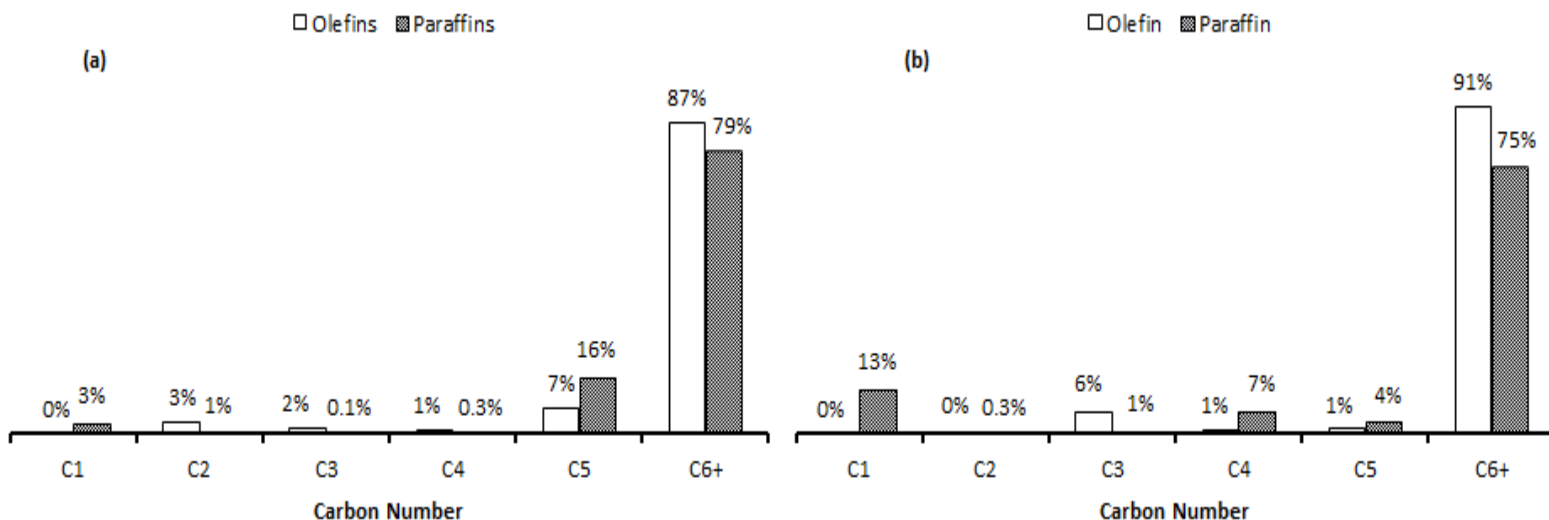


Figure 5.8: Hydrocarbon selectivity for (a) Co/H-ZSM-5 and (b) Co/SiO₂

In terms of the commercial Co/SiO₂ catalyst activity, it was found that it is less selective to C₆₊ paraffins (75 %), when compared to the bi-functional Co/H-ZSM-5 catalyst, which is 79 % selective to C₆₊ paraffin as shown in Figure 5.8. However Co/SiO₂ catalyst resulted in a higher selectivity to higher olefin (C₆₊) hydrocarbon production, about 91 % while selectivity of 87 % was obtained by using Co/H-ZSM-5 catalyst for the same HCs. The commercial catalyst, Co/SiO₂, was found to be least selective to C₂ paraffin and C₃ Olefin, with no selectivity for C₂ paraffin.

Sartipi *et al.*, (2013b) obtained 16-18 % of olefins selectivity by Co/SiO₂ catalyst and 18-50 % selectivity to olefins by Co/H-ZSM-5 catalyst. For lower hydrocarbons, Co/SiO₂ is more selective to C₃ olefins, 6 % selectivity was achieved, and 13 % selective to methane, while for higher hydrocarbon a higher selectivity of 91 % was obtained for C₆₊ olefins as shown in Figure 5.8(a) which also led to a higher CO conversion of about 15.48 % by Co/SiO₂ catalyzed reaction. The bi-functional catalyst managed to be more selective to C₆₊ paraffin and less selective to C₆₊ olefin with a minimum methane production as opposed to the commercial catalyst (compare Figure 5.8(a) with Figure 5.8(b)) which is a positive characteristic of the Co/H-ZSM-5 catalyst under the process conditions stated in Table 5.6.

Yan *et al.*, (2009), modelled the reaction of syngas with a ratio of H₂/CO of 1 and predicted a methane selectivity of about 60 % at temperature of 240 °C and a pressure of 1 bar using

Co/SiO₂ catalyst, while All *et al.*, (1995) performed experimental work and obtained 22 % of methane selectivity at 220 °C, 1 bar and H₂/CO ratio of 2. This confirms that Co/SiO₂ has a high selectivity for methane; on the contrary Sartipi *et al.*, (2013b) reported 20 % and 7 % of methane selectivity by using a Co/H-ZSM-5 and Co/SiO₂ catalysts respectively. This effect of H₂ to CO ratio, temperature and pressure is further studied at 250 °C H₂/CO ratio of 2.5 and pressure of 15 bars as shown in Table 5.7.

Table 5.7: Comparison between Bi-functional and Commercial catalyst on Conversion

Catalyst	H ₂ /CO	GHSV (ml/gcat.hr)	Temperature (° C)	Pressure (bar)	% CO Conversion
Co/H-ZSM-5	2.5	1200	250	15	53.77
Co/SiO ₂					67.90

Table 5.7, shows the CO conversion obtained by Co/H-ZSM-5 and Co/SiO₂ catalyzed reaction at a syngas ratio of 2.5, flow rate of 1200 GHSV , temperature of 250 °C and pressure of 15 bars. The resulting conversion at these conditions was found to be 53.77 % for Co/H-ZSM-5 bi-functional catalyst and 67.90 % for Co/SiO₂ commercial catalyst. These CO conversions are much higher than the ones reported in Table 5.6 due to different conditions, since each catalyst will behave differently at different conditions. Sartipi *et al.*, (2013b) obtained CO conversion of about 65 – 80 % for Co/SiO₂ catalyzed reaction, while 65 – 85 % was obtained for Co/H-ZSM-5 catalyzed reaction at 15 bars and ratio of 2, the obtained results in Table 5.7 are in agreement with the conversion obtained by Sartipi. The resulting product selectivity associated with the conversion reported in Table 5.7 is depicted in Figure 5.9 for each catalyst.

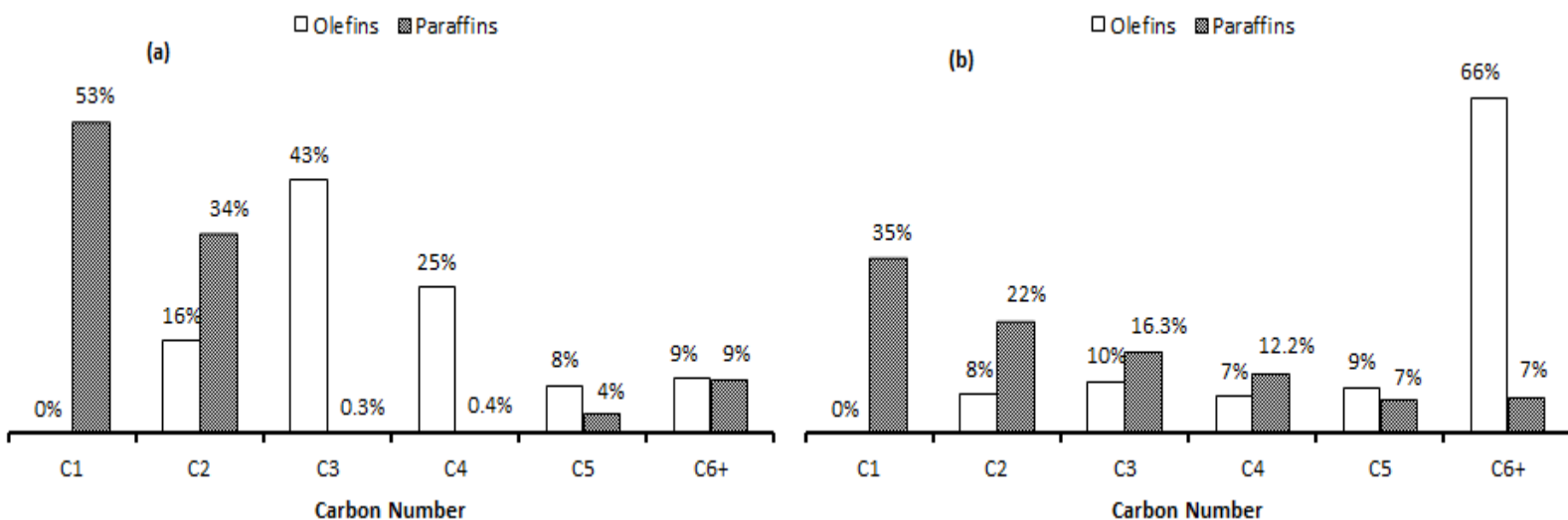


Figure 5. 9: olefin & Paraffin Selectivity based on (a) Co/H-ZSM-5 and (b) Co/SiO₂ catalyst

As mentioned above, Sartipi *et al.*, (2013b) obtained a higher methane selectivity of about 20 % by Co/H-ZSM-5 and 7 % by Co/SiO₂ catalyst. From Figure 5.9, the same characteristics was observed, were the bi-functional catalyst was highly selective to Methane over the commercial catalyst. A methane selectivity of 53 and 35 % was obtained by Co/H-ZSM-5 and Co/SiO₂ respectively, while 34 % and 2 % selectivity was obtained for C₂ paraffins. Sartipi *et al.*, (2013b) reported about 26 % of methane selectivity by Co/H-ZSM-5 catalyzed reaction which was three times higher than that obtained by Co/SiO₂ (8 %) and attributed this high methane selectivity to be a results of a higher diffusion of H₂ when compared to CO which also resulted in yields towards middle distillates as evident and reported in Figure 5.9. From Figure 5.9(b) it was observed that, paraffin selectivity decreased in an orderly manner while selectivity to olefin increased, thus an increase in olefin selectivity resulted in a decrease in paraffin selectivity of the same carbon number and vice versa. On the contrary for Co/H-ZMS-5 catalyzed reaction, Figure 5.9(a), the selectivity correlation of paraffins and olefins is random when compared to that of Co/SiO₂. Co/H-ZSM-5 produced a significant amount of C₂ - C₆₊ olefins with a maximum selectivity of 43 % and 25 % for C₃ and C₄ HCs respectively. 66 % selectivity to C₆₊ olefin is achieved as the maximum for Co/SiO₂ catalyzed reaction under similar conditions as Co/H-ZSM-5 catalyst. Sartipi *et al.*, (2013b), reported 15 % selectivity to paraffins by Co/SiO₂ catalyst and 18 % by Co/H-ZSM-5 with about 16 – 25 % of olefins by the SiO₂ supported catalysts and 18 -50 % by H-ZSM-5 supported catalyst, this is because Sartipi *et al.*, (2013b)

calculated iso-paraffin and olefin selectivity together. In general, comparing Figure 5.8 and Figure 5.9, increasing H₂ to Co ratio from 1.5 to 2.5, and temperature to 250 °C from 220 °C and a pressure of 15 bars, resulted in more production of lower hydrocarbons, with methane being more abundantly produced as the lower hydrocarbon per Co/H-ZSM-5 and Co/SiO₂ catalyst.

A significant drop of higher hydrocarbon selectivity was also observed, with a higher selectivity to C₆₊ olefin by using Co/SiO₂ catalyst. For Co/SiO₂ catalyzed reaction, about 0.5 - 1.5 g (by weight) of H₂O was formed by WGS reaction (Eq. (6), in section 2.1.3), while no water was formed by the bi-functional Co/H-ZSM-5 catalyst. CO₂ is neither formed nor produced by per Co/H-ZSM-5 and Co/SiO₂ catalyst under studied conditions reported in Table 5.7. These findings is in agreement with Yao *et al.*, (2010) and De Klerk & Furimsky, (2011) reported results in their studies. However based on Eq. (6), Co/SiO₂ was expected to form CO₂ of which all was converted to H₂O and CO by the reverse reaction of the WGS phenomena hence water was formed and no traces of CO₂ was detected or analyzed.

5.5. Summary

Chapter 5 dwelled on the results and discussion of the catalyst performance due to intended variations in process conditions i.e. Temperature, pressure, flow rate as well as the syngas feed composition. The discussed results were in terms of CO conversion and product selectivity. The Product distribution and or selectivity were based on two types of hydrocarbons, namely, olefins and paraffins. The FTS experimental setup was discussed in terms of how it was operated and how the process set-points were put in place during the course of the reaction. Effects of different pressure and flow rate were discussed as well as high and low temperature conditions (within the LTFT temperature range) were discussed in terms of CO conversion and selectivity. The bi-functional catalyst was compared to the commercial under similar conditions to determine which catalyst is more preferable for certain products and specific process conditions. The conclusion drawn from the results discussed in this chapter is reported in Chapter 7 of this dissertation.

5.6. References

- All S, Chen B, Goodwin Jr. J.G., 1995, Zr Promotion of Co/SiO₂ for Fischer-Tropsch Synthesis. *Journal of Catalysis*, 157(1), pp.35–41.
- Calleja G, de Lucas A, van Grieken R, 1995, Co/HZSM-5 catalyst for syngas conversion: influence of process variables. *Fuel*, 74(3), pp.445–451.
- Dagle R.A, Lizarazo-Adarme J.A, Dagle V.L, Gray M.J, White J.F, King D.L, Palo D.R, 2014, Syngas conversion to gasoline-range hydrocarbons over Pd/ZnO/Al₂O₃ and ZSM-5 composite catalyst system. *Fuel Processing Technology*, 123, pp.65–74. Available at: <http://dx.doi.org/10.1016/j.fuproc.2014.01.041>.
- De Klerk A, Furimsky E, 2011, Fischer – Tropsch Syncrude ” ,Platinum Metals Review, Vol. 55 (4), pp.263–267.
- Mohanty P, Pant K.K, Parikh J, Sharma D.K, 2011. Liquid fuel production from syngas using bifunctional CuO-CoO-Cr₂O₃ catalyst mixed with MFI zeolite. *Fuel Processing Technology*, 92(3), pp.600–608. Available at: <http://dx.doi.org/10.1016/j.fuproc.2010.11.017>.
- Motchelaho A.M.M, 2011, *Iron and Cobalt Catalyst Supported on Carbon Nanotubes for use in the Fischer-Tropsch Synthesis*, Msc Dissertation, University of The Witwatersrand.
- Moyo M, 2012. *Cobalt and Iron supported on Carbon Spheres Catalysts for Fischer-Tropsch Synthesis*, Msc Dissertation, University of The Witwatersrand, Johannesburg.
- Price J, 1994, *An Investigation into novel bimetallic catalysis for use in the FT reaction*, Msc Dissertation University of The Witwatersrand.
- Rao V.U.S, Gormley R.J, 1990, Bifunctional catalysis in Syngas Conversion, Elsevier Science Publishers, Pittsburg , pp.207–234.
- Sartipi S, van Dijk J.E., Kapteijn F, 2013a, Applied Catalysis A : General Toward bifunctional catalysts for the direct conversion of syngas to gasoline range hydrocarbons : H-ZSM-5 coated Co versus H-ZSM-5 supported Co. “*Applied Catalysis A, General*”, 456, pp.11–22. Available at: <http://dx.doi.org/10.1016/j.apcata.2013.02.012>.
- Sartipi S, Parashar K, Makkee M, Gascon J, Kapteijn F, 2013b, Breaking the Fischer–Tropsch synthesis

selectivity: direct conversion of syngas to gasoline over hierarchical Co/H-ZSM-5 catalysts. *Catalysis Science & Technology*, 3(3), p.572. Available at: <http://xlink.rsc.org/?DOI=c2cy20744c>.

Tristantini D, Logdberg S, Gevert B, Borg O, Holmen A, 2007, The effect of synthesis gas composition on the Fischer-Tropsch synthesis over Co/ γ -Al₂O₃ and Co-Re/ γ -Al₂O₃ catalysts. *Fuel Processing Technology*, 88(7), pp.643–649.

Yan Z, Wang Z, Bukur D.B, Goodman D.W, 2009, Fischer-Tropsch synthesis on a model Co/SiO₂ catalyst. *Journal of Catalysis*, 268(2), pp.196–200. Available at: <http://dx.doi.org/10.1016/j.jcat.2009.09.015>.

Yao Y, Hildebrandt D, Glasser D, Liu X, 2010, Fischer - Tropsch Synthesis Using H₂ / CO / CO₂ Syngas Mixtures over a Cobalt Catalyst, *Industrial & Engineering Chemistry Research*, Vol 49, pp.11061–11066.

Yoon S.J, Lee, J.G, 2012. Hydrogen-rich syngas production through coal and charcoal gasification using microwave steam and air plasma torch. *International Journal of Hydrogen Energy*, 37(22), pp.17093–17100. Available at: <http://dx.doi.org/10.1016/j.ijhydene.2012.08.054>.

CHAPTER 6: EFFECT OF CO₂ CO-FEEDING ON THE PERFORMANCE OF THE BI-FUNCTIONAL Co/H-ZSM-5 CATALYST DURING FTS

6.1. Introduction

Management of waste has always been a crucial and delegated responsibility, undertaken on behalf of the industry, public authorities and waste management specialist. Waste accumulation has been known to create various problems to the environment and to the human health. These problems are worsened when waste accumulates at incorrect landsite (Phale, 2005). However to solve environmental problems and ensure a sustainable living, we must rethink and restructure basic human systems, which includes waste management. Garbage control is also of greater concern to those interested in structuring a sustainable future. For this reason, the need for environmentally acceptable waste disposal has also become a priority in South Africa.

One of the ways of beneficiating the waste is to gasify them and convert the products of the gasification (typically syngas, CO and H₂) to liquid fuel via the Fischer-Tropsch synthesis. During the gasification of biomass waste, such as corncob, woody biomass to mention a few, 8-12 % of CO₂ is produced. Separation of CO₂ from the gasification products to obtain the syngas for FTS requires additional operating costs. The CO₂ co-feeding could have beneficial or detrimental effect on the FTS process, especially the reactivity of the catalyst. Therefore effect of CO₂ co-feeding on the performance of a bi-functional Co/H-ZSM-5 catalyst during FTS was investigated and the results discussed in this Chapter.

A bi-functional Co/H-ZSM-5 catalyst was prepared by the wetness impregnation of cobalt onto H-ZSM-5 as described in Chapter 3 of this dissertation. The prepared catalyst was characterized using N₂ physisorption at 77 K for BET surface area, pore volume and pore size. Textural and structural morphologies were checked with Transmission Electron Microscopy (TEM) and Scanning Electron Microscopy. Energy Dispersive Spectroscopy (EDS) was used to determine the elemental composition of the catalyst. The reduction temperature of the catalyst was determined by using H₂-TPR. Detailed information about the results of characterization of the catalyst is provided in Chapter 4. Evaluation of the effect of CO₂ co-feeding on the catalyst was carried out at as syngas flow-rate of 1200 GHSV (ml/gcat.hr), pressure of 15 bars, reaction temperature of 250 °C, and H₂/CO ratio of 2.5 with a gas mixture that contained 5 % of CO₂.

The reaction mixture was analyzed using a pre-calibrated gas chromatograph (GC); and the results were compared to the results obtained with syngas mixture that contained CO₂ under similar conditions.

6.2. Results and Discussion

Table 6.1 shows the results obtained for the effect of CO₂ co-feeding on the performance of the bi-functional Co/H-ZSM-5 catalyst. In the presence of CO₂ co-feeding, CO conversion of 73.7 % was obtained and CO conversion of 53.7% was obtained for the reaction without CO₂ co-feeding. In addition, the co-fed CO₂ was converted to hydrocarbons and a CO₂ conversion of 63.5 % was obtained.

Table 6.1: Effect of CO₂ co-feeding on the rate of conversion Co/H-ZSM-5 catalyzed reaction

H ₂ /CO	% CO ₂	GHSV (ml/gcat.hr)	Temperature (° C)	Pressure (bar)	% CO Conversion	% CO ₂ Conversion
2.5	0	1200	250	15	53.7	-
	5				73.7	63.5

A CO conversion of 53.7 % was obtained for Co/H-ZSM-5 catalyzed reaction at 250 °C, reactant flow rate of 1200 GHSV and a pressure of 15 bars with a syngas ratio of 2.5 without CO₂. Once a syngas mixture containing 5 % of CO₂ was used the CO conversion was observed to increase to 73.7 %, also the CO₂ was hydrogenated to form hydrocarbons, resulting in its conversion to be 63.5 % as shown in Table 6.1. Yao *et al.*, (2010) reported CO conversion of about 20 % of CO conversion when about 5 % of CO₂ was present in the feed, resulting in about 0.4 % of CO₂ conversion for Co-catalyzed reaction at 200 °C, pressure of 20 bar, flow rate of 3600 GHSV and H₂/CO ratio of 2, in the absence of CO₂ Yao *et al.*, (2010) obtained a CO conversion of 14.6 % which is lower than the one obtained in this study (see Table 6.1 for the Co-catalyzed reaction). From this it can be concluded that for a synthesized Co/H-ZSM-5 catalyzed reaction, the presence of CO₂ drove the rate at which CO is converted to products resulting in a high CO conversion when compared to reaction in which CO₂ is not present.

Figure 6.1 depicts a Co/H-ZSM-5 catalyzed reaction for a syngas mixture of H₂ to CO ratio of 2.5 with 0 % CO₂ and with 5 % CO₂ in the feed. It can be observed from Figure 6.1, that the presence of CO₂ gives a minor or no change in paraffin selectivity. In the presence of CO₂ co-

feeding, the selectivity of the bi-functional Co/H-ZSM-5 catalyst was 53 % to methane, 34 % to C₂, < 4 % to C₄-C₅ and less than 10 % to C₆₊. These values are more or less the same as the selectivity obtained to these HCs without CO₂ co-feeding. Yao *et al.*, (2010) reported that paraffin selectivity in particular methane, selectivity increased with a decrease in CO partial pressure. In this study the CO partial pressure was kept constant while the partial pressure of N₂ was affected with the introduction of CO₂ gas (changed from 15 % to 10 % while the CO₂ was 5 %). Therefore the results obtained in this study are in agreement with Yao *et al.*, (2010) regarding selectivity to paraffin, in particular methane. It was observed that co-feeding CO₂ affected the selectivity to olefins as well. The selectivity of C₃ olefin decreased from 43 % to 35 % while C₄ olefin increased from 25 % to 32 %. In addition, the C₆₊ olefin increased from 9 % to 15 % when the syngas was co-fed with CO₂. The findings in this study are not in agreement with the report of Yao *et al.*, (2010).

Yao *et al.*, (2010) in their study reported that if the ratio of CO₂ to CO in the CO₂ co-feeding is less than 50 % for a Co catalyzed reaction, the CO₂ will behave as an inert gas and will not be hydrogenated. In contrary to this report, results from this study show that in the presence of CO₂ and at a CO₂/CO ratio much more less than 50 % hydrogenation of CO₂ occurs to an extent, thus making CO₂ not fully an inert gas under conditions stated in Table 6.1. The increase in the selectivity to higher olefin from 9 % to 15 % in the presence of CO₂ could be attributed to the speculation that when most of the CO has been hydrogenated to methane and ethane, the remaining CO is not enough to produce C₃₊ paraffin. Hence, the reaction opted for CO₂ to react, resulting thereby in more olefins since CO₂ reaction favors olefin production. Also Yao *et al.*, (2010) obtained selectivity of 15 % to methane in the presence of CO₂, but failed to have identified distinctively other hydrocarbons formed during the reaction but rather grouped them as C₂₊ with which 85 % selectivity was obtained.

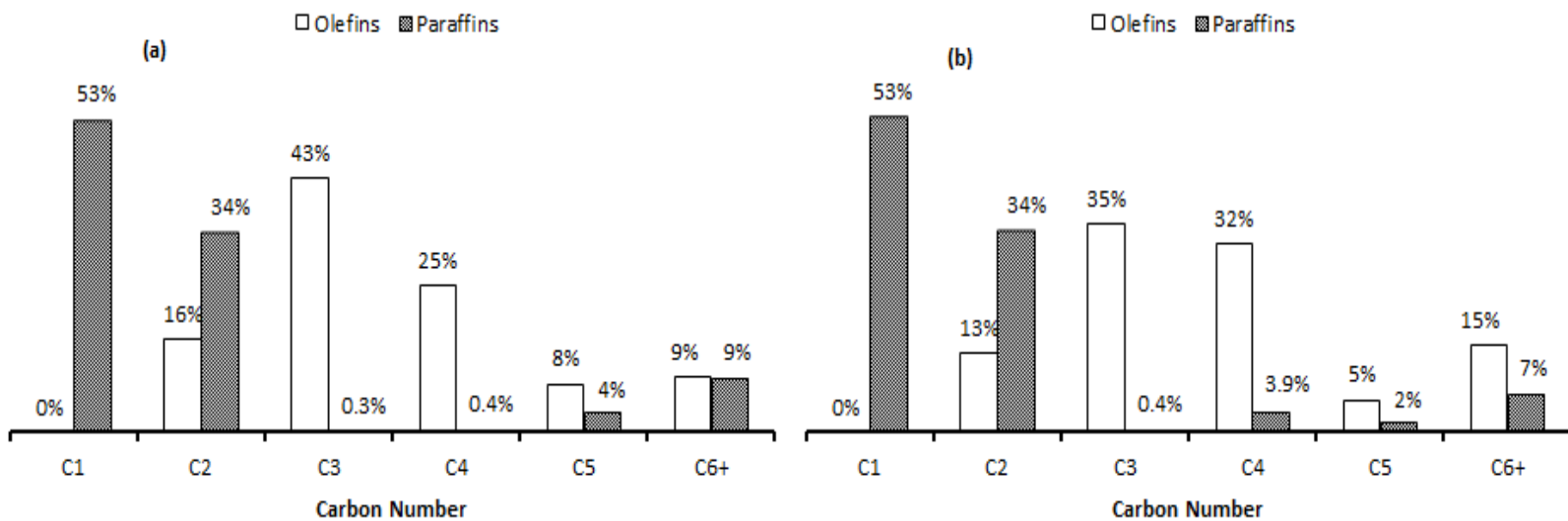


Figure 6.1: Change in Olefin & Paraffin Selectivity in the absence of CO₂ (a) and in presence of CO₂ (b)

It could be concluded that CO₂ co-feeding increases the catalyst selectivity to intermediate olefin carbon number and enhances CO conversion. The enhanced CO conversion when CO₂ is present could be attributed to olefin formation; also the CO₂ is converted to olefins since no change in the obtained paraffin selectivity was observed. Therefore under similar conditions, a syngas with or without CO₂ content will offer the same paraffin selectivity with a higher CO conversion, however when CO₂ is introduced more olefins are produced and production of paraffin remains the same throughout the reaction duration when using Co/H-ZSM-5 to catalyze the reaction.

6.3. Comparison of the bi-functional catalyst and commercial catalyst in the presence of CO₂

Table 6.2, shows the performance of the bi-functional Co/H-ZSM-5 catalyst compared with commercial Co/SiO₂ catalyst in the presence of CO₂ co-feeding under similar conditions.

Table 6.2: Comparison between Bi-functional and Commercial catalyst on Conversion in the presence of CO₂

Catalyst	H ₂ /CO	% CO ₂	GHSV (ml/gcat.hr)	Temperature (° C)	Pressure (bar)	% CO Conversion	% CO ₂ Conversion
Co/H-ZSM-5	2.5	5	1200	250	15	73.75	63.59
Co/SiO ₂						70.35	75.30

From Table 6.2, CO conversion of 73.75 % and 70.35 % were obtained for Co/H-ZSM-5 and Co/SiO₂ catalysts respectively, in the presence of CO₂ co-feeding, making the conversion from the Co/H-ZSM-5 catalyst to be about 3 % higher than that of the commercial catalyst. Figure 6.2 shows that the selectivity of the catalyst to methane was 53 % (see Figure 6.2(a)). In the presence of CO₂ co-feeding, the CO₂ conversion of the bi-functional catalyst was 63.59 % and it was 75.3 % for the commercial catalyst. Most of the CO₂ that reacted contributed mainly to olefin production; hence a high selectivity of 76 % to C₆₊ olefin was for the Co/SiO₂ catalyzed reaction (see Figure 6.2(b)), resulting in a CO₂ conversion of 75.3 %. On the other hand, CO₂ reacted when Co/H-ZSM-5 catalyst was used and yielded almost uniform distribution of C₂ to C₄ olefins.

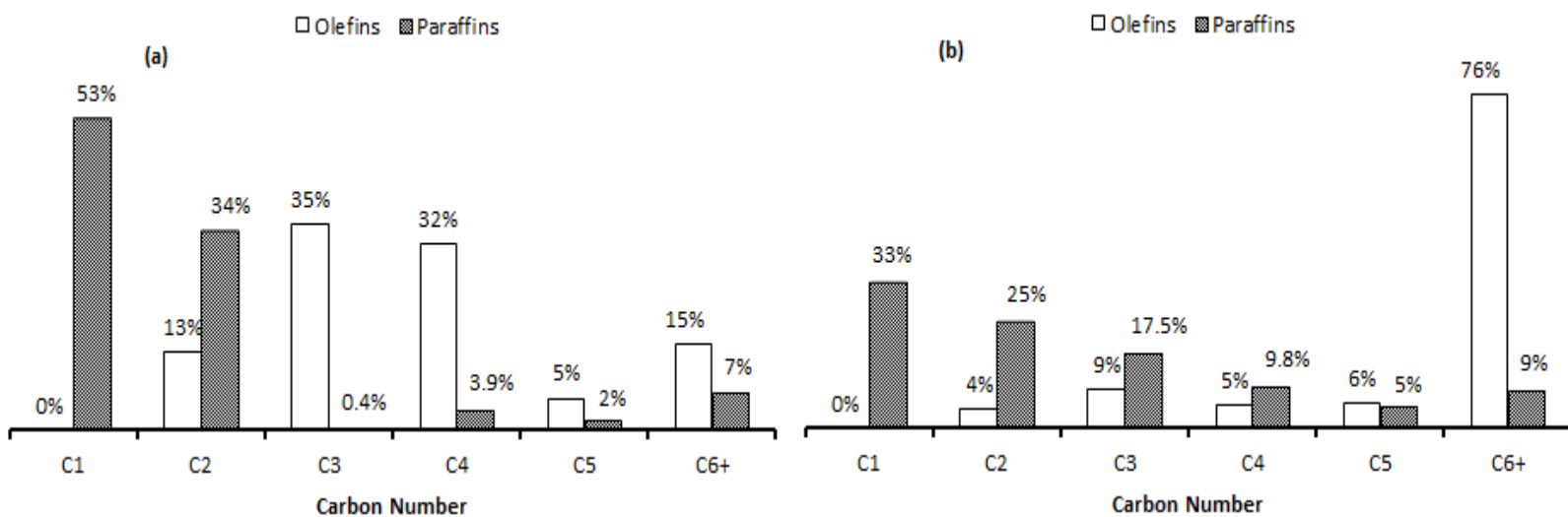


Figure 6.2: Olefin and Selectivity in the presence of CO₂ for (a) Co/H-ZSM-5 and (b) Co/SiO₂ catalyst

From Figure 5.9(b) (in Chapter 5) and Figure 6.2(b) it can be observed that a syngas mixture with a higher H₂ to CO ratio and CO₂ present, results in a slight increase in paraffin selectivity for a Co/SiO₂ catalyzed reaction. However a significant increase in selectivity to C₆₊ olefin was recorded in the presence of CO₂ co-feeding (compare Figure 5.9 in Chapter 5 to Figure 6.2 in Chapter 6). When comparing Figure 6.2(a), which is the product selectivity of Co/H-ZSM-5 catalyzed reaction, to Figure 6.5(b), which is the product selectivity of Co/SiO₂ catalyzed reaction, it is observed that the presence of CO₂ in the feed increased the selectivity to olefin with Co/H-ZSM-5 producing more middle olefin hydrocarbons, meanwhile for Co/SiO₂ catalyst, selectivity to lower and middle olefin increased, their counterpart paraffin also slightly increased.

Thus for Co/SiO₂ catalyzed reaction in the presence of 5 % CO₂, both C₁ to C₆₊ hydrocarbon selectivity increased with the catalyst being more selective to C₆₊ olefin. On the contrary for Co/H-ZSM-5 an increase in selectivity to olefin resulted in a decreased or no change in selectivity to paraffin hydrocarbons. However the presence of CO₂ co-feeding only affected selectivity to olefins. Thus selectivity to olefins increased while selectivity to paraffins remained the same or slightly decreased (see Figure 6.1(a) and Figure 6.2(a)). The water formation increased from 0.5 – 1.5 g, when no CO₂ is present (see selectivity to HCs in Figure 5.9) to about 2 - 3.5 g (by weight) for Co/SiO₂ catalyzed reaction (see equation (6) which is the WGS reaction, producing H₂O by its reverse reaction) when CO₂ is present (see Figure 6.2 for selectivity to HCs) this also contributed to higher CO₂ conversion. These results agree with findings of Dorner *et al.*, (2009) where water production due to reverse WGS reaction in the presence of CO₂ is reported.

6.4. Summary

Similarly to Chapter 5, Chapter 6 outlined in detail the performance of the bi-functional Co/H-ZSM-5 catalyst and the commercial Co/SiO₂ catalyst in the presence of CO₂ co-feeding. The effect of CO₂ co-feeding was evaluated under specified process conditions as stated in Table 6.2. Conversion and selectivity results obtained when CO₂ was present in feed were compared to results obtained in the absence of CO₂. Also the performance of the bi-functional catalyst was compared to that of a commercial catalyst in terms of, which products are favoured as well as how the conversion of CO was affected. The co-fed CO₂ was converted to hydrocarbons and a CO₂ conversion of 63 % was obtained for the bi-functional catalyst. In terms of selectivity, both syngas (with CO₂ co-feeding and without CO₂ co-feeding) gave similar product selectivity to paraffins. The bi-functional catalyst was 53 % selective to methane, 34 % to C₂, < 4 % to C₃-C₅ and less than 10 % selective to C₆₊ HCs. It was observed that co-feeding CO₂ affected the olefin selectivity as well, for most olefin HCs selectivity increased. However, the C₆₊ increased from 9 % to 15 % when the syngas was co-fed with CO₂. The results reported in this chapter have been accepted as a contribution in the form of an oral presentation at the 33rd Pittsburgh International Coal Conference, 8-12 August 2016, Cape Town, South Africa. A full length paper is in preparation for submission to the conference for inclusion in the conference proceedings.

6.5. References

- Dorner R.W, Hardy D.R, Williams F.W, Davis B.H, Willauer H.D, 2009, Influence of Gas Feed Composition and Pressure on the Catalytic Conversion of CO₂ to Hydrocarbons Using a Traditional Cobalt-Based Fischer- Tropsch Catalyst. *Energy & Fuels*, 23(August 2008), pp.4190–4195. Available at: <http://pubs.acs.org/doi/abs/10.1021/ef900275m>.
- Yao Y, Hildebrandt D, Glasser D, Liu X, 2010, Fischer - Tropsch Synthesis Using H₂ / CO / CO₂ Syngas Mixtures over a Cobalt Catalyst, *Industrial & Engineering Chemistry Research*, Vol 49, pp.11061–11066

CHAPTER 7: CONCLUSION & RECOMMENDATIONS

The conclusion from this study and recommendations for future research are discussed in this chapter.

7.1. Conclusion

Management of waste has always been an important factor to ensure a healthy and clean environment, in an ever increasing population. Industries, waste management authorities and the public have taken interest and responsibility on management of waste; this is because accumulation of waste with no control has resulted in environmental and health problems. However to ensure a sustainable living and solve health and environmental problems which are a results of illegally dumped waste, different processes and studies have been devoted in either reuse, recycle and reducing waste materials. Other studied processes include gasification of waste biomass, garbage and used tyres. Gasification process results in syngas as the final product, this syngas is a mixture of H_2 , CO and CO_2 in different proportion depending on the gasification feed material. In South Africa it was found that about 20-28 million of tyres (in number) are dumped illegally in landsite with an average increase of 9.3 million a year as it was predicted in 2005 (Mahlangu, 2009). This is because no regulations or measurement are put in place to reduce tyre accumulation and to control their disposal; hence this study was devoted in recovering energy from biomass and used tyres to produce liquid fuel from a simulated syngas obtained from gasification of these waste. This was approached by implementing the following research questions and objectives:

The following research questions were attended to in this study:

- Can the use of bi-functional Co-based catalyst supported on H-ZSM-5 yield liquid fuel from waste-based syngas via FTS?
- How does the performance of this synthesized catalyst during FTS compare with the performance of the commercial Co-based FTS Catalyst?
- What will be the effect of CO_2 co-feeding with H_2/CO on the performance of the catalyst during FTS?
- What will be the effect of operating variables such as reaction temperature, pressure, reaction time and H_2/CO ratio on the performance of the catalyst?

To fulfill the above research questions the following objectives were implemented:

- Synthesis and characterization of a bi-functional Co-based catalyst supported on H-ZSM-5 zeolite.
- Evaluation of the performance of the synthesized catalyst in terms of reactivity (activity and selectivity) and hydrocarbon distribution during the conversion of syngas to liquid fuels via FTS and comparison between this performance and that of a commercial Co-based FTS catalyst (Co/SiO₂).
- Studying the effect of CO₂ co-feeding on the performance of the catalyst during FTS reaction
- Investigation of the effect of operating variables such as temperature, pressure, reaction time, H₂/CO ratio on the performance of the catalyst.

A Co-based bi-functional catalyst (Co/H-ZSM-5) was successfully synthesized by wetness impregnation method of a cobalt-solution (prepared by dissolving cobalt-hexahydrate crystals in deionized water) onto an H-ZSM-5 support, which is a calcined form of ammonium ZSM-5. This method of synthesis was outlined in detail in Chapter 4 of this dissertation. The bi-functional Co/H-ZSM-5 catalyst was characterized by several techniques, including N₂ physisorption, XRD, SEM/EDS, TPR TEM and TGA, and these results were presented in Chapter 4 of this dissertation. BET surface area, pore volume and pore size were obtained from the N₂ physisorption. Crystallinity and composition was checked by an XRD analysis at a 0° to 90 ° 2θ region. Catalyst reduction condition, from metal-oxide to metallic-cobalt was determined by TPR, while thermal stability and decomposition of the catalyst was determined by TGA. Catalyst morphology and elemental composition was checked by a TEM analysis as well as the metal dispersion throughout the zeolite support.

From the XRD analysis discussed, section 4.3.2, it was concluded that ZSM-5 is a highly crystalline structured material, which is mostly composed of simple cubic, body-centred and face-centred structured elements such as silicon, aluminium, oxygen and hydrogen resulting in an overall orthorhombic crystal structure. The comparison of synthesized ZSM-5 and H-ZSM-5 with the simulated International Zeolite Association database of the same zeolites showed the best correlation between these data as depicted in Figure 4.5. The presence of metallic Cobalt was confirmed by comparing the diffracted peaks of Co/H-ZSM-5 to those of Cobalt metal

obtained from The American Mineralogists Crystal Structure database. The use of Scanning Electron Microscopy analysis coupled with Energy Dispersion X-ray Spectroscopy (SEM/EDX/EDS) also confirmed the presence cobalt metal in Co/H-ZSM-5 catalyst as well as other elements of interest.

From section 4.3.1 , ZSM-5 had the highest total surface area of 369 m²/g while Co/H-ZSM-5_1 had the least total surface area of 273 m²/g, Sartipi *et al.*, (2013b) obtained the total surface area of zeolite to be in the range of 52 – 414 m²/g, with H-ZSM-5 having the least surface area of 52 m²/g. Each sample was classified as meso-porous to intermediate pore size, by using Che & Védrine (2012) pore size classification range, although Du & Wu (2007) stated that zeolites are known to be micro-porous materials with a pore size of about 0.57 nm. H-ZSM-5 had the highest pore size of 3.034 nm with Co/H-ZSM-5 having the least pore size of 2.828 nm which correspond well to that obtained by Sartipi *et al.*, (2013b) which was in the range of about 4-8 nm. Lastly the pore volume of the samples ranged between 0.185 - 0.244 cm³/g, while ZSM-5 and Co/H-ZSM-5_1 samples had the highest and the least pore volume respectively.

The catalyst morphology was obtained to be rounded and aggregated with little or no presence of void between the solid particles (high level of agglomeration) and a cobalt-metal composition of 25 % due to a two-step impregnation of the solution on the support was obtained. The high interaction of the cobalt-metal with the zeolite support increased the catalyst thermal-stability and about 2 % of mass was lost at temperatures below 200 °C which is the mass (%) of catalyst expected to be lost during the Fischer-Tropsch catalyst evaluation process at Low-Temperature Fischer-Tropsch (LTFT), this was determined by a TGA analysis. From the catalyst reduction profile it can be concluded that the reduction temperature is between 320-330 ° C and the bi-functional catalyst is fully reduced at about 330 °C. Also from the TPR analysis it was found that cobalt has a high oxidation state due to its high reduction temperature resulting in strong interaction of the Cobalt-metal with the H-form of zeolite support (H-ZSM).

With respect to operating conditions: low flow rate yielded a higher conversion and a higher flow-rate resulted in a lower conversion i.e. when the flow-rate was increased, the rate at which the reactants were converted to products decreased, this is due to insufficient contact time of the reactants with the catalyst active sites. The bi-functional catalyst, Co/H-ZSM-5, was more selective to olefins in particular, C₅ and C₆₊ olefins, at all studied flow rates (1200, 2800 and

3600 GHSV), also high flow-rates offered an efficient separation between the formed products which was easily distinguished from each other during analysis since no overlap of peaks occurred. For a bi-functional Co/H-ZSM-5 catalyzed reaction, olefin selectivity decreased with an increasing flow-rate while selectivity to paraffin increased under similar conditions. At low process conditions such as pressure, temperature and flow rate as well as a low H₂ to CO ratio, the bi-functional catalyst yielded a minimum amount of methane and the catalyst was less prone to middle distillates hydrocarbon production, and also no CO₂ formation and water production.

When temperature was increased, CO conversion increased significantly, and a sharp drop or cut-off of higher hydrocarbon (C₆₊) production is noted (see Figure 5.7(b)). This higher hydrocarbon cut-off mostly occurs at higher process conditions, i.e. at 250 °C, pressure of 15 bars and H₂/CO ratio of 2.5 as experienced in this study. Sartipi *et al.*, (2013b) also experienced the same higher hydrocarbon cut-off for Co/H-ZSM-5 catalyzed reaction at 240 °C, pressure of 15 bars and H₂ to CO ratio of 2. At this point, Fischer-Tropsch-Synthesis ASF distribution gets broken at the upper limit of gasoline range hydrocarbons, since longer hydrocarbons are more prone to conversion reactions. This hydrocarbon cut-off is what Dagle *et al.*, (2014) and Mohanty *et al.*, (2011) reported in their studies, that hydrocracking and hydro-isomerization of the primary Fischer-Tropsch products is considered to occur on the acidic sites of zeolite supported catalyst by breaking the Anderson-Schultz-Flory (ASF) hydrocarbon product distribution thus facilitating direct conversion of liquid fuel without the need for further hydro-treatment and limiting the FT product spectrum to C₄ – C₅, which is in contrast to petroleum derived products that requires downstream hydrocracking and hydro-isomerization stages (Sartipi *et al.*, 2013b). Hence Sartipi *et al.*, (2013b) titled their studies “Breaking the Fischer-Tropsch Synthesis Selectivity...” due to this outcome, which is a positive characteristic of the bi-functional catalyst.

For syngas with an increased H₂ to CO ratio, conversion of the reactants to products increased significantly and resulting in selectivity to shift towards methane and lower hydrocarbons, with middle distillates olefin being produced in large quantities while C₆₊ paraffin hydrocarbons simultaneously get cut-off. At a low pressure (2 bar), low temperature (220 °C) , low flow-rate (1200 GHSV) and H₂ to CO ratio of 1.5, the commercial catalyst (Co/SiO₂) catalyst readily converted CO to products when compared to the bi-functional catalyst , this is because the

conversion obtained by SiO₂ supported catalyst (about 15.48 %) is higher than that obtained by H-ZSM-5 supported catalyst (about 2.64 %) under similar conditions. However in terms of selectivity, Co/H-ZSM-5 was more selective to higher hydrocarbons (79 % selective to C₆₊ paraffin), while Co/SiO₂ was more selective to methane (13 % selectivity) and 91 % selective to C₆₊ olefins (at 220 °C as depicted in Figure 5.8).

At a high process conditions (250 °C, 15 bars and H₂/CO of 2.5) the two catalysts, Co/H-ZSM-5 and Co/SiO₂, almost attained the same conversion with about 53 % and 67 % for H-ZSM-5 and SiO₂ supported catalyst respectively. At this stated conditions the bi-functional catalyst was observed to produce 53 % selectivity to methane as opposed to 31 % selectivity by the commercial catalyst. Sartipi *et al.*, (2013b) obtained 26 % and 8 % methane selectivity for Co/H-ZSM-5 and Co/SiO₂ catalyst respectively. It was concluded that higher methane level above expected AFS distribution by Cobalt-based catalysts, implies that a secondary reaction of CO hydrogenation occurred in addition to the primary FTS reactions. The commercial catalyst distributed the formed products in an orderly manner (i.e. increasing olefins while paraffins are decreasing see Figure 6.2) as opposed to the bi-functional catalyst in which the products were randomly distributed at high process conditions. CO₂ was produced by the two catalysts; however Co/SiO₂ resulted in some amounts of water due to the reverse path of the water gas shift (WGS) reaction.

When co-feeding CO₂ into the FTS system, CO conversion increased and was converted at a higher rate than CO₂, thus the rate of hydrogenation is higher for CO than for CO₂ as it is adsorbed faster on the catalyst surface than CO₂, this was with regard to H-ZSM-5 supported catalyst. Although Yao *et al.*, (2010) stated that if the CO₂ to CO ratio is less than 50 % no hydrogenation of CO₂ will occur, it will act as an inert gas or inhibitor, this was proven otherwise, since CO₂ was hydrogenated to form hydrocarbons at a low CO₂ to CO ratio of 16.667 %. Hyun *et al.*, (2014) stated that the presence of CO₂ will negatively influence the performance of the catalyst due to partial competition between CO and CO₂ adsorption behavior, this was proven otherwise since the presence of CO₂ increased the adsorption of CO on the catalyst surface resulting in a higher conversion of CO for both H-ZSM-5 and SiO₂ supported catalyst, the only negativity noted was that, if one desires higher paraffins hydrocarbon production, the presence of CO₂ will result in more methane and olefin formation. For H-ZSM-5

supported cobalt catalyst the presence of CO₂ does not affect paraffin product distribution, thus no change or insignificant change occurred in paraffin selectivity, however the olefin selectivity of higher hydrocarbon decreased and attempted to evenly distribute middle olefin distillates selectivity, no water formation by WGS in Zeolite supported catalyst, therefore CO₂ is directly converted to products, in particular olefins. For Co/SiO₂ catalyzed reaction, also no change in selectivity to paraffin however the olefin selectivity increased in an orderly manner from lower, middle to higher olefins, also in the presence of CO₂ water production doubles, Dorner *et al.*, (2009) also mentioned that the presence of CO₂ results in the reverse of WGS reaction. Similarly to the bi-functional catalyst the commercial catalyst CO conversion increases when CO₂ is present however CO and CO₂ are almost adsorbed at the same rate on the SiO₂ supported catalyst; this is evident with the obtained conversion being almost the same as depicted in Table 6.2. Thus, they both follow the same adsorption path (Yao *et al.*, 2010) on SiO₂ supported catalyst. Also the presence of CO₂ has been a known factor, to contribute in shifting the reaction to more methane production; this was evident in both catalysts. In general CO₂ can be hydrogenated successfully along with CO in FTS over cobalt-based catalyst, this is in support of Yao *et al.*, (2010) and Dorner *et al.*, (2009) findings, even at low ratio (see Eq. (11) in section 6.2) as opposed to Yao *et al.*, (2010). It was also proven that CO₂ is neither formed or produced during Co-catalyzed FTS reaction this is in agreement well with Yao *et al.*, (2010).

In general based on the performance evaluation, the bi-functional catalyst in deed can yield liquid fuel production or higher hydrocarbons from waste based synthetic gas. The bi-functional catalyst also displayed evident for no requirement of downstream hydrocracking processes by cutting-off higher hydrocarbons to gasoline range products of which the commercial catalyst was unable to achieve. The comparison of Co/H-ZSM-5 to Co/SiO₂ catalyst on performance is more related to process conditions. At low process conditions (see Table 5.6 and Figure 5.8) the Co/SiO₂ resulted in a higher conversion but high methane production and water also C₆₊ olefin (undesired product) selectivity was high while Co/H-ZSM-5 resulted in low methane production, no water formation and high C₆₊ paraffins were produced which are the desired products. So the Co/HZSM-5 bi-functional catalyst is preferred at these conditions.

For high process conditions (see Table 5.7 and Figure 5.9), similar to low process conditions, Co/SiO₂ resulted in a higher conversion with paraffins produced in an orderly manner for all

carbon numbers (C_1 to C_{6+}) but the Co/SiO_2 was more favorable to C_{6+} olefins which is an undesired product. On the contrary the bi-functional $Co/H-ZSM-5$ catalyst, produced more methane than Co/SiO_2 with middle distillates olefins (but no paraffins) and 9 % of C_{6+} paraffin (desired product) as opposed to 7 % by Co/SiO_2 , so the commercial catalyst is preferred under this conditions since it offers paraffin oaf all carbon number range. In terms of CO_2 co-feeding, the presence of CO_2 increases conversion of CO to olefin at low or high process conditions and CO_2 itself is hydrogenated to form products for either catalyst with no or little change in paraffin product distribution, so either catalyst can be used when CO_2 isco-fed, but preferably the bi-functional will perform better than Co/SiO_2 due to its water elimination and no CO_2 formation and still offers hydrocracking abilities of which Co/SiO_2 did not possess. For more details on maximizing production of gasoline and diesel range products (C_{6+} paraffin's), see section 7.2 which gives some few recommendations that can be applied.

7.2. Recommendations

The following recommendations can be implemented in order to shift production to desired hydrocarbon range, in particular gasoline-diesel range HCs and more precise data for good interpretation.

- Use electronic gas flow control valves instead of manual ball valves control to offer more stability of flow and hence conversion.
- Bi-functional catalyst ($Co/H-ZSM-5$) performs better with syngas at low process conditions Low-Temperature-Fischer-Tropsch (see Sartipi *et al.*, 2013b; Huang *et al.*, 2011; Liu *et al.*, 2013), hence the commercial catalyst was still offering high conversion under studied conditions.
- For methane and middle distillate hydrocarbon production, the commercial catalyst will be suitable for such processes but for C_5 and higher hydrocarbons the bi-functional catalyst is recommended.
- In higher Olefin hydrocarbon production the commercial catalyst is recommended since it's more selective to these compounds, and are produced in more quantities.
- Increase analysis time on the GC by increasing the column length which increases separation efficiency, care must be taken when increasing column length since heavy hydrocarbon might saturate within the column resulting in blockages.

7.3. Process Optimization

Some of the key points that can be used for process optimization are stated below. One of the challenges that can occur is when implementing these recommendations simultaneously; the two stated optimization cannot be implemented at once:

- Operating conditions should be set at low flow rate to obtain a higher syngas conversion, although a high flow rate offers an optimum hydrocarbon separation within the GC column.
- To produce more C₆₊ hydrocarbons or gasoline and diesel range hydrocarbons, lower and middle hydrocarbons (C₁-C₅), specifically C₅ for Co/H-ZSM-5 and C₁ for Co/SiO₂, should be minimized by increasing flow rate, this shifts selectivity and production to C₆₊ compounds, thus a higher flow rate yields higher hydrocarbons.

7.4. References

- Che M, Védrine J.C (ed.), 2012, Characterization of Solid Materials and Heterogeneous Catalyst- From structure to Surface Reactivity, Volume 2, Wiley-VCH Verlag GmbH & CO. KGaA, Weinheim, Germany
- Dagle R.A, Lizarazo-Adarme J.A, Dagle V.L, Gray M.J, White J.F, King D.L, Palo D.R, 2014, Syngas conversion to gasoline-range hydrocarbons over Pd/ZnO/Al₂O₃ and ZSM-5 composite catalyst system. *Fuel Processing Technology*, 123, pp.65–74. Available at: <http://dx.doi.org/10.1016/j.fuproc.2014.01.041>.
- Dorner R.W, Hardy D.R, Williams F.W, Davis B.H, Willauer H.D, 2009, Influence of Gas Feed Composition and Pressure on the Catalytic Conversion of CO₂ to Hydrocarbons Using a Traditional Cobalt-Based Fischer- Tropsch Catalyst. *Energy & Fuels*, 23(August 2008), pp.4190–4195. Available at: <http://pubs.acs.org/doi/abs/10.1021/ef900275m>.
- Du X, Wu E, 2007. Porosity of microporous zeolites A, X and ZSM-5 studied by small angle X-ray scattering and nitrogen adsorption. *Journal of Physics and Chemistry of Solids*, 68(9), pp.1692–1699.
- Huang X, Hou B, Wang J, Li D, Jia L, Chen J, Sun Y, 2011, CoZr / H-ZSM-5 hybrid catalysts for synthesis of gasoline-range isoparaffins from syngas. “*Applied Catalysis A, General*”, 408(1-2), pp.38–46. Available at: <http://dx.doi.org/10.1016/j.apcata.2011.09.004>.
- Hyun D C, Park J.C, Hong S.Y, Lim J.T, Kim C.S, Lee H-T, Yang J-I, Hiong S, Jung H, 2014, Highly selective iron-based Fischer – Tropsch catalysts activated by CO₂-containing syngas. *Journal of Catalysis*, 317, pp.135–143. Available at: <http://dx.doi.org/10.1016/j.jcat.2014.06.014>.
- Liu J, Chen J, Zhang Y, 20013, Cobalt-imbedded Zeolite Catalyst for direct synthesis of Gasoline via Fischer-Tropsch Synthesis , *The Royal Society of Chemistry* , Vol. 3, Issue 10, pp.2559.
- Mahlangu M.L, 2009. Waste Tyre Management Problems in South Africa and the Possible Opportunities that can be created through Recycling Thereof. ,Msc dissertation, University

of South Africa

Mohanty P, Pant K.K, Parikh J, Sharma D.K, 2011. Liquid fuel production from syngas using bifunctional CuO-CoO-Cr 2O₃ catalyst mixed with MFI zeolite. *Fuel Processing Technology*, 92(3), pp.600–608. Available at: <http://dx.doi.org/10.1016/j.fuproc.2010.11.017>.

Sartipi S, van Dijk J.E., Kapteijn F, 2013a, Applied Catalysis A : General Toward bifunctional catalysts for the direct conversion of syngas to gasoline range hydrocarbons : H-ZSM-5 coated Co versus H-ZSM-5 supported Co. “*Applied Catalysis A, General*”, 456, pp.11–22. Available at: <http://dx.doi.org/10.1016/j.apcata.2013.02.012>.

Sartipi S, Parashar K, Makkee M, Gascon J, Kapteijn F, 2013b, Breaking the Fischer–Tropsch synthesis selectivity: direct conversion of syngas to gasoline over hierarchical Co/H-ZSM-5 catalysts. *Catalysis Science & Technology*, 3(3), p.572. Available at: <http://xlink.rsc.org/?DOI=c2cy20744c>.

Yao Y, Hildebrandt D, Glasser D, Liu X, 2010, Fischer - Tropsch Synthesis Using H₂ / CO / CO₂ Syngas Mixtures over a Cobalt Catalyst, *Industrial & Engineering Chemistry Research*, Vol 49, pp.11061–11066

APPENDICES

Appendix A: CATALYST SYNTHESIS IMAGES

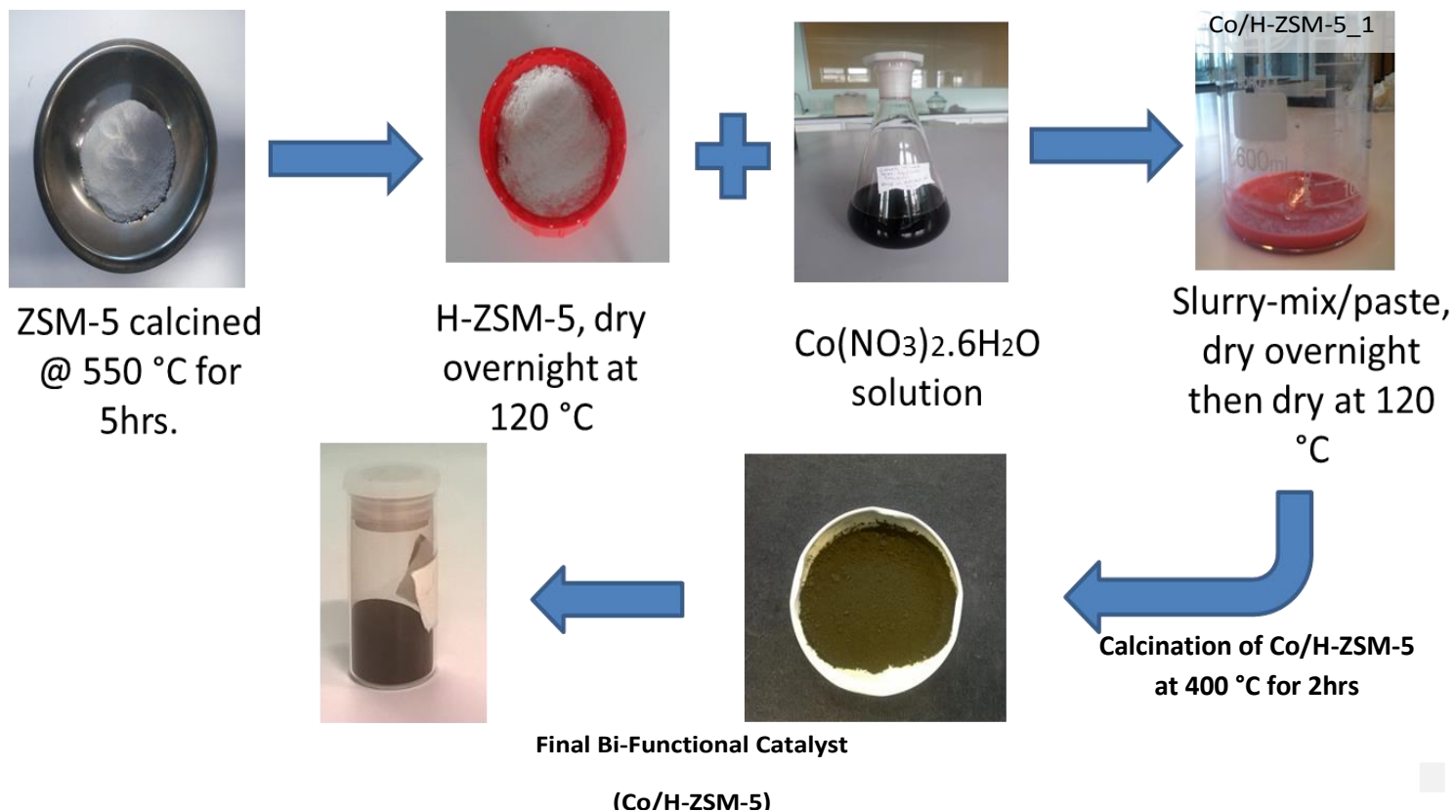


Figure A. 1: Bifunctional catalyst Synthesis images

Figure A.1 depicts the process of the catalyst synthesis method outlined in section 4.2. It shows the transformation of ammonium form of ZSM-5 to an H-form zeolite, thus H-ZSM-5, after calcination. The ammonium ion (NH₄⁺) in the ZSM-5 zeolite serves as the source of hydrogen ion; hence the H-form zeolite (H-ZSM-5) is formed after calcination. The prepared cobalt-Nitrate solution, its mixture with the support as labelled Co/H-ZSM-5_1 throughout this document and the final bi-functional catalyst that was characterized and used in the performance evaluation.

Appendix B: N₂ PHYSISORPTION AND BET DATA

Figure of Tables, B1 to B4 shows the data that was obtained from the N₂ Physisorption at 77 K. These include the surface area, pore volume and size as well as data from the Adsorption Isotherms, BET and Langmuir model of surface area.

sample		Surface Area (m ² /g)	
ZSM-5		369.5425	
H-ZSM-5		333.0928	
Co/H-ZSM-5_1		273.4548	
Co/H-ZSM-5		292.2497	

sample	Pore Volume (cm ³ /g)	sample	Pore Size (nm)
ZSM-5	0.243519	ZSM-5	2.90199
H-ZSM-5	0.231254	H-ZSM-5	3.03364
Co/H-ZSM-5_1	0.188458	Co/H-ZSM-5_1	2.95844
Co/H-ZSM-5	0.188458	Co/H-ZSM-5	2.82825

Figure B. 1: Sample Surface area, pore Volume and Size

Sample_10 - Adsorption	ZSM-5	Sample11 - Adsorption	H-ZSM-5
Relative Pressure (P/Po)	Quantity Adsorbed (cm ³ /g STP)	Relative Pressure (P/Po)	Quantity Adsorbed (cm ³ /g STP)
0.049401721	104.4316305	0.051979191	94.00835853
0.125030755	112.1866466	0.127191005	100.0275385
0.218712978	116.9711518	0.212167939	105.0040479
0.28965691	119.5054588	0.297263852	108.8840873
0.367030455	121.8812828	0.370961652	111.6916252
0.993571927	157.4341566	0.994533518	149.5047433
Sample12 - Adsorption	Co/H-ZSM-5_1	Sample_14 - Adsorption	Co/H-ZSM-5
Relative Pressure (P/Po)	Quantity Adsorbed (cm ³ /g STP)	Relative Pressure (P/Po)	Quantity Adsorbed (cm ³ /g STP)
0.054311869	79.2674472	0.050297508	83.08197949
0.132585439	83.0347051	0.123762716	88.90468231
0.211117722	85.77815226	0.214552173	93.14786951
0.286134038	87.99547882	0.298926484	95.75952479
0.356181563	89.86068	0.371474279	97.53711099
0.987491453	119.290995	0.98886526	121.8375343

Figure B. 2: Catalyst and Support Adsorption Isotherm Data

Sample_10	ZSM-5	Sample_11	H-ZSM-5
Relative Pressure (P/Po)	$1/[Q(Po/P - 1)]$	Relative Pressure (P/Po)	$1/[Q(Po/P - 1)]$
0.049401721	0.000497637	0.051979191	0.000583237
0.125030755	0.001273746	0.127191005	0.001456859
0.218712978	0.002393234	0.212167939	0.002564721
0.28965691	0.003412149	0.297263852	0.00388495
0.367030455	0.004757538	0.370961652	0.005279968
Sample_12	Co/H-ZSM-5_1	Sample_14	Co/H-ZSM-5
Relative Pressure (P/Po)	$1/[Q(Po/P - 1)]$	Relative Pressure (P/Po)	$1/[Q(Po/P - 1)]$
0.054311869	0.000724523	0.050297508	0.000637459
0.132585439	0.001840812	0.123762716	0.001588706
0.211117722	0.003119865	0.214552173	0.002932531
0.286134038	0.004555043	0.298926484	0.004452653
0.356181563	0.006156563	0.371474279	0.006059486

Figure B. 3: Sample Surface Area based on BET model

Sample_10	ZSM-5	Sample11	H-ZSM-5
Pressure (mmHg)	P/Q (mmHg-g/cm ³ STP)	Pressure (mmHg)	P/Q (mmHg-g/cm ³ STP)
30.82144547	0.295135155	32.41457748	0.34480527
78.00595856	0.695323026	79.31717682	0.792953401
136.4537506	1.166559006	132.3093719	1.26004068
180.7152557	1.512192477	185.3757629	1.70250555
228.9881592	1.87878035	231.3342133	2.071186742
Sample12	Co/H-ZSM-5_1	Sample_14	Co/H-ZSM-5
Pressure (mmHg)	P/Q (mmHg-g/cm ³ STP)	Pressure (mmHg)	P/Q (mmHg-g/cm ³ STP)
33.86925125	0.427278189	31.3803215	0.377703104
82.68118286	0.995742476	77.21483612	0.868512592
131.6544495	1.534824964	133.8578491	1.437046814
178.4351349	2.027776169	186.4984894	1.947571166
222.1172485	2.471795768	231.7606354	2.376127743

Figure B. 4: Sample Surface Area based on Langmuir model

Every sample step of Co/H-ZSM-5 catalyst synthesis was analyzed by Brunauer–Emmett–Teller (BET) analysis, in order to determine their adsorptive and surface property.

From the N₂ physisorption/ BET analysis data, Adsorption Isotherms of each sample were plotted on the same axis using Microsoft Excel. The relationship of the surface area with

pressure was determined by the BET and the Langmuir model and the results of each model were compared to the other. While the total surface area, pore size and volume were plotted as a bar graph from the obtained BET data as discussed in section 4.3.1 above. The results obtained from the N₂ Physisorption analysis are summarized below:

- ZSM-5 had the highest absorptivity while Co/H-ZSM-5_1 had the least absorptivity.
- Co/H-ZSM-5_1 surface area increases with increasing pressure while ZSM-5 had the least increase in surface area, by both the BET and the Langmuir surface area model.
- The highest total surface area was obtained by ZSM-5 when compared to the other zeolite samples, with Co/H-ZSM-5_1 having the least total surface area.
- Co/H-ZSM-5 had the smallest pore size whereas H-ZSM-5 had the highest pore size.
- The pore volume of ZSM-5 was obtained to be the highest, resulting in the high absorptivity of the adsorbate as stated above, while Co/H-ZSM-5_1 had the smallest pore volume.

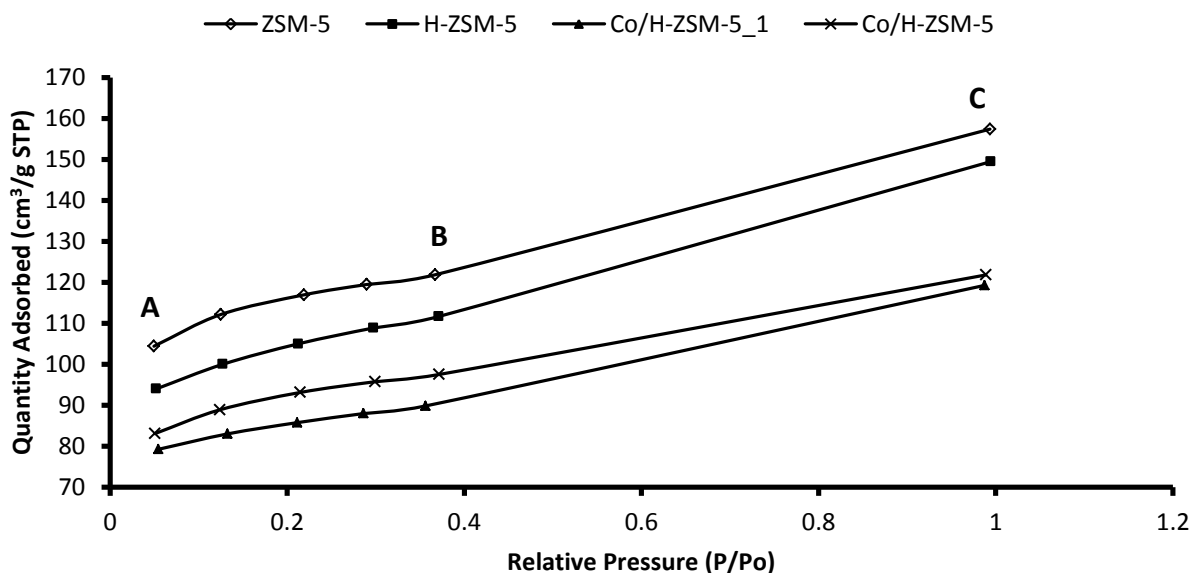


Figure B.5: Catalyst and Supports Adsorption Isotherms

Figure B.5, depicts a relationship between the relative pressure (P/P_o) and the quantity or amount adsorbed (Q) by the solid layer, which give rise to the adsorption isotherm curves. It can be seen that the quantity adsorbed increases with the relative pressure, point A to B, however from point B to C it can be concluded that no adsorption occurred until P/P_o is unity, at point C. From

Figure B.5, it is noted that Nitrogen at 77.4 K, results in the highest adsorptivity of ammonium form of ZSM-5 which is 104.431 (point A), 121.881 (point B) and 157.434 cm³/g STP (point C) when compared to H-ZSM-5, Co/H-ZSM-5_1 and Co/H-ZSM-5 samples. With Co/H-ZSM-5 having the least adsorptivity of 83.081, 97.537 and 121.837 cm³/g STP at points A,B and C respectively. Hence adsorption isotherm of ZSM-5 is above that of H-ZSM-5, Co/H-ZSM-5_1 and Co/H-ZSM-5 with Co/H-ZSM-5 adsorption isotherm being the lowest. It is also observed that the adsorption isotherm of Co/H-ZSM-5_1 and Co/H-ZSM-5 at A,B and C nearly intersect, this might be due to the fact that Co/H-ZSM-5 is the calcined (400 °C for 2 hrs) form of Co/H-ZSM-5_1, and analyzing these samples using nitrogen at its normal temperature of liquefaction (77.4 K) might have resulted in the calcination of Co/H-ZSM-5_1 to Co/H-ZSM-5 form, hence the similarity.

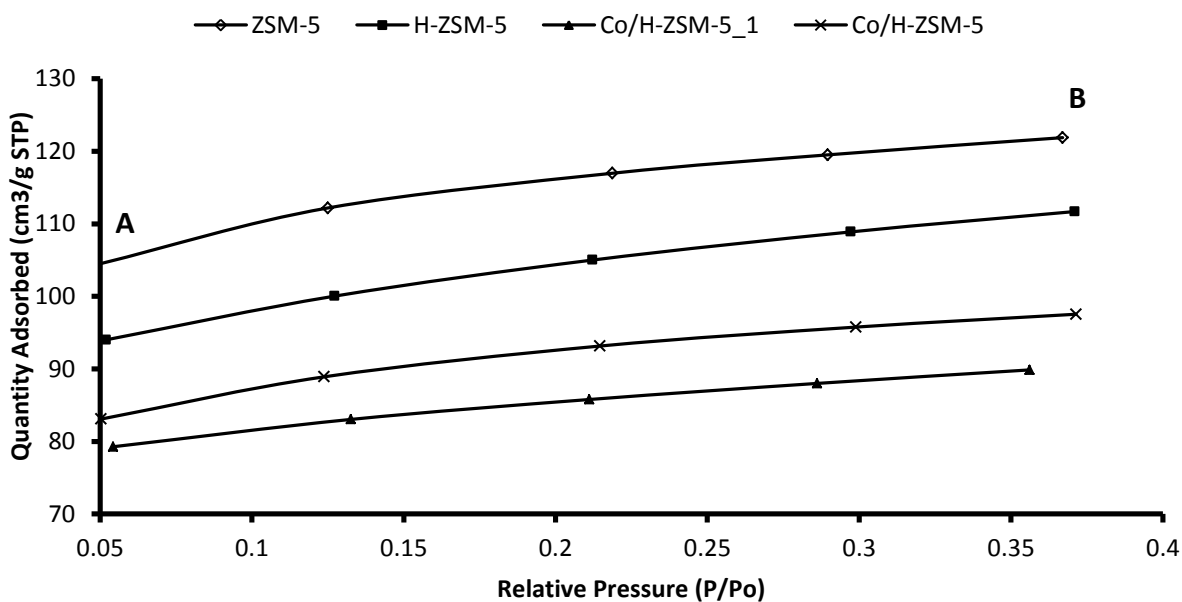


Figure B. 6: Point A and B of the Adsorption Isotherms

Figure B.6, is a semi-plot of points A and B in Figure B.5. The main aim of this Figure is to depict the behavior of the amount adsorbed in relation to the relative pressure and its classification in terms of the type of the adsorption isotherm. The curves of each sample in Figure B.6, can be classified as a Type I adsorption isotherm, which is characterized of microporous samples with an increase intake of the gas adsorbed at relative low pressure. This can simply be interpreted by an initial micro-pore filling then followed by adsorption on the external

surface of the sample. According to Che & Védrine (2012), micro-porous solids such as zeolite usually give rise to Type I isotherm, which is mostly distinguished by an increase in the amount adsorbed by the adsorbent at low pressure then followed by a distinct plateau. Instead of a plateau the zeolite samples show an increase in the isotherm at relative high pressure this is mainly due to weak adsorbate (gas)-adsorbent layer (solid) interaction, and such behavior is mostly observed in a Type III and V adsorption isotherm, this can be seen by a steep increase of the isotherm in Figure 10, between point B and C in each sample.

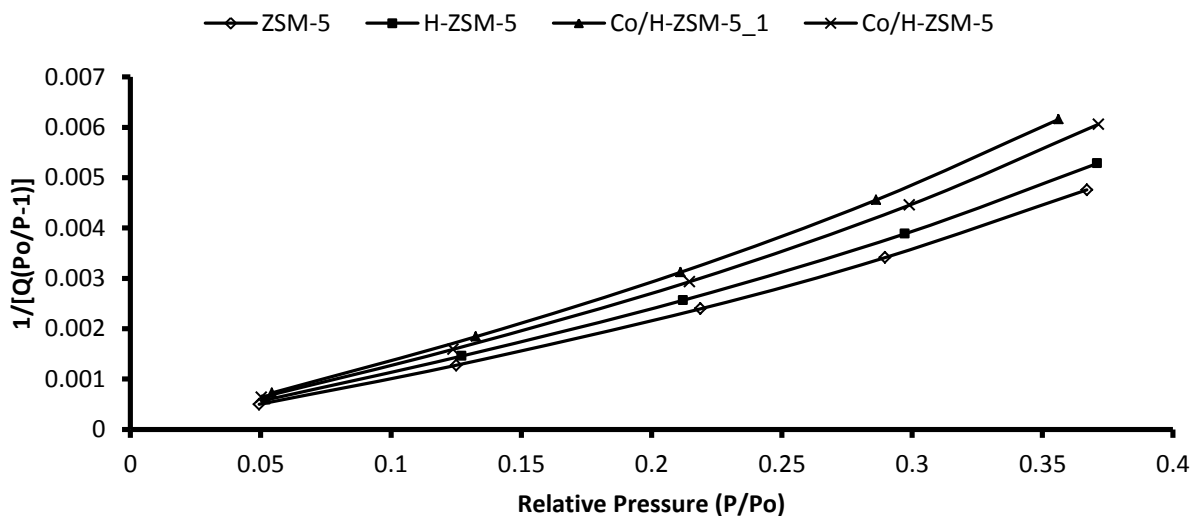


Figure B.7: BET Model Surface Area Plot

The BET-plot is a plot of $1/Q[P_o/p - 1]$ versus P/P_o , and one looks for a linear region in the accepted domain of validity, which is $0.05 < P/P_o < 0.35$, otherwise beyond this region the BET-plot may give a negative intercept (Che & Védrine, 2012). Figure B.7, depicts the BET-plot which gives a relationship of the surface area in relation to the relative pressure. From the same Figure, it can be seen that the surface area increases with an increase in the relative pressure for the region stated above. Both the cobalt samples results in a higher surface area when compared to the ammonium- and H-form of zeolite, with a higher surface area of $0.00615 \text{ g STP/cm}^3$ and $0.00605 \text{ g STP/cm}^3$ for Co/H-ZSM-5_1 and Co/H-ZSM-5 respectively. The similarity of the surface area of Co/H-ZSM-5_1 and Co/H-ZSM-5 could be due to reasons mentioned above. Ammonium form of zeolite, thus ZSM-5, has the least value of the surface area of about $0.00475 \text{ g STP/cm}^3$ and the H-form zeolite, thus H-ZSM-5 has a surface area of about $0.00527 \text{ g STP/cm}^3$.

STP/cm³. Ammonium form of zeolite is a micro-porous substance however after calcination, to form the H-form zeolite most of the solid powder had agglomerated this could have had an effect on the surface area of each sample. For Co/H-ZSM-5_1, which is a dried mixture of cobalt (II) Nitrate Hexa-hydrate solution on H-ZSM-5, the solid powder had an increased in the size of the particles after drying, and after calcination to form Co/H-ZSM-5, most of the nitrate hexa-hydrate and any other elements that might have contributed to the increase in solid particles might have been released, hence this explains the higher surface area of Co/H-ZSM-5_1 when compared to Co/H-ZSM-5 and the other zeolite samples in the accepted range of validity.

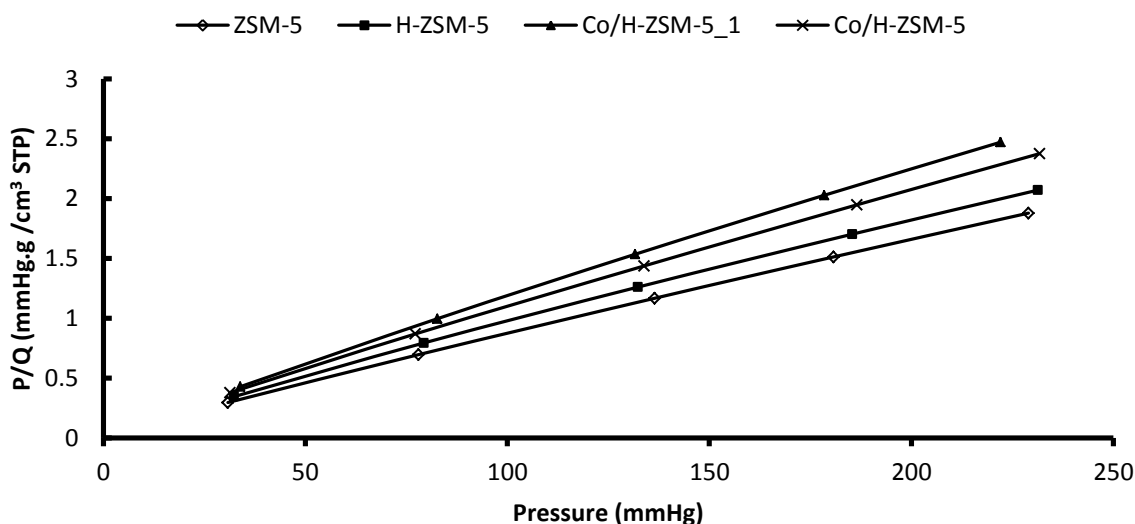


Figure B.8: Langmuir Model Surface Area

The Langmuir surface area plot behaves the same way as the BET surface area plot, but the Langmuir is known to be more accurate and does in fact result in a linear relationship between the surface area and the pressure (Che & Védrine, 2012) as it can be seen in Figure B.8. In the Langmuir model, the surface area is expressed in terms of P/Q (mm Hg.g /cm³). The same characteristics as the BET surface area model is obtained for each of the samples, with a higher surface area of 1.878, 2.071, 2.471, 2.376 mmHg.g/cm³ STP for ZSM-5, H-ZSM-5, Co/H-ZSM-5_1 and Co/H-ZMS-5 respectively at a pressure of about 230 mm Hg.

Appendix C: PERFORMANCE EVALUATION AND GC PICS



Figure C. 1: The Experimental Setup Components used for Catalyst Performance Evaluation

- A – Set of Gases used for the experiment on the gas bank/ stand
- B – Set of regulators up stream, gas cylinder outlet regulators
- C – Reactor, covered by a thermal blanket to maintain constant temperature
- D – TCD (Thermal Conductivity Detector) Gas Chromatograph
- E – FID (Flame Ionized Detector) connected to the apparatus online
- F - Computer used , installed with Clarity[®] program for peak analysis
- G – Offline FID for Wax and oils

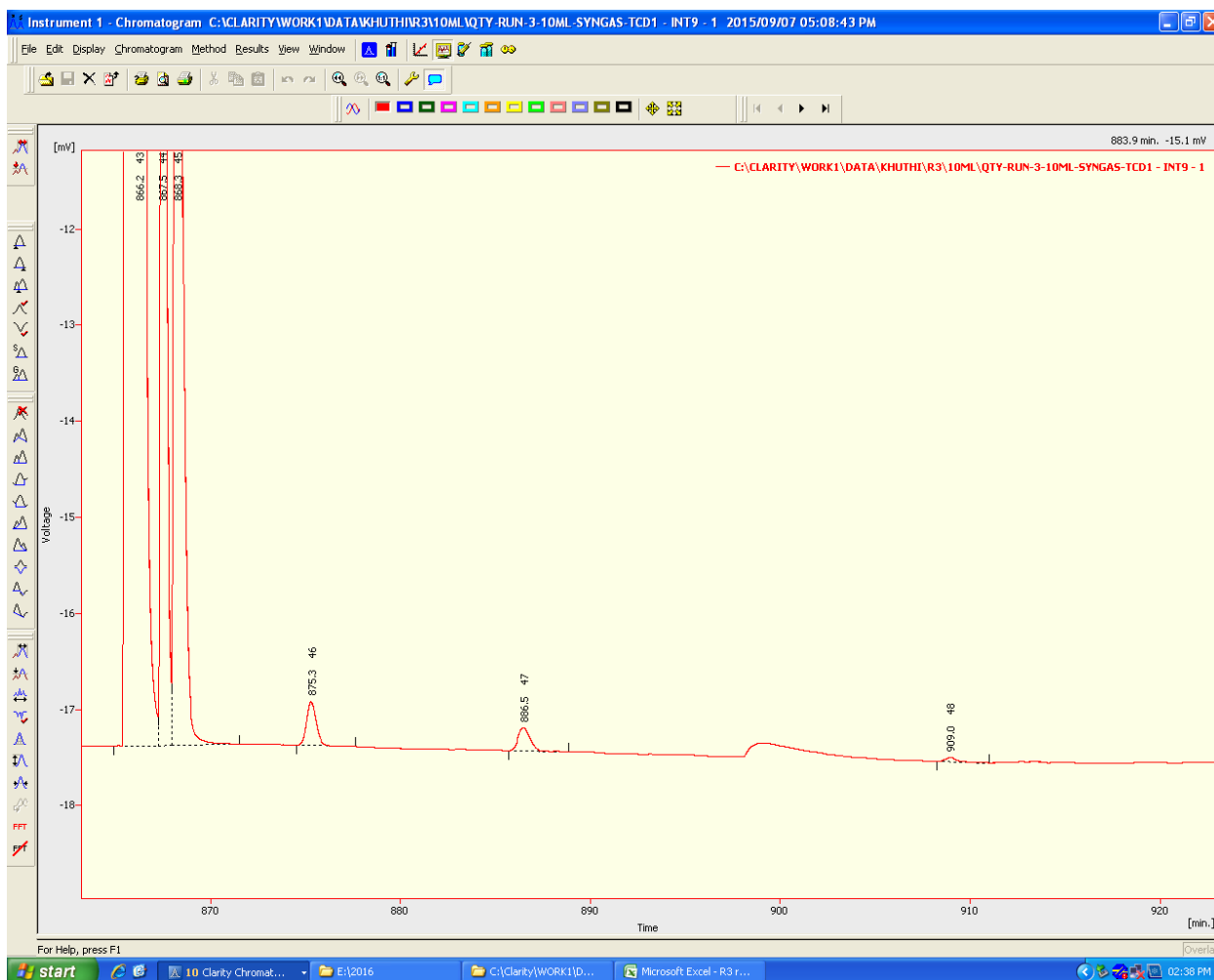


Figure C. 2: Thermal Conductivity Detector Gas Chromatograph peak image during reaction

Figure C.2 shows the peaks from the TCD chromatogram which detects inorganic compounds. The depicted in the Figure above are for unreacted H_2 , N_2 and CO the first three peaks respectively and lower hydrocarbons such as C_1 to C_2 can be detected at a low signal

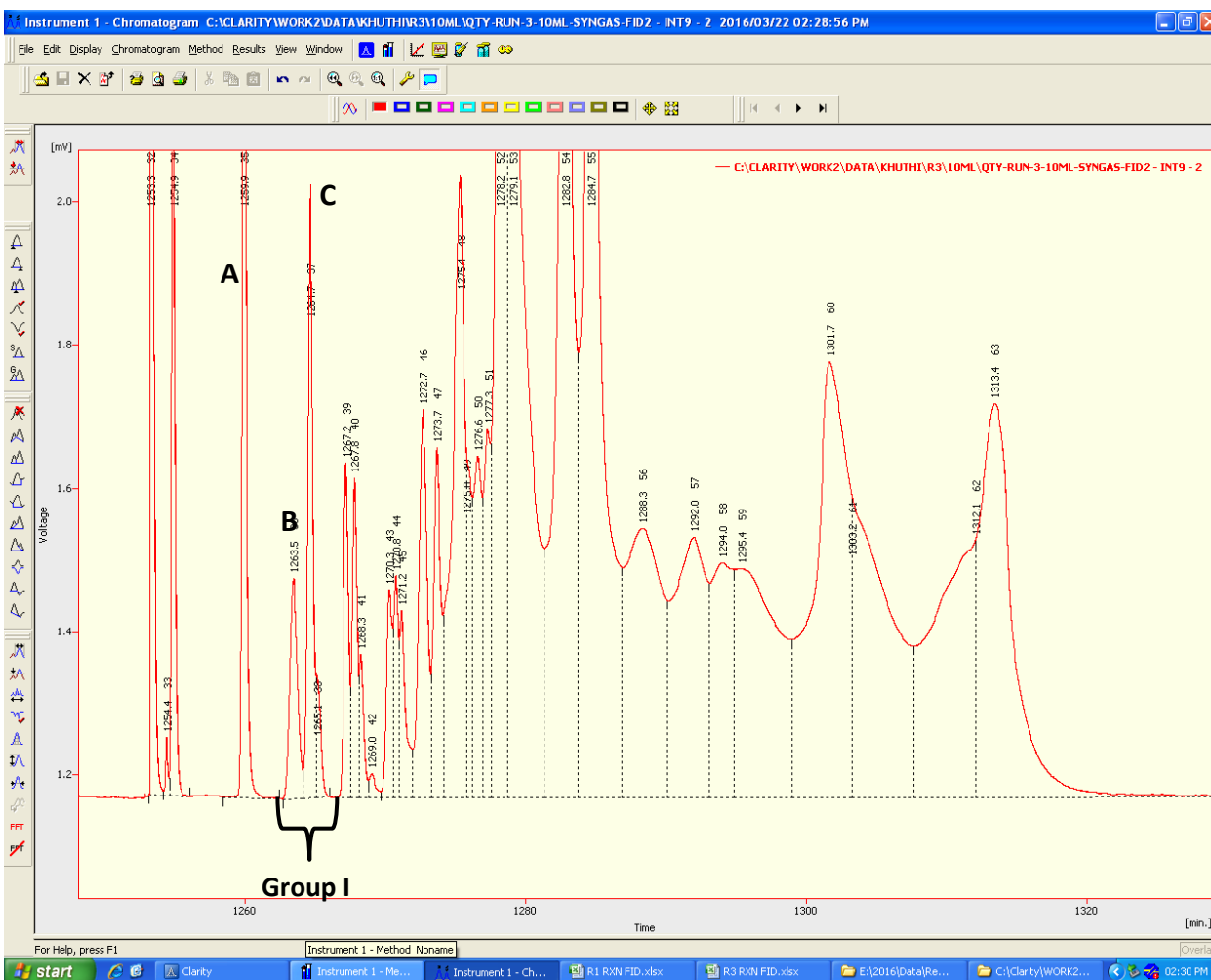


Figure C. 3: Flame Ionized Detector Gas Chromatograph peak image during reaction

Figure C.3, depicts the peak signal of unreacted H_2 , N_2 and CO the first three peaks respectively, as well as the peaks of Hydrocarbons formed. In a group of peaks (say Group I) the first peak is considered as an olefin (Peak B: Ethene) then the second one as a paraffin (Peak C: Ethane) of that Hydrocarbon number, C_2 in this case, but a stand-alone peak is considered as a paraffin (Peak A: Methane)

Appendix D: CONVERSION AND SELECTIVITY CALCULATIONS

In this section an example on how conversion and selectivity was obtained will be performed. Method of calculation used is based on Price (1994); Motchelaho (2011) and Moyo (2012) who submitted their Thesis and obtained their qualification from the University of Witwatersrand.

D1. Conversion Calculations

Table D1. 1: Syngas Calibration peaks before reaction

CALIBRATION PEAKS before rxn			
Peak #	H ₂	N ₂	CO
1	8179.085	297.5	325.937
2	8731.889	261.016	352.189
3	8972.554	247.103	364.438
4	9136.824	238.626	368.8
5	9246.526	236.442	367.879
6	8871.887	224.453	356.969
7	8692.762	220.442	354.188
8	8942.636	231.421	369.559
9	8802.056	223.92	360.599
10	8747.929	224.174	359.571
11	9049.934	230.776	372.822
12	9078.612	231.564	372.967
Average	8871.058	238.9531	360.4932

Table D1.1 shows the TCD calibration peak areas of Hydrogen (60 %), Nitrogen (15 %) and Carbon-monoxide (25 %) composition as the syngas mixture. This peaks were obtain before reaction takes place and an average of the peaks calculated as tabulated above.

Table D1. 2: Peak Composition Area

% H ₂	147.851
% CO	14.41973
% N ₂	15.93021

The values in Table D1.2 were calculated by using the following equation:

$$\text{for } H_2 = \frac{\text{average } H_2 \text{ peak area}}{\% H_2 \text{ in syngas}} = \frac{8871.058}{\% 60} = 147.851$$

Table D1. 3: Thermal Conductivity Detector Syngas mixture Peak Areas after reaction

TCD Peak Areas after rxn			
Peak #	H ₂	N ₂	CO
9	6602.65	352.207	256.446
10	6563.526	344.68	255.265
11	6864.347	351.629	266.229
12	7321.552	340.19	281.733
13	7414.641	340.767	284.613
14	7379.293	340.079	281.567
15	7210.529	338.164	277.101
16	6864.025	334.199	264.79
17	6624.919	334.387	256.18
18	6751.253	344.428	261.574
19	6669.48	336.564	259.521

The Table D1.3 above shows the TCD peaks of the syngas content after reaction. This data from the above tables will be used to calculate conversion and selectivity.

Table D1. 4: Product Moles and Conversion

Time, hours	% Mole after rxn			% Conversion	
	H ₂	N ₂	CO	H ₂	CO
19	44.39285	21.63688	17.70249	48.70697	50.91025
21	46.42748	22.0731	18.46283	47.41622	49.81357
23	49.51981	21.35503	19.53803	42.02793	45.10513
25	50.14943	21.39125	19.73775	41.39026	44.63787
27	49.91035	21.34806	19.52651	41.55166	45.11957
29	48.7689	21.22785	19.2168	42.56495	45.68418
31	46.4253	20.97895	18.36304	44.67634	47.48153
33	44.80809	20.99075	17.76594	46.63354	49.21781
35	45.66256	21.62106	18.14001	47.20131	49.66017
37	45.10948	21.12741	17.99764	46.62209	48.88829
Average	47.11742	21.37503	18.6451	44.87913	47.65184

To calculate % conversion, product moles after reaction had to be calculated by using the equation below and tabulated in Table D1.4 above.

$$\% \text{ moles of } H_2 \text{ after rxn} = \frac{\text{peak area of } H_2 \text{ after rxn}}{\text{area to mole ratio of } H_2} = \frac{6602.65}{147.851} = 44.392 \%$$

Then % Conversion was calculated by the following equation:

$$CO \text{ Conversion} = \left\{ \frac{\left[\text{Moles of CO before rxn} - \left(\text{moles of CO after rxn} \left(\frac{\text{moles of N}_2 \text{ before rxn}}{\text{moles of N}_2 \text{ after rxn}} \right) \right) \right]}{\text{moles of CO before reaction}} \right\} \times 100 \%$$

$$= \left\{ \frac{\left[25 - \left(17.702 \left(\frac{15}{21.63} \right) \right) \right]}{25} \right\} \times 100 = 50.91 \%$$

Of which is the conversion of CO at that point in time. This was done for 51 points and the average CO conversion is what is stated in the results and discussion in Chapter 5 and 6, which is the average conversion per reaction run. The change in conversion with time can also be shown as a plot (see Figure D1.1) for syngas composition of 1.5; 2.5 and 2.5 with CO₂ co-feeding. For the above example the conversion calculated was for 2.5 syngas ratio which resulted in a CO conversion of 53 % on average basis over the 100 hr. reaction time. The conversion tabulated in Table D1.4 was between the reaction time of 19- 37 hrs. this can also be seen from the Figure D1.1 below, of which the reaction was performed at different H₂/CO (1.5; 2.5; 2.5 + 5 % CO₂) ratios , Temperature 250 °C and 15 bars of Pressure.

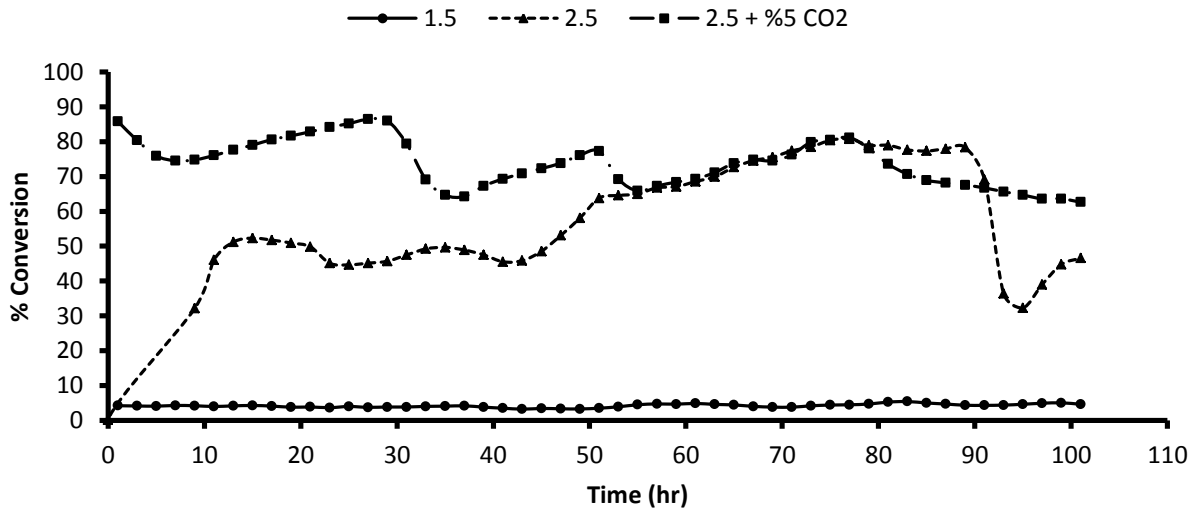


Figure D1. 1: Change of Conversion with Time at 250 °C, 15 bars and 1200 GHSV and various H₂/CO ratios

D2. Selectivity Calculations

For selectivity calculations the FID peak areas as depicted in Figure C.3 are used. A gas mixture of composition stated in Table D2.1 was used as the calibration gas. The calibration peaks were used to determine the hydrocarbon selectivity per carbon numbers.

Table D2. 1: Calibration Gas Composition

FROM FID CALIBRATION		
	AREA	Peak %
H ₂	302.482	55.5496
N ₂	52.942	9.722584
CO	144.76	26.58459
CH ₄	4.532	0.832283
C ₂ H ₄	3.209	0.58932
C ₂ H ₆	4.236	0.777924
CO ₂	32.365	5.943701
TOTAL	544.526	100

Table D2.2 shows the peak areas of C1 to C8 for their respective hydrocarbon i.e. Olefin or Paraffin, these peaks are obtained after reaction and would be used with the calibration peak areas to calculate the selectivities of these compounds.

Table D2. 2: Hydrocarbon Products Peak Areas

FROM REACTION		
	PEAK AREA	
	Olefin	Paraffin
CH ₄	0	2.09
C ₂	0.522	0.077
C ₃	7.228	0.916
C ₄	25.501	69.058
C ₅	51.9	54.631
C ₆	38.515	84.352
C ₇	62.799	69.034
C ₈	56.28	59.964

When calculating selectivity's each hydrocarbon for each carbon number is assumed to exhibit a certain molar factor of which these factors are useful when calculating selectivity (references). These factors are shown in Table D2.3.

Table D2. 3: Hydrocarbon Molar Response Factor adopted from Motchelaho (2011) and Moyo (2012)

CN	Olefin	Paraffin
1	0	1
2	1	1
3	0.7	0.74
4	0.78	0.55
5	0.47	0.47
6	0.4	0.4
7	0.35	0.35
8	0.32	0.32
9	0.28	0.28
10	0.24	0.24
11	0.21	0.21
12	0.19	0.19
13	0.18	0.18
14	0.17	0.17
15	0.15	0.15

Table D2. 4: Product moles and Selwectivity

CN	Peak Area		Mole %		Moles (mol)		Selectivity		% Selectivity	
	Olefin	Paraffin	Olefin	Paraffin	Olefin	Paraffin	Olefin	Paraffin	Olefin	Paraffin
	$A_{HC,i}$	$A_{HC,i}$	$X_{HC,i}$	$X_{HC,i}$	$N_{HC,i}$	$N_{HC,i}$	$S_{HC,i}$	$S_{HC,i}$	$S_{HC,i}$	$S_{HC,i}$
1	0	2.09	0	0.383820056	0	0.010280894	0.00000	30.621	0	0.614485
2	0.522	0.077	0.0958632	0.014140739	0.002567764	0.00037877	0.05152	1.128	0.21504	0.022639
3	7.228	0.916	0.9291751	0.124482578	0.03555517	0.004505885	0.71334	13.421	2.97761	0.269315
4	25.501	69.058	3.6528614	6.975222487	0.125441669	0.339702394	2.51672	1011.793	10.50526	20.30389
5	51.9	54.631	4.4796759	4.715398346	0.255300678	0.268734708	5.12207	800.418	21.38046	16.06218
6	38.515	84.352	2.8292497	6.196361606	0.189458683	0.414934929	3.80109	1235.871	15.86644	24.80051
7	62.799	69.034	4.0364739	4.43723532	0.308913821	0.339584336	6.19770	1011.442	25.87036	20.29683
8	56.28	59.964	3.3073903	3.52388683	0.276846285	0.294968206	5.55434	878.554	23.18482	17.63014
TOTAL	242.745	340.122	19.330689	26.37054796	1.194084068	1.673090121	23.95677	4983.248	100	100

Table D2.1 to D2.4 will be used to calculate data obtained in Table D2.4. After obtaining peak areas from calibration and reaction, moles of Olefin and paraffin's can be calculated per carbon

number. The moles of the formed products were calculated by the following equation and example for calculating Methane Selectivity.

- Calculate the average area and % mole of C₂ in calibration Gas by using data in Table D2.1

$$\text{Area of } C_2 \text{ in calibration gas} = \frac{3.209 + 4.236}{2} = 3.723$$

$$\begin{aligned} \text{average } C_2 \text{ moles in calibration gas} &= \frac{\text{Area of } C_2 \text{ in calibration gas}}{\text{Total component Area in syngas}} \\ &= \frac{3.723}{544.526} \times 100 = 0.684 \% \end{aligned}$$

- Calculate moles of each compound, e.g. for methane, C₁ use the formula:

$$N_{HC,i} = X_{C_2,cal} \times F_{tot,out} \times t_{rxn} \times \left(\frac{A_{HC,i}}{A_{C_2,cal}} \right) = 0.684 \times 4.64 \times 10^{-4} \times 60 \times \left(\frac{2.09}{3.723} \right) = 0.01 \text{ mol}$$

Where: $X_{C_2,cal}$ – is the average % of C₂ hydrocarbons in the calibration gas.

$F_{tot,out}$ – The total gas flow rate out of the system

t_{rxn} – Total time for reaction

$A_{HC,i}$ – Peak area of produced Hydrocarbon *i*

$A_{C_2,cal}$ –Peak area of C₂ hydrocarbon in calibration gas

- Calculate Selectivity in moles of the hydrocarbon i.e. Methane as C₁

$$\text{Selectivity (moles)} = \left(\frac{N_{HC,i}}{\Delta W} \right) \left(\frac{t_{rxn}}{-r_{CO}} \right) = \left(\frac{0.01}{0.5} \right) \left(\frac{60}{1.12 \times 10^{-5}} \right) = 30.621 \text{ moles}$$

- Calculate % Selectivity by using total selectivity of all the hydrocarbons for paraffin/olefin depending on the bonds of the produced hydrocarbon.

$$\begin{aligned} \% \text{ Selectivity} &= \frac{\text{moles produced of paraffin, } i}{\text{total paraffin moles produced}} = \frac{30.621 \text{ moles}}{4983.248 \text{ moles}} \times 100 \\ &= 0.614 \% \end{aligned}$$

Therefore the % selectivity of Methane is 0.614 % which was rounded off as 1 % in the Figure D2.1 below for plotting. In the same Figure D2.1, the selectivity of other hydrocarbons is depicted and data Tabulated in Table D2.5.

Table D2. 5: Olefin and Selectivity Data in Fractions

CN	Selectivity fraction	
	Olefin	Paraffin
	$S_{HC,i}$	$S_{HC,i}$
C ₁	0	0.006145
C ₂	0.00215	0.000226
C ₃	0.029776	0.002693
C ₄	0.105053	0.203039
C ₅	0.213805	0.160622
C ₆₊	0.649216	0.627275
Total	1	1

The selectivity's shown in Table D2.5 are in terms of fraction, there after converted to percentage while plotting the bar graphs as depicted in Chapter 5 and 6 as well as Figure D2.1 below. To obtain C₆₊ hydrocarbons selectivity an average of C₆ and higher carbon number hydrocarbons selectivity was calculated.

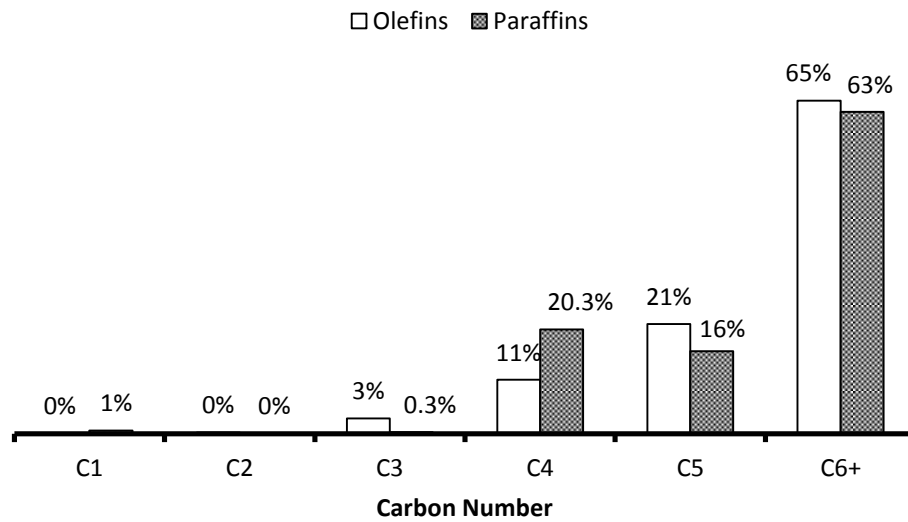


Figure D2. 1: Hydrocarbon Selectivity at 250 °C, 15 bars and H₂/CO ratio of 1.5